Power electronic activation for active magnetic bearings

A dissertation presented to

The School of Electrical, Electronic and Computer Engineering

North-West University

In partial fulfilment of the requirements for the degree

Magister Ingeneriae

in Electrical and Electronic Engineering

by

Tshepo Elias Seiphetlho

Supervisor: Prof. G. van Schoor
Assistant supervisor: Mr. E.O. Ranft

June 2006

Potchefstroom Campus

"[21]For me to live is Christ, and to die is gain. [22]If I am to live in the flesh, that means fruitful labor for me. Yet which I shall choose I cannot tell. [23]I am hard pressed between the two. My desire is to depart and be with Christ for that is far better. [24]But to remain in the flesh is more necessary on your account"

Philippians 1:21-24

DECLARATION

I hereby declare that all the material incorporated in this thesis is my own original unaided work except where specific reference is made by name or in the form of a numbered reference. The work herein has not been submitted for a degree at another university.

Signed: 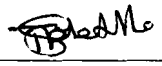

Tshepo Elias Seiphetlho

SUMMARY

The School of Electrical, Electronic and Computer Engineering of the North-West University is currently doing research on active magnetic bearing (AMB) systems. One of the latest developments is the flexible rotor double radial AMB model. Various studies on the AMB sub-systems are being conducted using the model.

The focus of this study is on AMB power amplifiers (PAs). The aim is to develop a platform to facilitate the analysis of the two-state and the three-state switching techniques that are possible for the AMB switch-mode PAs. An average current controlled PA prototype board is designed to facilitate the study.

The design of the switch-mode PA for the two-state and the three-state switching techniques is conducted and analysed based on the design specification. The switching techniques are realised in a digital signal processing (DSP) environment with a TMS320P2812 eZdsp DSP starter kit (DSK). A TMS320P2812 eZdsp DSK is programmed in VisSim® development software.

The simulation model for the two switching techniques was developed in MATLAB® simulink. The simulation models are used to verify the design specifications, to predict the experimental set-up behaviour and to compare the two-state and the three-state switch-mode PA topologies. The two switching techniques showed good correlation in system performance, small signal bandwidth and power bandwidth. The simulation models' responses are also in agreement with the theoretical analysis.

Testing of the PA's switching techniques was conducted on the double radial AMB system. The two switching techniques are analysed on the basis of how well they can regulate the coil current. The power bandwidth as well as the power loss analysis was used to evaluate the two switching techniques.

The experimental results showed good correlation with the simulation results in terms of the dynamic response and the power losses. The power bandwidth measurements could not be performed at the specified dc levels due to noise problems. The power bandwidth prediction was however verified by reducing the voltage level to minimum values and the switching frequency to lower value. Recommendations for future improvements on the PAs are given based on the results.

OPSOMMING

Die skool vir Elektriese, Elektroniese en Rekenaaringenieurswese van die Noordwes- Universiteit is tans besig om navorsing te doen op aktiewe magnetiese laer (AML) sisteme. Een van die nuutste ontwikkelings is die buigbare rotor dubbelradiale rotor AML model. Verskeie studies op AML substelsels word gedoen met die model.

Die fokus van hierdie studie is op AML kragversterkers (KVs). Die doel is om 'n platform te ontwikkel vir die fasilitering van die twee-toestand en drie-toestand skakeltegnieke, wat moontlik is vir AML skakelmodus KVs. 'n Gemiddelde stroom beheerde KV prototipe bord is ontwerp om hierdie studie te fasiliteer.

Die ontwerp van die skakelmodus KV vir die twee- toestand en drie- toestand skakeltegnieke is uitgevoer en ge-analiseer, gebaseer op die ontwerpspesifikasie. Die skakeltegnieke word geïmplementeer in 'n digitale seinverwerking (DSP) omgewing met behulp van 'n "TMS320P2812 eZdsp DSP starter kit (DSK)". 'n TMS320P2812 eZdsp DSK word geprogrammeer in VisSim® ontwikkelingsagteware.

Die simulasiemodel vir die twee skakeltegnieke is ontwikkel in MATLAB® simulink. Die simulasiemodelle word gebruik om die ontwerpspesifikasies te verifieer, om die eksperimentele opstelling se gedrag te voorspel om die twee-toestand en drie-toestand skakelmodus KV topologieë. Die twee skakeltegnieke het goeie korrelasie getoon in stelselsgedrag, kleinsein bandwydte en drywings bandwydte. Die simulasiemodelle se respons stem ook ooreen met die teoriese analise.

Die KV se skakeltegnieke is getoets op die dubbelradiale AML sisteem. Die twee skakeltegnieke is ge-analiseer op grond van hulle vermoë om die spoelstroom te reguleer. Die drywingsbandwydte sowel as die drywingsverliese analise is gebruik om die twee skakeltegnieke te evalueer.

Die eksperimentele resultate het goeie korrelasie getoon met die gesimuleerde resultate in terme van die dinamiese respons en drywingsverliese. Die drywingsbandwydte metings kon nie by spesifieke dc vlakke uitgevoer word nie weens ruisprobleme. Die drywingsbandwydte voorspelling is egter g-everifieer, deur die spanning vlak na minimum waardes teverstel en die skakel frekwensie na laer waarde. Aanbevelings vir toekomstige verbeteringe op die KVs, gebaseer op die resultate, word gegee.

ACKNOWLEDGEMENTS

I would like to thank M-tech industrial and THRIP for funding this research and for giving me the opportunity to further my studies.

I would also like to thank Prof. G. van Schoor, my supervisor and Mr. E.O. Ranft, my assistant-supervisor for granting me the privilege to work under their guidance. Their continued support, guidance and technical advice lead to the successful completion of my project.

I also wish to acknowledge the inputs and support of the following people in no particular order

- My brother, Lebeko and my sister, Bridgette for their love and support
- My cousin Oumanyana Lemme for her support and constant guidance
- My friends Desmond, Dolly and Motlatsi for always encouraging me to work hard
- And finally my friends from the MBMC research group; Charl, Deon, and Markus.

TABLE OF CONTENTS

NOMENCLATURE

LIST OF FIGURES

LIST OF TABLES

LIST OF ABBREVIATIONS

AMB	Active Magnetic Bearing
MBMC	Magnetic Bearing Modelling and Control
PA	Power Amplifier
PWM	Pulse-Width-Modulation
VMC	Voltage Mode Control
CMC	Current Mode Control
PCMC	Peak Current Mode Control
ACMC	Average Current Mode Control
PE	Power Electronics
DSP	Digital Signal Processing
DSK	DSP Starter Kit
ADC	Analogue-to-digital converter
PCB	Printed Circuit Board
MOSFET	Metal-oxide-semiconductor field effect transistor
IGBT	Insulated gate bipolar transistor
SMPS	Switch-mode power supply
TP	Test point
rms	root-mean-square

FPGA	Field Programmable Gate Array

LIST OF SYMBOLS

i	Instantaneous current
V_{BUS}	H-bridge voltage rail
A_t	Power amplifier's carrier signal's amplitude
L, L_{Load}	Coil/Load inductance
T_s	Switching time
f_{sw}	Switching frequency
d	Duty cycle
R, R_{Load}	Coil/Load resistance
R_θ	Thermal resistance
τ	AMB load time constant
I_{act}, I_{ref}, I_{max}	Actual coil current, Reference current and maximum current
K_p	Proportional gain
K_i	Integral gain
ω_{bw}, ω_{pbw}	Small signal bandwidth and power bandwidth (rad/s)
C_{rect}, C_{dec}	Rectifier capacitor and decoupling capacitor
f_{ref}	Reference signal frequency
Hx, Lx	High side and Low side IGBT
T_d	Deadband time

1
Chapter
Introduction

Chapter 1 provides a general background on power electronic (PE) application in active magnetic bearing (AMB) systems. The focus is on the problem statement, issues to be addressed and the research methodology. An overview of the dissertation is provided at the end of this chapter.

1.1 Background

The School of Electrical, Electronic and Computer Engineering of the North-West University is currently doing research on AMB systems. A number of AMB models have been developed. One of the latest developments is the flexible rotor double radial AMB model. Various studies on the AMB sub-systems are being conducted using the model. This model is currently in the Magnetic Bearing Modelling and Control (MBMC) laboratory of the North-West University.

1.1.1 Active Magnetic Bearings

AMB systems suspend a load in space by means of magnetic forces. The advantages of AMBs have given AMB systems an upper hand over the conventional bearings in the technology of rotating machines. An AMB's system performance mostly depends on its sub-systems. The sub-systems of AMB systems are the position sensors, a controller, power amplifiers (PAs), electromagnetic actuators and the load.

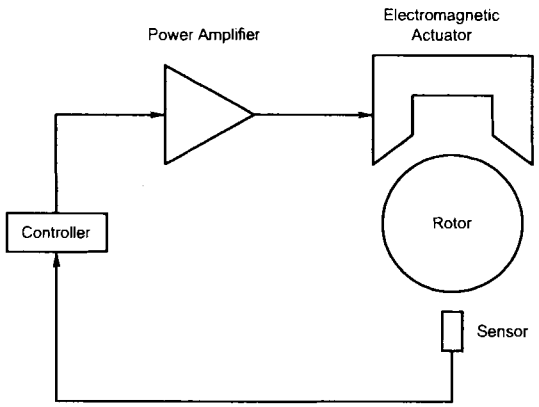

Figure 1-1: A functional block diagram of an AMB system

Figure 1-1 displays a functional block diagram of an AMB system. The position sensor senses the position of the load and supplies a position signal to the controller which generates appropriate control signal. The control signal is fed to the PAs. The PAs are responsible for establishing currents in the electromagnetic actuator which result in magnetic forces required to stably suspend the load in space.

1.1.2 AMB power amplifiers

PAs are one of the major sub-systems of AMB systems. They convert the control command from the position controller into current signals. The PA converts low power controller output signals into high power actuator input signals by regulating the flow of energy between the power source and magnetic circuit. The power amplification stage in an AMB system is constrained by power efficiency and size. A low efficiency amplifier result in high losses which can cause the load to generate heat which will in turn reduce the functionality and reliability of the AMB system. The size of the PA is a constraint because more than 8 PAs may be needed for AMB systems.

There are three types of PAs that may be used in AMBs. They are linear amplifiers, switch-mode amplifiers and hybrid amplifiers. Linear PAs are mostly applicable in AMB systems that require low voltage and current because of their low power efficiency. The advantage of the linear PA is the low level of noise that it produces when it operates. For large AMB systems, the switch-mode PAs are the more viable choice when compared to linear PAs due to the high power efficiency that is required. The only drawback of switch-mode PAs is the noise resulting from the switching process. A hybrid PA is basically a switch-mode linear assisted PA. It combines the advantages of both the linear and switch-mode PAs. This type of amplifier is aimed at reducing the noise produced by the switch-mode amplifiers and also at improving the efficiency of linear amplifier application in large AMB systems. The only drawback of the hybrid amplifier is the complexity of the circuit and control strategy [1].

AMB PAs may be controlled in two different ways; current controlled or voltage controlled. The control methods depend on whether the magnetic circuit's current or voltage is being regulated. A PA regulating current is classified as a current controlled while a voltage regulating PA is termed a voltage controlled PA. The advantage of the current controlled PA is the elimination of the pole introduced by the load inductance which reduces the systems order. This reduces the controller complexity allowing the use of a simple PD controller [2].

The pulse-width-modulation (PWM) signals of switch-mode PAs can be generated in two different ways, the voltage mode control (VMC) in which a carrier signal is used to generate the switching signals or the current mode control (CMC) in which the slope of the actual current through the load is used to generate the PWM signals.

The switch-mode PA PWM generator can be realised in two different ways, the two-state and the three-state technique. The two techniques control the pattern in which the H-bridge is change states. The H-bridge circuit is shown in Figure 1-2. In the two-state switching technique, a single PWM signal is applied to switches S1 and S4 and the complement of that PWM signal to S2 and S3. As a result, the coil voltage is switched between the positive voltage rail and the negative voltage rail. The three-state switching technique utilises two individual PWM signals. One PWM signal to drive switch S1 and S3 with the signal and its complement respectively; and the other to drive switches S2 and S4 with the signal and its complement respectively. The coil voltage now has three states i.e. positive voltage rail, negative voltage rail and 0 V. A three-state technique is considered the best choice of PA for AMB systems due to the fact that the current ripple component is drastically reduced, resulting in lower losses in the AMB magnetic circuit [1, 2, 3].

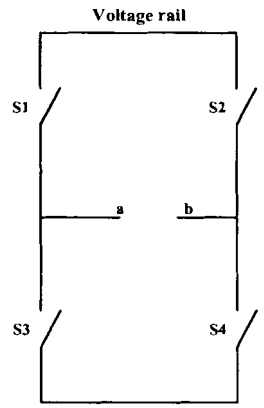

Figure 1-2: H-bridge circuit diagram

1.2 Problem statement

The purpose of the study is to develop a platform to facilitate the analysis of the two-state and the three-state switching techniques that are possible for an AMB switch-mode PAs. The focus will be placed on PA topology, the efficiency, reliability and control of the H-bridge circuit in the two different modes. The study will take an in-depth look at reducing the losses caused by PAs in AMB systems.

Due to the advantages of current controlled PAs over voltage controlled PAs, an average current controlled PA will be implemented. Figure 1-3 displays the proposed switch-mode PA that will be controlled by either the two-state or three-state PWM generation technique. A basic switch-mode PA comprises a power circuit, feedback circuit, a controller and a PWM generator.

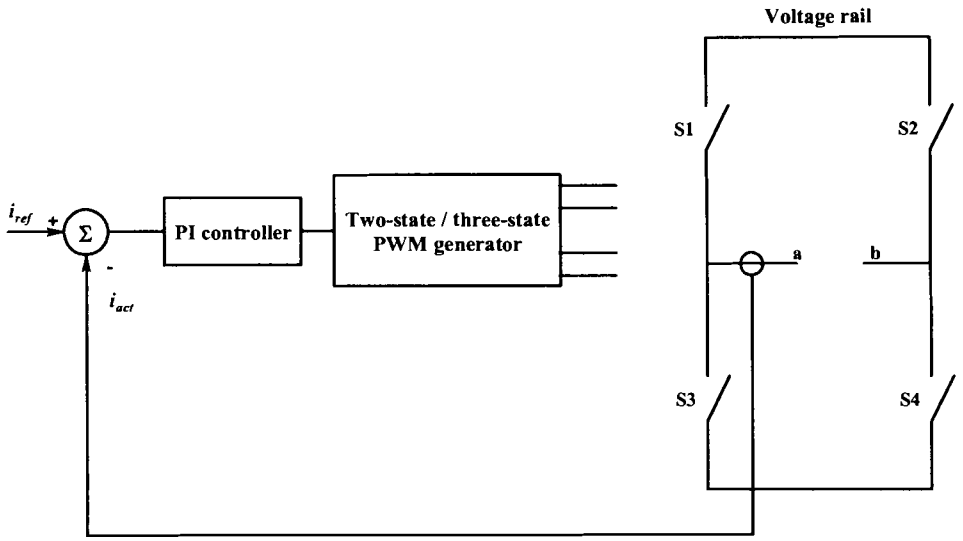

Figure 1-3: A proposed switch-mode PA

1.3 Issues to be addressed

1.3.1 PA specifications

The first step in the design and development of the PA is to generate a detailed specification addressing all the relevant information that will guarantee good results and performance. The specifications must also be aligned with the current development in the MBMC laboratory of the North-West University. The PA parameters which include high efficiency, a wide power bandwidth, small signal bandwidth and the current level will be specified and used as a point of departure for the system design.

1.3.2 PA design and simulation

For the complete realisation of a two-state and three-state PA using the same prototype board, a detailed AMB PA design will include component specifications and the design of every sub-system of the PA to accommodate both the switching techniques on the power electronic (PE) board. The design and the comparison of the two switching techniques are done by means of a simulation model. The simulation model should include most of the sub-components of the prototype PA.

1.3.3 PA design implementation

Before the final prototype board is developed, a method of practically realising the two switching techniques should be devised. PE circuits are controlled by either an analogue or digital controller. A digital controller will be used for accomplishing the switching techniques. The use of dSpace and TMS320 digital signal processing (DSP) board will be considered in realising the switching techniques.

1.3.4 PA design evaluation

Once the design of the PA is completed, factors that can affect the overall performance of the PE circuit will be considered. These factors include the printed circuit board (PCB) layout for the prototype board, the protection circuits and the integration of the PA with the AMB magnetic coil for evaluation purposes.

1.4 Research methodology

1.4.1 PA specifications

The study will be conducted by firstly consulting the available literature on the AMB PAs and by studying the previously developed PA for the flexible rotor double radial AMB model. The two PWM switching techniques are studied and the PA specifications will be compiled from information gathered from the literature and the specifications of the existing PA of the flexible rotor double radial AMB model in the MBMC laboratory.

1.4.2 PA design and simulation

At this stage, a complete PA model with a two-state and three-state switching technique will be designed based on the system's specifications. Before the development of the PA prototype; analytical calculations will be done to specify the PA devices. The simulation models of the two techniques will be conducted in order to verify the design. Simulation packages used include MATLAB®/Simulink power system block set. The PE board will include the power circuit, the H-bridge driver, the feedback circuit and the protection circuits.

1.4.3 PA design implementation

A method for efficiently generating the required control signals with the identified DSP boards will be selected. The two techniques will be realised on the DSP boards by means of MATLAB®/Simulink toolbox and VisSim® development software.

1.4.4 PA design verification

At this stage, a prototype board will be developed. The two-state and the three-state switching techniques will be tested on the AMB load. The experimental/practical results of the two switching strategies will be compared in terms of the control, the power losses, the power bandwidth and the small signal bandwidth. The practical model and the simulation model will be compared in order to draw a sound conclusion on the switching techniques. The reliability of the PA will be tested with the implemented protection circuits.

1.5 Overview of the dissertation

The topic of the study is the design, development, testing and comparison of an average current controlled PA operating in a two-state and a three-state switching mode. The dissertation constitutes 6 chapters. Chapter 2 contains the literature study on the existing AMB amplifiers, the different modes of control and the switching techniques. The chapter starts by briefly highlighting the reasons behind the use of switch-mode PAs in AMB systems. The reasons are established by examining the linear and switch-mode amplifier and thereafter, the background on switch-mode PA is given.

In chapter 3, a detailed step by step design of the switch-mode PA is carried out. The PE prototype circuit board and sub-circuits are designed. The two PWM controller strategies under investigation are further investigated and a concept is realised for controlling the PEs.

Chapter 4 contains a more in-depth analysis of the two-state and the three-state PWM technique through the use of simulation models. The simulations are conducted in order to predict the performance and response of the practical system. The main focus of this chapter is on the analysis and comparison of the two-state and the three-state techniques.

The practical implementation of the PA design and the results from the testing of the prototype board are outlined in chapter 5. The chapter explores the reliability of the PE board and the operation of the two developed PWM control techniques by driving an AMB load with the developed PA. Emphasis is placed on the dynamic response, the power bandwidth, the small signal bandwidth and the power losses of the two PWM techniques.

In chapter 6, conclusions are drawn from the simulation and practical results. Some recommendations on improving the performance of the practical system are discussed.

Chapter 1 gave some background on the MBMC research activities, AMB operation in general and PAs. The objective of the study, issues that will be addressed and the methodology that will be followed in reaching the goals of the study formed part of this chapter. An overview of the document is also included. Chapter 2 will discuss the literature on the AMB PAs.

2
Chapter
Introduction to AMB power amplifiers

Chapter 2 contains the literature regarding the power electronics (PE) of an active magnetic bearing (AMB) system. This chapter discusses the working principles of AMBs in short and the fundamental role of power amplifiers (PAs) in an AMB system. Different types of amplifiers, amplifier switching methods, control strategies and current sensing techniques for feedback implementation make-up the core subjects of this chapter.

2.1 Active Magnetic Bearings

AMB systems provide means of stably suspending a rotating rotor without mechanical contact. The basic functional block diagram of an AMB system is illustrated in Figure 2-1. The AMB system comprises sensors, a controller, PAs, magnetic actuators and the rotor. The sensor measures the position of the rotor in the form of a voltage signal which serves as input to the controller. The controller determines the appropriate current or voltage reference to position the rotor at the desired position. The current or voltage reference signal serves as control command for the PA. The PA converts this reference into a power signal which is used to drive the magnetic actuator coil. The magnetic actuator in turn produces the force required to suspend the rotor in air and at the desired position. The scope of this work is limited to AMB PEs.

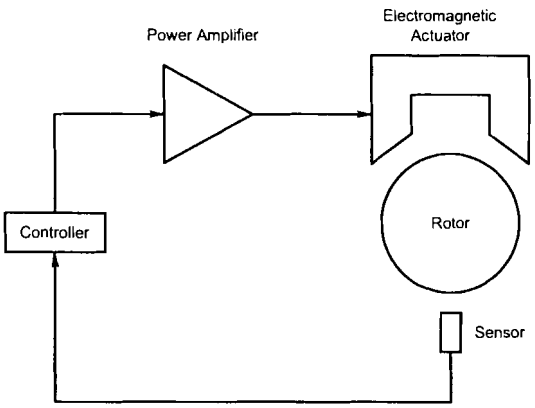

Figure 2-1: A functional block diagram of an AMB system

2.2 Power amplifier introduction

PEs in AMB systems refer to PAs which are important sub-components of AMB systems. They are responsible for generating control currents required to stably suspend the rotor in air. The PA receives a current or a voltage command from the controller. The controller command is proportional to the position error signal of the rotor which is normally in the form of a small signal voltage [3] representing the desired coil current or voltage. The PA adjusts its output to closely match the control reference with an actual coil voltage or current.

AMB system loads are reactive loads that require high apparent power (*VA* rating) to achieve high frequency actuation dynamics. The basic function of the PA is to regulate the energy flow in the magnetic circuit according to the controller's output i.e. to track the current or voltage command within the PA's bandwidth limit [4]. The resulting current flows through the actuator producing the required forces.

The operation of AMB PAs is analogous to the tank model shown in Figure 2-2. The reservoirs serve as the sources of energy. In actual systems, it is the power supply. Pumps 1 and 2 are the mechanism used to provide energy to the load and are analogous to the switching devices in Figure 2-3.

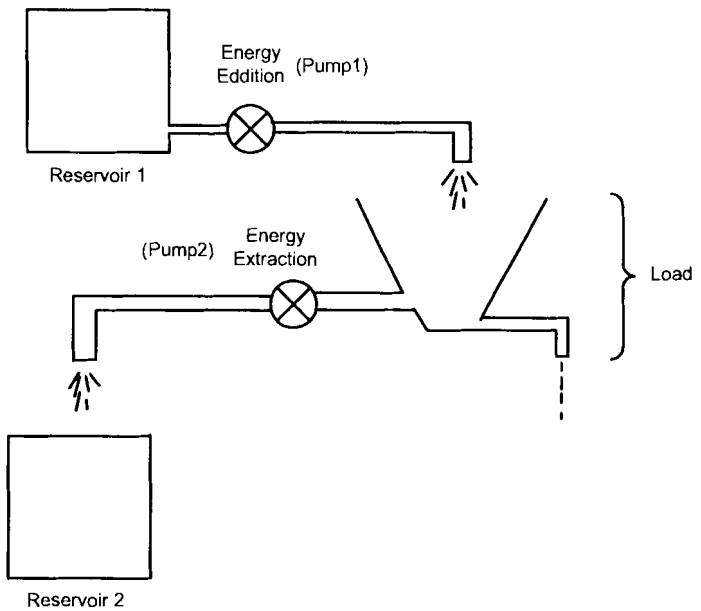

Figure 2-2: Tank model [5]

The amplifier operates by adding energy to the load when required, removing energy when there is a surplus and maintaining energy at the required level. The mechanism of controlling the energy is coordinated in such a way that the energy in the load matches the desired energy [3].

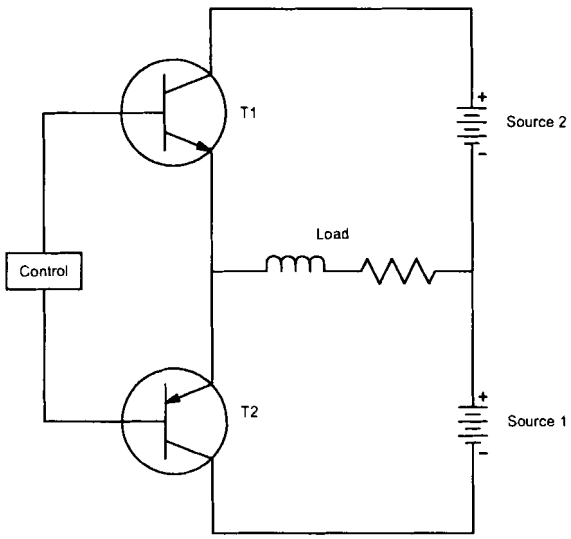

Figure 2-3: Ideal amplifier [5]

Different types of PAs may be employed to regulate the energy in an AMB load and each has its own advantages and disadvantages. They are linear PAs which track the desired signal at the expense of efficiency but with excellent noise immunity, switch-mode PAs which offer better efficiency than linear PAs but generate high levels of noise, and the switch-mode linear assistance PAs (hybrid amplifier) which combine the advantages of both the linear and switching PA [1, 6].

AMB systems have two control strategies that may be employed during the design process; the current control and voltage control [2]. The PAs are specified according to the employed AMB control strategy. The control strategies are based on the AMB coil current or voltage. In the current controlled AMB systems, the current into the magnetic circuit is regulated and in the voltage controlled AMB systems the voltage across the magnetic circuit is regulated. For a current controlled AMB system, the linearised relation between the generated magnetic forces and current is given by (2-1).

$$F = k_i i + k_s x \tag{2-1}$$

with F the magnetic force, k_i the force-current factor, k_s the force-displacement factor, I the coil current and x the position of the rotor.

In a voltage controlled AMB, the relation between the magnetic forces and the voltage is given by (2-2).

$$F = \frac{4B_0}{u_0 N} \int v_r dt \tag{2-2}$$

B_0 is the flux density in the air gap, N the number of turns per pole and v_l the coil voltage. The strategy employed in AMB systems therefore influences the design of the PA.

2.3 Losses due to power amplifiers

AMBs operate by introducing a constant bias current in each electromagnet. The system is subjected to constant electrical losses which may cause rotor heating and reduce efficiency of the system. The losses are divided into the copper losses and the iron losses of the electromagnets [6]. The iron losses are classified as eddy current losses which are proportional to the square of the alternating currents flowing through the coils and rotating hysteresis losses which are proportional to the alternating current passing through the coils of the magnetic circuit [6, 7]. These losses can be reduced by the design of the PAs which determines the alternating current component of the load.

2.4 Linear power amplifier

Linear PAs operate switching devices in their linear regions. The output devices (transistors) are modelled as voltage controlled variable resistors. Figure 2-4 displays a linear PA used to deliver power to the load. The voltage controlled variable resistor is represented by the pass element which continuously varies the magnetic circuit voltage. The linear PA features a very high signal quality due to their continuous signal control. This is associated with a low efficiency as the power is dissipated in both the load and the pass element [3].

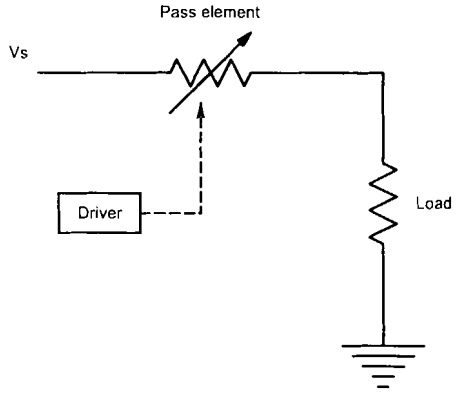

Figure 2-4: Linear PA

A maximum current reference causes the resistance of the pass element to reduce to a minimum value allowing maximum current to flow through the load, resulting in minimal losses. A minimum current reference causes the resistance of the pass element to approach infinity and the losses are still minimal. The problem with linear PAs arises when the resistance of the pass element is almost equal to the load resistance. At this point the power loss in the transistor will equal the power dissipated in the load.

Due to the high *VA* rating required by AMBs, linear PAs are not sufficient in driving magnetic coils with high inductance and low resistance [8]. When used to drive such magnetic coils requiring high dynamic performances, the efficiency of the amplifier is reduced to approximately less than 5 % due the high voltage rating of the systems [1]. The linear PAs are useful in systems requiring a low voltage [2]. Linear PA will not be investigated due to its low efficiency.

2.5 Switching power amplifier

Switching PAs are mostly employed in AMB systems due to their high efficiency. These amplifiers have an efficiency of higher than 80 %. The use of switching PAs in AMB systems has its own advantages and disadvantages. The major drawback of switching PAs includes electromagnetic interference with the position sensors and heating of the rotor due to induced eddy currents [2, 4, 9]. The induced eddy currents are due to the ripple component of the coil current. For AMB systems, the required PA characteristics include a wide power bandwidth and reduced switching losses [6].

Figure 2-5 displays a basic switch-mode PA schematic. A PWM control block generates a variable duty cycle to control the amount of energy delivered to the load. When maximum or high currents are desired, the PWM controller generates maximum duty cycles required to turn the switch on for longer periods of time. The resulting losses are mainly due to the on-resistance of the switch. When minimum current is desired, the PWM controller generates minimum duty cycles to turn the switch on for shorter period of time. When constant current is desired, the controller provides 50 % duty cycle to the switch.

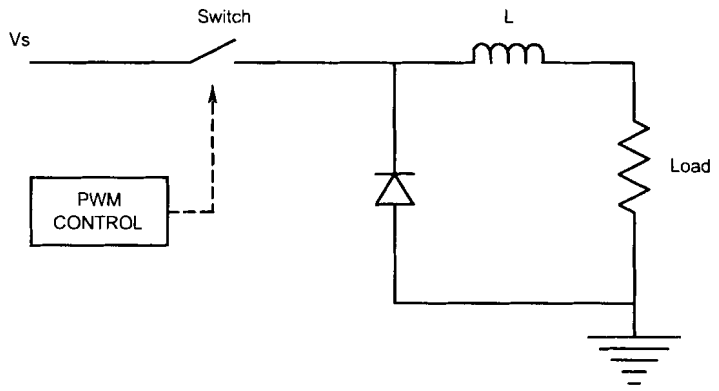

Figure 2-5: Switch-mode PA

Due to low losses, switch-mode PAs are very efficient means of controlling power flow in an AMB system. Depending on the intended application, the characteristics of switch-mode amplifiers depend on factors such as:

- power circuit topology,
- switching methods, and

- modes of control

The characteristic factors of the switching PAs are discussed in the following sub-sections.

2.5.1 Switch-mode PA power circuit topology

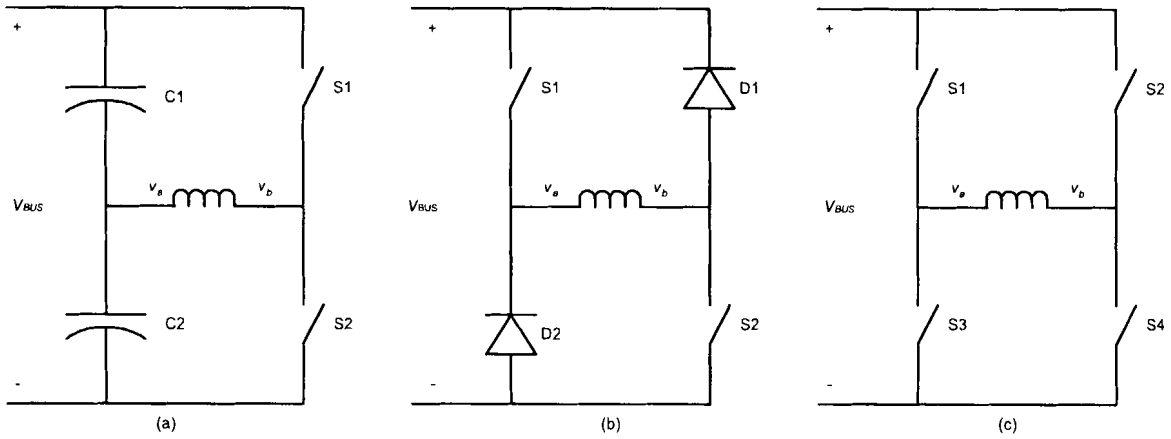

Figure 2-6: Power circuit structure (a) half-bridge (b) full-bridge with unidirectional current flow and (c) full bridge with bidirectional current flow

The most popular power circuit topologies available for use in AMB PAs are displayed in Figure 2-6. Figure 2-6(a) displays the half-bridge power circuit topology, which can only be switched between two states, energy addition and energy extraction resulting in significant current ripple. Figure 2-6(b) displays an H-bridge power circuit topology with two switches and two diodes; the power circuit allows only unidirectional flow of current. The third power circuit topology is a full H-bridge circuit shown in Figure 2-6(c). It has four switches and allows bi-directional flow of current through the load. The voltage at each coil terminal is controlled by a pair of switches; switch S1 and S3 controlling v_a and switches S2 and S4 controlling v_b [10].

An H-bridge power circuit of Figure 2.6(c) has three states of operation; forward conduction, reverse conduction and freewheeling conduction. In the forward conduction state, switches S1 and S4 are switched on while S2 and S3 are switched off and a positive voltage is applied across the load. In the reverse conduction state, switches S2 and S3 are switched on while S1 and S4 are switched off and a negative voltage is applied across the load. In the freewheeling state, switches S1 and S2 (or S3 and S4) are active and the current freewheels, a zero voltage is applied across the load.

With reference to the requested signal, the control electronics which is normally the PWM generator, initiates the switching sequence which the power circuit needs to respond to. One complete sequence is

referred to as a complete H-bridge cycle. Figure 2-7 and Figure 2-8 illustrates the complete switching cycle a PWM generator may initiate. These two possible PWM generators are discussed in section 2.5.2.

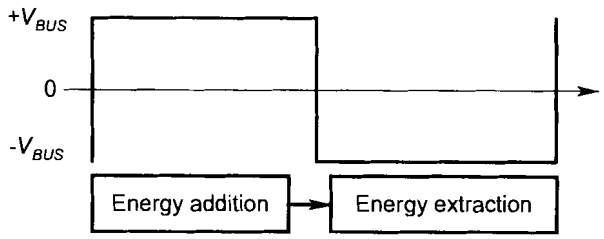

Figure 2-7: Two-state switching cycle

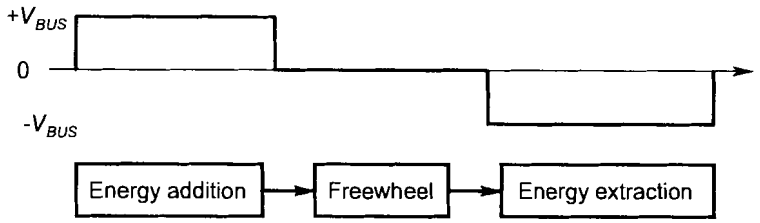

Figure 2-8: Three-state switching cycle

Due to the inductive nature of an AMB load, the load current does not change instantaneously. The power circuit topology incorporates freewheeling diodes across the switches ensuring that there is always a path for the current to flow. A deadband time is also included in the switching sequence to ensure that the two switches on the same leg of the bridge are never turned on at the same time.

2.5.2 Power amplifier switching techniques

There are two switching techniques to control the H-bridge power circuit topology. The techniques are the two-state and the three-state switching technique. The switching techniques are realised by means of a PWM controller. The PWM controller varies the duty cycle of the switch with respect to the desired load current. The duty cycle is produced by comparing a control signal with the carrier signal or the slope of the actual coil current.

Two-state switching technique

A two-state switching technique is a traditional PWM switching method. It is achieved by using a single PWM controller in order to produce the desired duty cycle for switching a pair of switching devices. Figure 2-9 displays an H-bridge power circuit controlled with the two-state switching technique. With this technique, diagonal switches are switched simultaneously. During the switching cycle, the PA will generate an output voltage switching between positive supply and negative supply voltage.

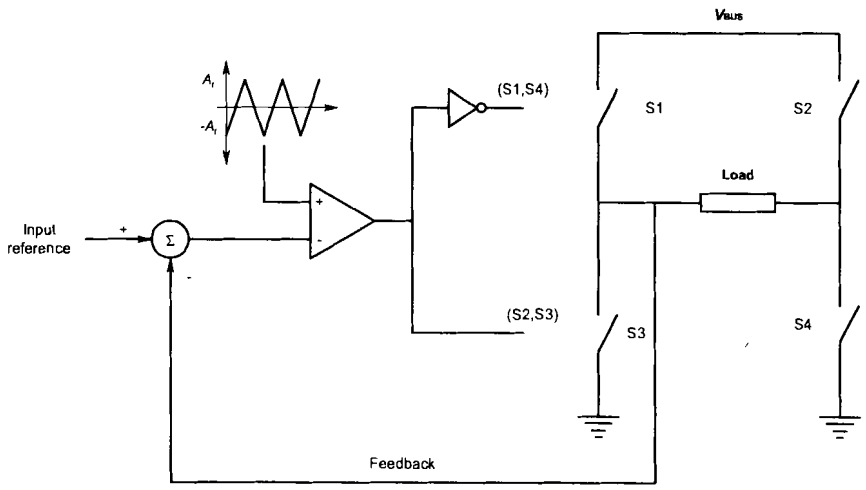

Figure 2-9: Two-state H-bridge switching configuration

Table 2-1 shows the switching states in a two-state controlled H-bridge. In state 1, switches S1 and S4 are switched on while switches S2 and S3 are switched off. A positive voltage is applied to the load and as a result the load current is increasing. When the load current is decreasing, state 2 is entered. Switches S2 and S3 are turned on while S1 and S4 are turned off. Figure 2-10 displays two-state PWM output load waveforms.

Table 2-1 Two-state PA switching states

	S1 and S4	S2 and S3	V_{Load}
State 1	1	0	$+V_{BUS}$
State 2	0	1	$-V_{BUS}$

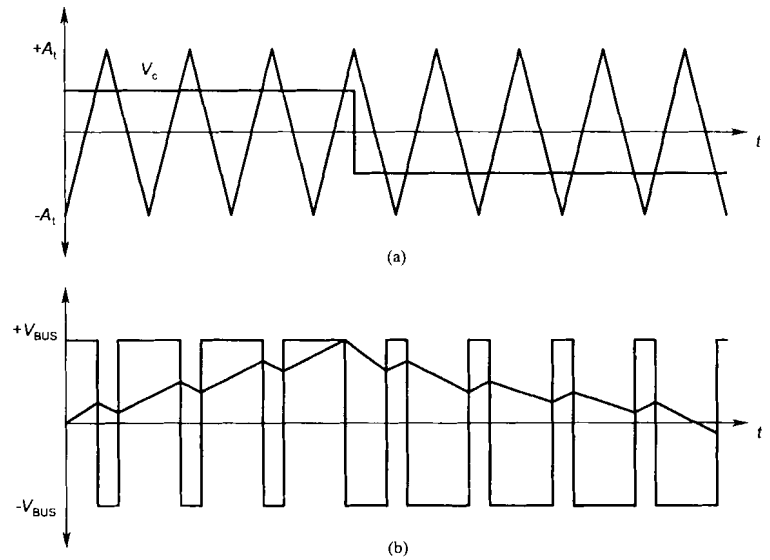

Figure 2-10: Two-state switching waveforms (a) control waveforms and (b) coil waveforms

As a result of the square voltage waveform that is applied to the load, the current has both a positive and a negative slope and the ripple value is defined by (2-3).

$$\Delta i = \frac{V_{BUS}}{L} T_{on} \tag{2-3}$$

T_{on} is the period of time a pair of switches remains on, V_{BUS} is the supply voltage and L is the inductance of the coil. When the PA supplies an average current of 0 A, the PWM duty cycle is 50 % and the current ripple is defined by (2-4).

$$\Delta i = \frac{V_{BUS}}{2L} T_s \tag{2-4}$$

T_s is the switching period. Equation (2-4) shows that the magnitude of the current ripple depends on the supply voltage and the switching frequency. The ripple value is inversely proportional to the switching frequency and directly proportional to the supply voltage (V_{BUS}).

A two-state switching technique has a number of disadvantages when used to drive an AMB load. The PA will have higher switching losses and high current ripple which occur due to the two levels of output voltage. To limit the high current ripple to acceptable levels, the switching frequency must be increased. Due to the desired high power efficiency, the switching frequency cannot be increased indefinitely because the switching losses of semiconductor devices increase proportional to the switching frequency.

Another important drawback of two-state PAs which relates to the switching frequency is highlighted in [6]. The reduction of the switching frequency in order to reduce the switching losses results in severe current ripple which will induce high eddy current losses and also limit the operating range of the PA. The operating range of the PA is the frequency range in which the actual current can follow the reference signal.

Three-state switching technique

The three-state technique is another method of controlling switching PA circuit. It is realised by controlling a power circuit with two single PWM signals [3]. Figure 2-11 displays an H-bridge circuit with three-state PWM implementation. Two PWM generators are used; one to control the left leg and another to control the right leg of the H-bridge. The diagonal switches are controlled independently which is different from a two-state controlled power circuit.

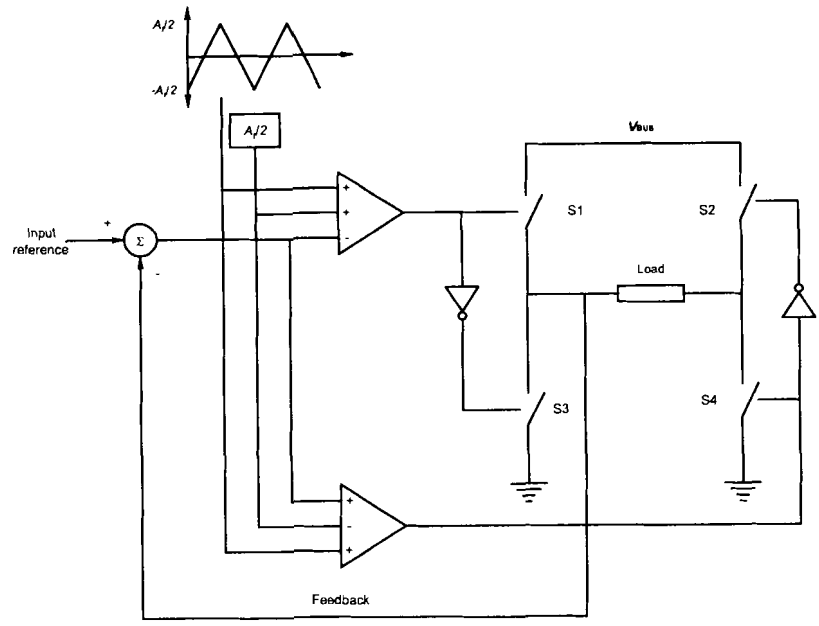

Figure 2-11: Three-state H-bridge switching configuration [3]

The operation of a three-state PWM is explained in Figure 2-12 and Figure 2-13. There are three switching states possible with three-state PMW technique. The states are related to the addition, extraction and maintenance of energy in the AMB load. Figure 2-13(a) displays the first state in three-state controlled power circuit where switches S1 and S4 are activated. This switching state is responsible for addition of energy to the AMB load i.e. the increase in coil current.

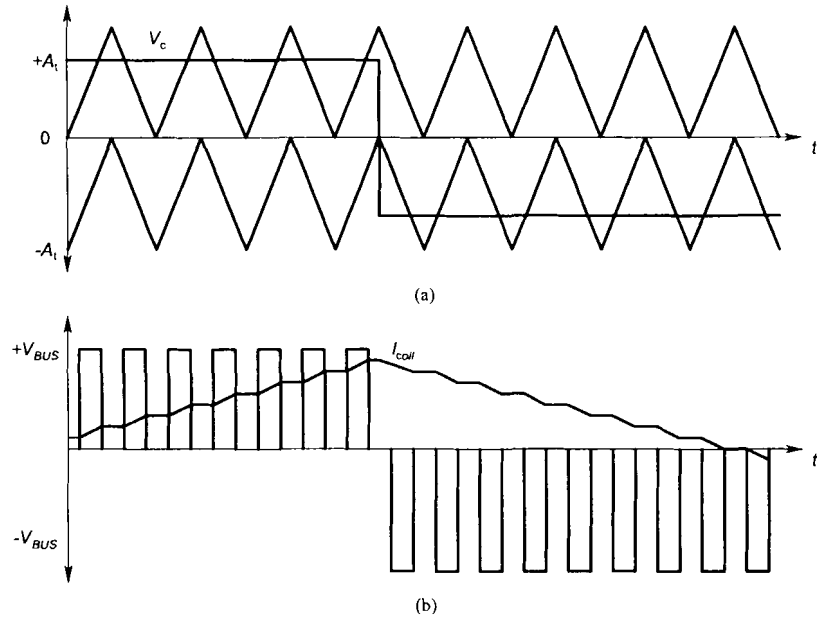

Figure 2-12: Three-state switching waveforms (a) control waveforms and (b) coil waveforms

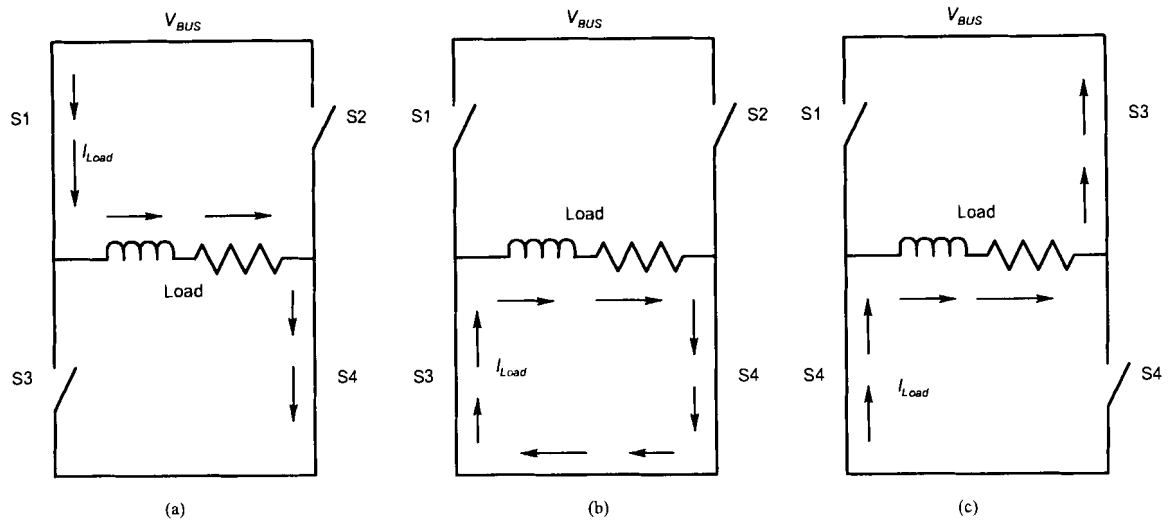

Figure 2-13: Three-state switching sequence (a) energy addition, (b) freewheeling and (b) energy extraction

Figure 2-13(b) represents the second state where the current freewheels through switches S3 and S4. The applied voltage across the load is zero. This switching state maintains the energy in the load and it is termed a freewheeling state. During the freewheeling state, the current through the AMB load decreases due to the resistance of the AMB coil. The PA will respond to this energy loss by initiating the next required state.

Figure 2-13(c) displays the third state in which switches S2 and S3 are active and the energy is extracted from the AMB load. The load current decreases and the energy is fed back to the supply [3, 6]. Table 2-2 shows the three-state switching states with corresponding voltage and current. A positive voltage is applied across the AMB load during state 1, a zero voltage during state 2 and a negative voltage during state 3.

Table 2-2 Three-state PA switching states

	S1	S2	S3	S4	V_{Load}	I_{load}
State 1	1	0	0	1	$+V_{BUS}$	Increasing
State 2	1 (0)	1 (0)	0 (1)	0 (1)	Zero	Constant
State 3	0	1	1	0	$-V_{BUS}$	Decreasing

Due to the addition, maintenance and extraction principle of controlling the AMB load; a full voltage is applied across the load for shorter periods of time. The load current changes slowly which results in a small ripple current [3]. When a constant current is flowing through the load, the current ripple is obtained by (2-5).

$$\Delta i = \left(I + \frac{2U_{on}}{R} \right) \frac{1 - e^{\left(-\frac{T_s}{2\tau}\right)}}{1 + e^{\left(-\frac{T_s}{2\tau}\right)}} \tag{2-5}$$

I is the bias current, U_{on} is the on-state voltage of a conducting switch, T_s is the switching period and τ is the time constant of AMB load. The time constant is defined by (2-6).

$$\tau = \frac{L}{R} \tag{2-6}$$

Equation (2-5) implies that the ripple current depends on the coil's properties and the switching frequency. One of the advantages of using the three-state switching technique is that the load ripple current is independent of the supply voltage. This implies that the AMB stiffness can be increased by increasing the supply voltage without producing additional load losses [1, 4, 6]. Other added advantages of the three-state switching technique are the reduced switching losses due to low switching frequency and the reduced eddy current losses in the AMB load due to minimum current ripple [4].

Three-state controlled PAs have their own disadvantages added to AMB systems especially in the self-sensing AMB system. The self-sensing AMB uses the ripple component [11] of the load current in order to estimate the air-gap length. To successfully implement a reliable self-sensing AMB system, the ripple current will have to be significant.

2.5.3 *Modes of control*

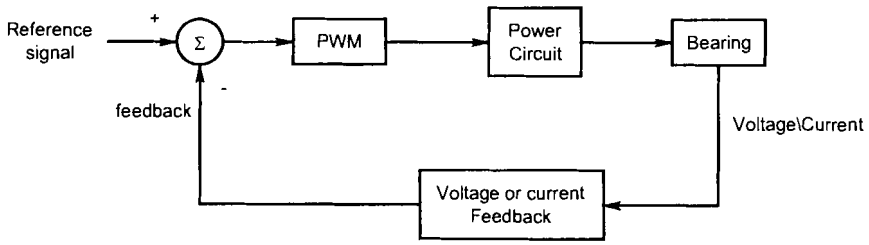

Figure 2-14: Feedback control loop in PAs

The PA control signal is motivated by the control strategy employed in AMB systems. The control strategy in PAs is basically a feedback control which can be established either for the load current, load voltage or air gap flux [5]. The PA uses feedback control in order to achieve design objectives for the load regulation and dynamic responses [12]. Figure 2-14 displays the PA feedback control loop. The control loop monitors the control variable and compares it to the reference signal to produce an error signal. When a voltage signal is monitored, the PA is termed a voltage controlled PA. Similarly, the PA is

termed a current controlled PA when the load current is monitored. The error signal is fed to the PI-controller to derive the control signal which is either compared to a carrier signal or the slope of the load current to produce the appropriate PWM signals.

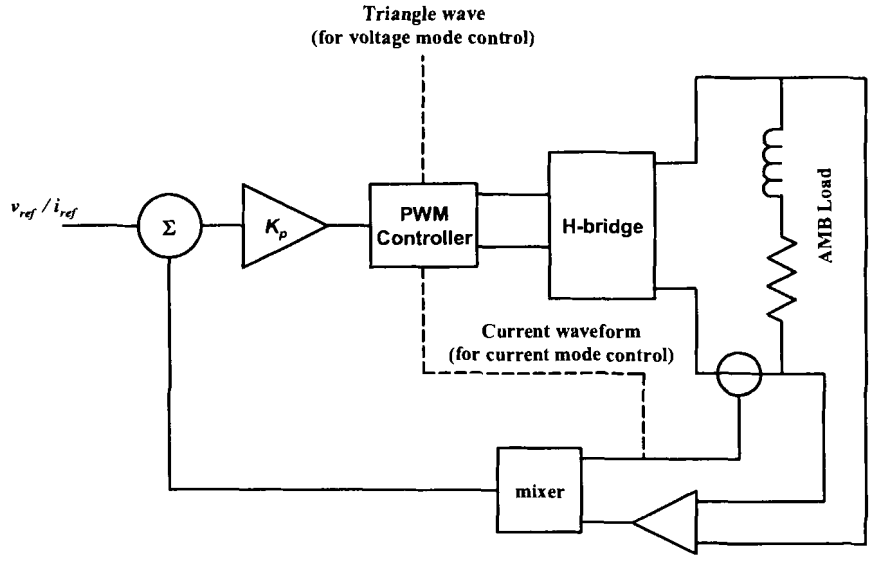

Figure 2-15: PA schematic with either VMC or CMC [3]

The generation of PWM signal with a carrier signal is defined as voltage mode control (VMC) while the generation of the PWM signal with a signal representing the slope of the actual load current is defined as the current mode control (CMC). Figure 2-15 illustrates the PA circuit with either VMC or CMC

Voltage mode control

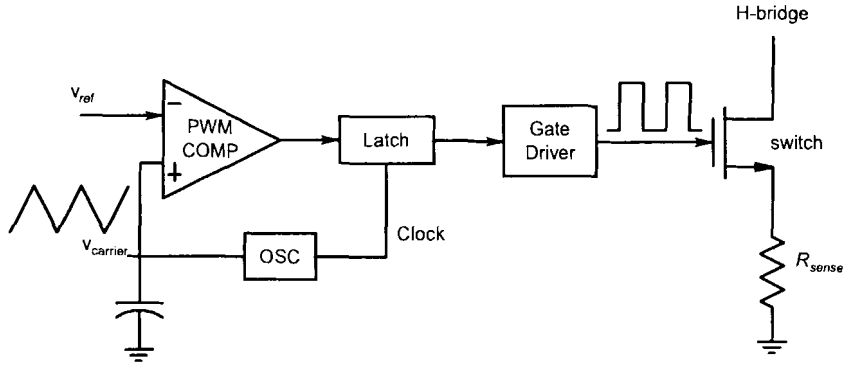

Figure 2-16: A voltage mode controlled PA

Figure 2-16 displays a basic voltage mode controlled PA. The PA is employed with one feedback loop as compared to the CMC PA. The appropriate PWM signals are produced by comparing an error signal with a carrier signal of constant amplitude and frequency. When the control signal exceeds the carrier signal, the oscillator set the latch and the produced PWM signal turns the switch off. The switch turns on when the carrier signal exceeds the error signal.

Current mode control

Figure 2-17 displays a basic circuit diagram of a current mode controlled PA. A fixed switching frequency is produced by an oscillator clock and a carrier signal is replaced with the output signal derived from the load current [13]. The derived signal is a voltage across a sense resistor device. The PWM signals are then generated by comparing an error signal with a voltage across a sense resistor (R_{sense}).

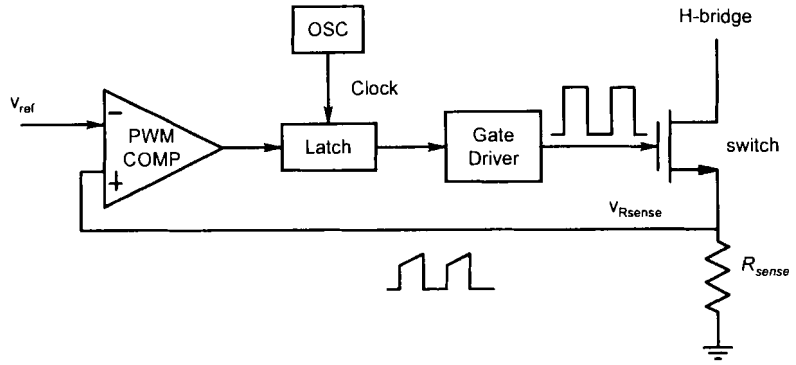

Figure 2-17: A current mode controlled PA

CMC can be employed in two different methods depending on the application. The two methods are peak current mode control (PCMC) and average current mode control (ACMC) [14]. For a PCMC, the PWM signals are derived by comparing the upslope of V_{Rsense} to the error signal derived from the reference signal and the actual signal. The appropriate on commands are sent to the switch when the latch is set. The switch will turn off when V_{Rsense} equals the error signal. In an ACMC, the converter actual load current is sensed. A compensation circuit is added as part of an inner feedback loop. The actual load current is compared to the error signal and amplified. The output of the compensation circuit is compared to an amplified oscillator signal to produce the PWM signal [13, 14].

2.5.4 Power amplifier bandwidth

The bandwidth of a PA is specified in terms of both a small-signal bandwidth and a power bandwidth. The small signal bandwidth describes the small signal behaviour of the magnetic actuator while the power bandwidth describes the large signal behaviour and specifically the frequency where a current of half the specified maximum current of the PA can still be supplied without being deformed. Deformation will occur above the power bandwidth due to the finite voltage at the bus.

Small signal bandwidth

The small signal bandwidth is defined as the frequency where the actual current is attenuated by -3dB for arbitrarily small reference currents. In AMB systems, the small signal bandwidth is limited by the load,

the PA, the voltage rail (V_{BUS}) and it is controlled by the proportional gain (K_p) of the PI-controller [3, 4]. The integral gain (K_i) is responsible for compensating the influence of the back-emf of the system [15].

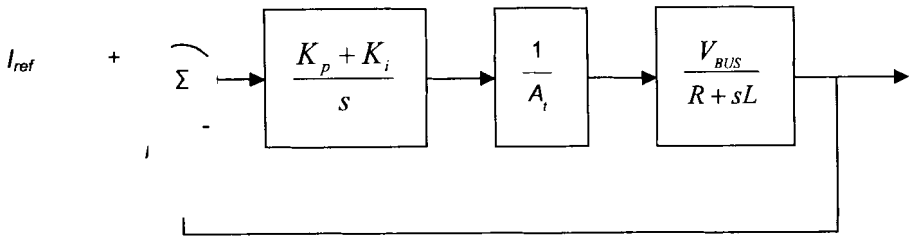

Figure 2-18: PA small signal bandwidth prediction

Figure 2-18 displays the closed loop block diagram used to determine the small signal bandwidth of the AMB PAs. The closed loop transfer function of the PA is determined as (2-7),

$$\frac{I_{act}}{I_{ref}} = \frac{\frac{K_p}{A_t}\frac{V_{BUS}}{R+sL}}{1+\frac{K_p}{A_t}\frac{V_{BUS}}{R+sL}} = \frac{K_p V_{BUS}}{A_t(R+sL)+K_p V_{BUS}} \tag{2-7}$$

I_{act} is the actual load current, I_{ref} the reference signal, R the resistance of the load and L the inductance of the load. The small signal bandwidth of the amplifier occurs when (2-8) is satisfied [3].

$$\omega_{bw} L A_t = R A_t + K_p V_{BUS} \tag{2-8}$$

From (2-8), the small signal bandwidth is determined as (2-9).

$$\omega_{bw} = \frac{R A_t + K_p V_{BUS}}{L A_t} \tag{2-9}$$

From (2-9) the K_p value of the controller is used to specify the small signal bandwidth of the PA. In order to achieve a wide small signal bandwidth for a specific AMB load with a fixed voltage rail or VA rating, the K_p value of the controller is increased. Care should be taken to avoid exceeding the linear limits of the controller's proportional gain as this will cause instability in control loop.

The maximum value of K_p is restricted by the slope of the carrier signal (2-10) and the maximum slew rate (current response) (2-11) of the PA. The dynamic performance of AMB systems depend on the maximum current slope limited by the maximum voltage of the amplifier and the inductance of the AMB load [1, 3, 6].

$$K_p \frac{d}{dt}\left(i_{ref} - i_{act}\right) < \frac{d}{dt} A_t f(2\pi f_{sw} t) \tag{2-10}$$

$$K_p \frac{d}{dt}\left(i_{ref} - i_{act}\right) \leq \frac{V_{BUS}}{L} \tag{2-11}$$

Equations (2-10) and (2-11) imply that the slope of the control signal should be less than the slope of the carrier signal. The slope of control signal should also be less or equal to the maximum slew rate to guarantee stable switching of the PA circuit and linear dynamic behaviour. With the help of (2-10) and (2-11), (2-12) is derived.

$$\begin{aligned} \frac{d}{dt} A_t f(2\pi f_{sw} t) &> \frac{V_{BUS}}{L} \\ 4 A_t f_{sw} &> \frac{V_{BUS}}{L} \\ A_t &> \frac{V_{BUS}}{4 L f_{sw}} \end{aligned} \tag{2-12}$$

Using (2-12) and (2-9), the maximum limit of the small signal bandwidth of the amplifier is determined as (2-13).

$$\begin{aligned} f_{bw_{\max}} &= \frac{4 f_{sw}}{2\pi} \\ &= 0.64 f_{sw} \end{aligned} \tag{2-13}$$

By Shannon's sampling theorem, a maximum usable small signal bandwidth of $0.2 f_s$ can be expected [3].

Power bandwidth

The power bandwidth of the PA is the frequency at which the PA can produce half the maximum current without distortion. At the power bandwidth, the actual current can still follow the reference signal without attenuation or distortion. The power bandwidth is limited by the slew rate of the PA and has nothing to do

with the switching frequency and the controller. The maximum slew rate of the switching PA is defined by (2-14).

$$\frac{di}{dt} \leq \frac{V_{BUS}}{L} \tag{2-14}$$

Assuming the sinusoidal input reference signal is limited to half the maximum signal as given by (2-15), the maximum rate of change of the input signal is expressed as (2-16).

$$i_{0.5ref} = 0.5I_{\max} \sin(\omega t) \tag{2-15}$$

$$\left.\frac{di_{0.5ref}}{dt}\right|_{\max} = 0.5I_{\max}\omega \tag{2-16}$$

The switching PA will respond to the desired half reference signal when the maximum rate of change of the input signal is below the maximum slew rate of the PA.

$$0.5I_{\max} 2\pi f \leq \frac{V_{BUS}}{L} \tag{2-17}$$

From (2-11), the power bandwidth of the PA is limited to a maximum frequency of (2-18).

$$f_{pbw} = \frac{V_{BUS}}{\pi I_{\max} L} \tag{2-18}$$

For AMB loads, the power bandwidth is usually less than the signal bandwidth [2, 16]. The power bandwidth depends on the supply voltage, the maximum input current level and the inductance of the AMB load.

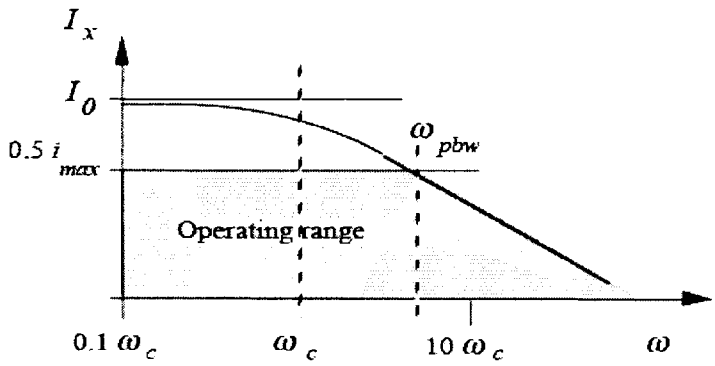

Figure 2-19: Operating range of the magnetic actuator [16]

Figure 2-19 displays the dynamic performance of the PA. From the figure, the frequency band in which the switching PA can achieve the desired performance when half the maximum current level is desired is defined as the operating range of the AMB system. At frequencies above the power bandwidth, the output voltage signal will enter saturation and the dynamic performance of the PA becomes nonlinear.

2.5.5 Current sensing

Measuring and controlling the current in a PE circuits is a major contributor to the success or failure of PE circuit design [17]. The current is monitored and measured for fault protection and control purposes. The employment of a current controlled PA with current mode control requires that the current flowing through the load be constantly monitored. Current measurements in PE circuits are performed by inserting a sensing device which may negatively influence the performance of the circuit if not chosen properly and not placed at the right location. The most common devices are non-inductive sense resistors and Hall Effect current sensors. These devices produce a voltage signal proportional to the current flowing through the device.

Resistive sensing

The use of a sense resistor for monitoring the load current is the simplest and most cost effective method. A sense resistor has the disadvantage of adding extra losses (I^2R) to the circuit. The resistive sensing will give accurate measurements when low currents are sensed [18]. The characteristics related to the appropriate choice of current sensing resistor and reliability of the sensing circuitry are:

- Low resistance value to minimise power losses
- Low inductance because of high di/dt
- Tight tolerance on initial value and low temperature coefficient for accuracy
- High peak power rating to handle short duration high current pulses
- High temperature rating for reliability [17]

Figure 2-20 displays an H-bridge circuit with a sense resistor. The placement of the resistor is at the location where the load current can be monitored at all times. The resistor continuously measures the current flowing through the active switching devices.

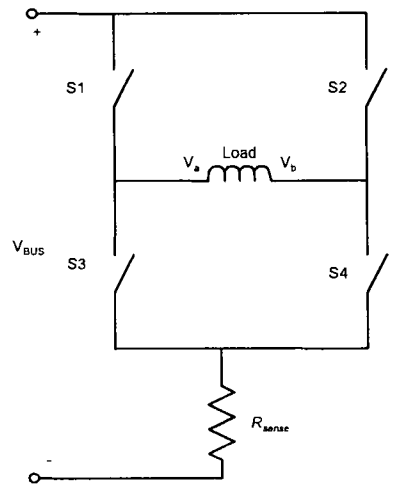

Figure 2-20: Resistive current sensing

Hall sensors are the most effective means of measuring currents for feedback control purposes. Average and peak-to-peak CMC are effectively implemented with hall sensors and the location of the sensor should be carefully selected. The advantage of using hall sensors is the electrical isolation it provides between the control and the power circuits [3].

Different locations of placing a sensing device for specific applications are explained in [17]. In order to sense an average current flowing through the load, a current sensor is placed in line with the load. The location of the device is illustrated in Figure 2-21. For measuring a peak current, the location of the sensor is in line with one of the switches forming an H-bridge circuit. The hall sensor is selected based on the bandwidth requirement. The bandwidth of the sensor provides accurate tracking of the change in the load current.

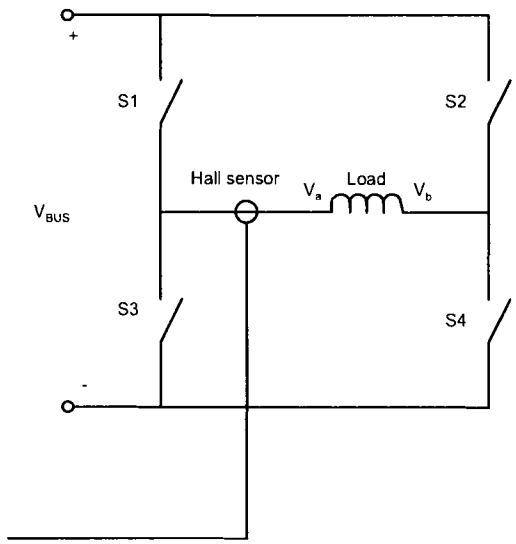

Figure 2-21: Average current sensing with Hall sensor device

Chapter 2 discussed the theory in AMB PAs. Two-state and three-state switching techniques were explored and the components of the switching PAs were studied. The next chapter will be involved in the design of the PEs and the two switching techniques.

3
Chapter

Power amplifier design

Chapter 3 contains a detailed design of the switching power amplifier (PA) circuit. The chapter aims at explaining and conducting the design of each building block of an AMB switching PA. Aspects concerning the reliability of the sub-components of PAs will be thoroughly looked at. The chapter starts by providing the PA specifications and then proceeds to a detailed design.

3.1 Power amplifier specification

Table 3-1 Power amplifier design specifications

Name	Description
Voltage	V_{min} = 150 V and V_{max} = 310 V
Efficiency	>80 %
Switching frequency	30 kHz
Output	Current, maximum of 10 A
Power bandwidth	1.5 kHz
Small signal bandwidth	2 kHz
Protection	Thermal and short circuit

Table 3-1 shows the design specifications for a two-state and three-state PA. A variable bus voltage is specified with a minimum dc voltage of 150 V and a maximum dc voltage of 310 V. The 220 V alternating-current (ac) mains voltage is adjusted to voltages that will produce dc voltages in a range between 150 V and 310 V when rectified. The coil current must be adjustable from -10 A to a maximum current of 10 A. At low reference signal frequencies, the coil current must track the reference signal with minimum error. The switching frequency of the amplifier is specified to a maximum of 30 kHz and the PA must have a power bandwidth of 1.5 kHz and a small signal bandwidth of 2 kHz. Since immunity against failure is one of the important factors not to be ignored, the amplifier must incorporate thermal and short circuit protection.

The specifications imply that the PA should be a switch-mode PA with a full H-bridge configuration. The PA must be able to drive the load with two-state and three-state PWM techniques.

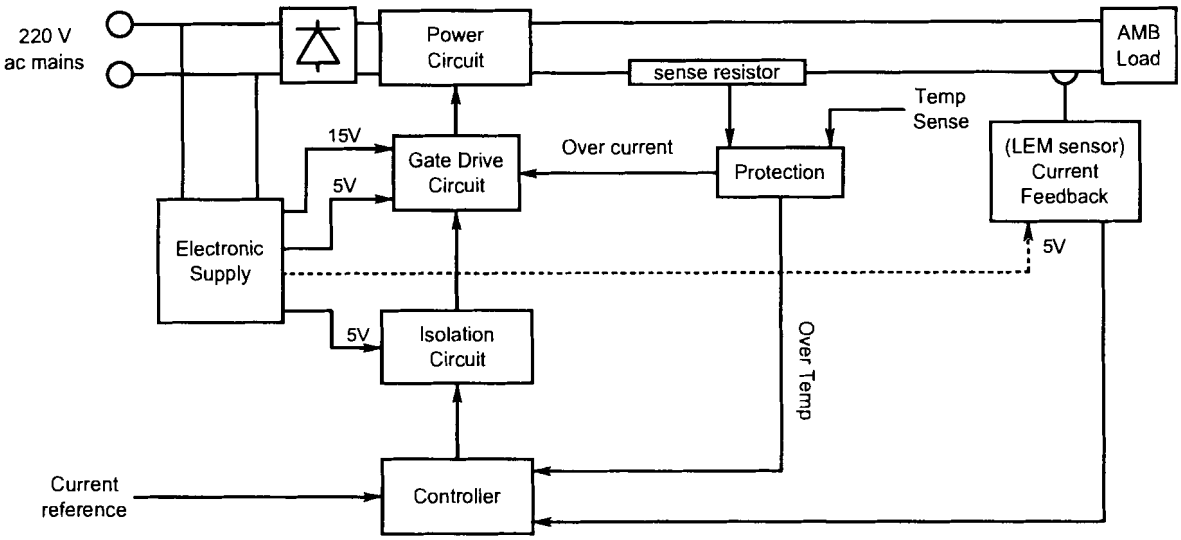

Figure 3-1: PA functional block diagram

Figure 3-1 displays the proposed functional block diagram of an AMB PA. The amplifier comprises a power circuit, gate drive circuitry, isolation circuitry, protection circuitry, feedback circuitry and a controller. A reference signal is compared to the current flowing through the load to determine the error signal. The error signal is converted to a voltage signal or control signal by a controller. The control signal is used to generate digital PWM signals i.e. two-state or three-state PWMs. The PWM signals serve as inputs to the isolation circuitry which provides a boundary between the digital and analogue circuits of the PA. The isolated PWM signals are used to control the power circuit which comprises an H-bridge circuit. The current is monitored for over-current protection and for providing feedback to the controller. The temperature of the operating PA is also monitored in order to protect the PA circuit against over-temperature conditions.

3.2 Power circuit design

Figure 3-2 displays a functional block diagram of the power circuit. The power circuit is responsible for supplying the load with voltage and consists of two parts; the rectifier for rectifying an ac voltage and the H-bridge circuit that allows the flow of energy to and from the load. The design of the H-bridge is explained in the following section.

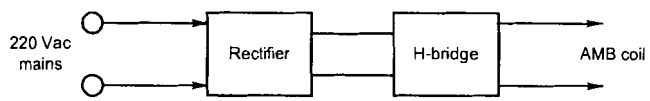

Figure 3-2: Power circuit functional block diagram

3.2.1 H-bridge design

An H-bridge circuit comprises a set of four controllable switches. The set of switches are the important components of the H-bridge as they connect the load to the supply voltage and provide a path for the requested load current. The structure of an H-bridge circuit and the connection of the load is shown in Figure 3-3. The four switches (S1 - S4) must be carefully specified in order to make an H-bridge circuit reliable.

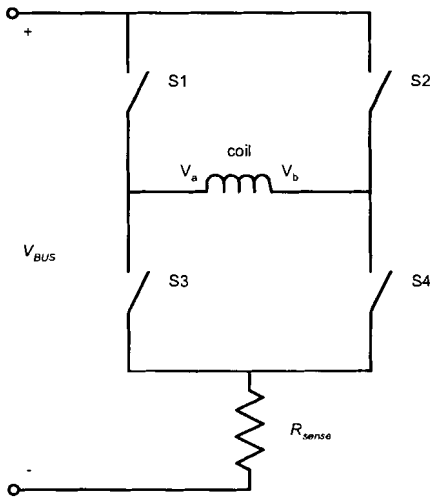

Figure 3-3: An H-bridge circuit diagram

Several factors need to be considered when specifying the controllable switches [19]:

- Power capability (Voltage and current rating)
- Switching speed (Hard/soft switching)
- Drive circuit requirements
- Protection and
- Losses

For this application, it is required that the switching devices be capable of withstanding a dc voltage of at least 310 V, conduct a maximum current of 10 A and be able to operate at a switching frequency of 30 kHz. The choice of the switching device is between Metal-oxide-semiconductor field effect transistor (MOSFET) and Insulated gate bipolar transistor (IGBT). At high switching frequencies, conducting MOSFET experience high losses and its on-state resistance ($R_{DS(on)}$) increases with increase in temperature [20].

An IGBT has a fixed voltage drop in the on-state, a high voltage and a high current rating. The major problem in the operation of the IGBT at high switching frequency is the resulting current tail for the duration of the turn-off process. Current tail implies that the IGBTs turn off time will be longer in which the results will be high turn-off switching losses. In order to operate the IGBT devices at high switching

frequency, the device needs to be controlled with soft switching mode or resonant switching technique [21]. In the soft switching mode, the collector-emitter voltage goes to zero before the device is turned-off. Operating the MOSFETs in temperatures between room temperature and 200 °C increases it on-state resistance which result in high conduction losses and decreased current rating at high temperature. With IGBTs, the operation at high temperatures does not influence the increase in the conduction losses [21, 22, 23].

Between the MOSFETs and IGBTs, IGBTs stands out due to low conducting losses under low switching frequencies. The switching devices chosen for this application are ultrafast 600 V 27 A IGBTs with built-in ultra-soft-recovery freewheeling diodes (IRG4PC50UD).

The freewheeling diodes serve a very important purpose. Due to the inductive nature of the AMB load, an H-bridge constructed with switches without freewheeling diodes will fail as the current through an inductor changes with time. The placement of freewheeling diodes guarantees continuity in the inductive load current. The diodes will provide path for the coil current when all the switches are switched off for a while. This takes place when the two switching devices in the same leg of the bridge are turned-off for a short period of time (deadband) to avoid cross conduction or short circuiting the bridge. Also, when the H-bridge changes states, the freewheeling diode conducts the current.

It is important to sense the current flowing while the IGBTs are conducting. The current is sensed for monitoring purposes and feedback circuitries. The design requires a sense resistor with a low resistance value in order to minimise power losses and low inductance value to avoid voltage spikes due to high *di/dt*. The choice of the sense resistor and the resistance value is discussed in section 3.7.

3.2.2 H-bridge losses

An H-bridge comprises switching devices and a sense resistor. Practical switching devices display non-ideal characteristics and exhibit both conductive and switching power losses while the sense resistor will only experience resistive losses.

Two-state PA H-bridge losses

Conduction and switching losses

Due to the finite time the switching devices take to change state, the product of the voltage across the device and the current through the device is non-zero. Thus, the device will dissipate power during turn-on and turn-off transitions. From the data sheet of the IRG4PC50UD, the total switching energy loss (E_{ts})

at a junction temperature (T_j) of 150 °C is obtained as 2.3 mJ. These testing conditions along with the conditions at which the IGBTs will be operated are shown in Table 3-2.

Table 3-2 Power amplifier design specifications

	Parameter	Test condition	Application condition
T_j	Junction temperature	150 °C	150 °C
I_C	Collector current	27 A	10 A
V_{CC}	Collector voltage	480 V	150 V and 310 V
V_{GE}	Gate-emitter voltage	15 V	15 V
R_G	Gate resistor	5 Ω	8 Ω

The switching energy lost in the device operated at a collector voltage of 150 V is approximated by (3-1).

$$\begin{aligned} E_{ts\_new} &= \frac{I_{c\_new}}{I_{c\_old}} \frac{V_{cc\_new}}{V_{cc\_new}} \frac{R_{g\_new}}{R_{g\_old}} E_{ts\_old} \\ &= \frac{10}{27} \frac{150}{480} \frac{8}{5} 2.3\times10^{-3} \text{ J} \\ &= 440\times10^{-6} \text{ J} \end{aligned} \tag{3-1}$$

Now, the switching power loss is determined using the switching energy loss multiplied by the switching frequency as it is proportional to the switching frequency and the energy lost during the switching period, (3-2).

$$\begin{aligned} P_{sw} &= E_{ts\_new} f_{sw} \\ &= 440\times10^{-6}\times30\times10^{3} \text{ W} \\ &= 13.2 \text{ W} \end{aligned} \tag{3-2}$$

For a collector voltage of 310 V, the switching energy is 880 μJ and the estimated switching losses of the device is 26.4 W. The switching loss of the diode at minimum voltage level is determined as (3-3).

$$\begin{aligned} P_{Dsw} &= \frac{V_{rr} I_{rr} t_{rr} f_{sw}}{2} \\ &= \frac{150\times10\times74\times10^{-9}\times30\times10^{3}}{2} \text{ W} \\ &= 1.67 \text{ W} \end{aligned} \tag{3-3}$$

For maximum voltage of 310 V, the diode switching losses are estimated as 3.34 W. Semiconductor devices also dissipate power while in the on-state. This loss is termed conduction loss and it is caused by the forward voltage drop in the conduction state of the switching devices. For a two-state switching technique, the conduction loss for the IGBT is determined by (3-4).

$$\begin{aligned} P_{on} &= V_{ce(on)} I_c d \\ &= \frac{1.65 \times 10}{2} \text{ W} \\ &= 8.25 \text{ W} \end{aligned} \tag{3-4}$$

The built-in freewheeling diodes also experience losses when conducting. The diode conduction losses are determined from (3-5).

$$\begin{aligned} P_{D\_on} &= V_c I_c d \\ &= \frac{1.25 \times 10}{2} \text{ W} \\ &= 6.25 \text{ W} \end{aligned} \tag{3-5}$$

Sense resistor losses

A non-inductive sense resistor of value 0.05 Ω was selected and connected to switches S3 and S4 as shown in Figure 3-3. The choice of the resistor will be discussed in section 3.7. The maximum sense resistor losses are computed in (3-6).

$$\begin{aligned} P_{Rsense} &= I^2 R_{sense} \\ &= 10^2 \times 0.05 \text{ W} \\ &= 5 \text{ W} \end{aligned} \tag{3-6}$$

The total power loss contribution due to the H-bridge components on the PA circuit at 150 V is determined using (3-2), (3-3), (3-4), (3-5) and (3-6). Equation (3-7) provides maximum losses of 63.76 W. At a typical steady state condition two IGBTs will conduct in the forward direction and two IGBT diodes will conduct in the freewheeling state, both set at 50 % duty cycle.

$$\begin{aligned} P_{H-bridge} &= 2P_{sw} + 2P_{Dsw} + 2P_{on} + 2P_{D\_on} + P_{Rsense} \\ &= 2 \times 13.2 + 2 \times 1.67 + 2 \times 8.25 + 2 \times 6.25 + 5 \text{ W} \\ &= 63.76 \text{ W} \end{aligned} \tag{3-7}$$

At a bus voltage of 310 V, the IGBT and the diode switching losses are twice the losses experienced when a 150 V is applied across the bridge. Thus, the total two-state H-bridge losses at a bus voltage of 310 V are given by (3-8).

$$\begin{aligned} P_{H-bridge} &= 2P_{sw} + 2P_{Dsw} + 2P_{on} + 2P_{D\_on} + P_{Rsense} \\ &= 2\times 26.4 + 2\times 3.34 + 2\times 8.25 + 2\times 6.25 + 5 \text{ W} \\ &= 93.48 \text{ W} \end{aligned} \quad \textbf{(3-8)}$$

Three-state PA H-bridge losses

Conduction and switching losses

The power losses in the switching devices for a three-state PA are determined in a similar manner as in the two-state PA. Assume that an H-bridge circuit is conducting the load's current in the forward direction and a minimum voltage (V_{BUS}) is applied across the H-bridge. The three-state duty cycle is determined as (3-9).

$$\begin{aligned} d \cdot V_{BUS} &= I \cdot R \\ d &= \frac{10\times 0.261}{150}\times 100\ \% \\ &= 1.74\ \% \end{aligned} \quad \textbf{(3-9)}$$

I is the maximum load current and R is the load resistance. The switching losses for a single IGBT and the freewheeling diode are the same as the switching losses experienced by the two-state PA IGBTs. For a maximum current of 10 A, the IGBT and freewheeling diode switching losses are given by (3-2) as 13.2 W and (3-3) as 1.67 W, respectively.

For the three-state controlled H-bridge, the high side IGBT (S1) will be on for 1.74 % of the time while the low side IGBT (S4) will conduct the current with a 100 % duty cycle. The conduction losses are determined as (3-10) for the high side IGBT (S1).

$$\begin{aligned} P_{on(S1)} &= V_{ce(on)} I_c d \\ &= 1.65\times 10\times 0.0174 \text{ W} \\ &= 0.3 \text{ W} \end{aligned} \quad \textbf{(3-10)}$$

For the low side IGBT, the conduction losses are given by (3-11).

$$\begin{aligned} P_{on(S4)} &= V_{ce(on)} I_c d \\ &= 1.65 \times 10 \text{ W} \\ &= 16.5 \text{ W} \end{aligned} \tag{3-11}$$

The conducting loss of the diode is determined as (3-12).

$$\begin{aligned} P_{D\_on} &= V_d I_c d \\ &= 1.25 \times 10 \times 0.983 \text{ W} \\ &= 12.29 \text{ W} \end{aligned} \tag{3-12}$$

Sense resistor losses

Because the two low side IGBTs (S3 and S4) connect to ground via the sense resistor, the current will only flow through the resistor when the high side IGBT (S1) is conducting. The loss dissipated by the sense resistor is given by (3-13).

$$\begin{aligned} P_{Rsense} &= I R d \\ &= 10 \times 0.05 \times 0.0174 \text{ W} \\ &= 8.7 \text{ mW} \end{aligned} \tag{3-13}$$

The sense resistor losses are negligible. For minimum bus voltage, the total losses in the H-bridge circuit are determined as (3-14).

$$\begin{aligned} P_{H-bridge\_3state} &= P_{sw} + P_{Dsw} + P_{on(S1)} + P_{on(S4)} + P_{D\_on} \\ &= 13.2 + 1.67 + 0.3 + 16.5 + 12.29 \\ &= 43.96 \text{ W} \end{aligned} \tag{3-14}$$

For maximum voltage across the H-bridge, the switching losses are twice the switching losses experienced at a bus voltage of 150 V. The three-state PA total H-bridge losses are thus determined as (3-15).

$$\begin{aligned} P_{H-bridge\_3state} &= P_{sw} + P_{Dsw} + P_{on(S1)} + P_{on(S4)} + P_{D\_on} + P_{Rsense} \\ &= 26.4 + 3.34 + 0.3 + 16.5 + 12.29 \\ &= 58.83 \text{ W} \end{aligned} \tag{3-15}$$

The theoretical analysis of the H-bridge losses shows that the three-state PA generates low H-bridge losses as compared to the two-state PA. The losses in the H-bridge translate to heat this is conducted

through an appropriate heat sink protecting the devices from over heating. Over-temperature protection is also implemented as discussed in section 3.2.5.

3.2.3 Decoupling capacitor design

Switch mode power supplies (SMPS) with high speed switching devices result in voltage waveforms with significant high frequency content. At high frequencies, parasitic elements due to the physical construction of the H-bridge become significant [24].

Figure 3-4 displays an H-bridge circuit with stray inductances and supply line inductances. L_{C1}, L_{C2}, L_{C3} and L_{C4} are the stray inductances at the collector side of switching device S1, S2, S3 and S4 respectively, L_{E1}, L_{E2}, L_{E3} and L_{E4} model the stray inductances at the emitter side of switching device S1, S2, S3 and S4 respectively, and L_{BUS+} and L_{BUS-} respectively models the inductances of the positive and negative supply terminals, respectively.

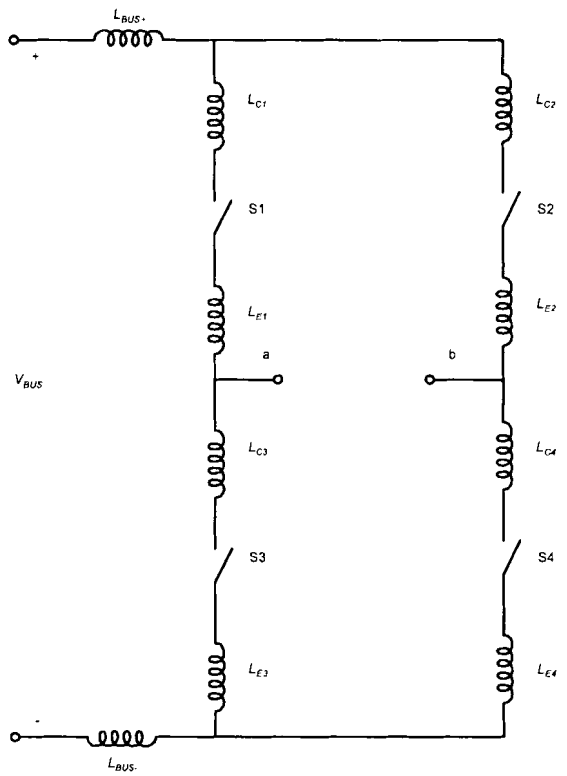

Figure 3-4: H-bridge model with parasitic elements [24]

The stray inductances of the positive and negative terminals of the switching devices are minimised by arranging the switching devices as close as possible to one another. This minimises the track lengths and high frequency loop areas between the devices and in effect the stray inductances. The inductances due to the power supply lines are reduced by using high frequency decoupling capacitors i.e. WIMA capacitors. The decoupling capacitors are inserted between the negative and positive supply rails and placed as close as possible to the switching devices.

The positioning of the low and high frequency decoupling capacitors reduce the voltage spikes due to the stray inductances of the power supply lines and reduces the noise transmission due to high frequency current loops. In order to the high frequency current loops, the power supply tracks from the low frequency capacitor (smoothing capacitor) are kept as short and direct as possible to the H-bridge circuit. By doing so, the power supply inductances (L_{BUS+} and L_{BUS-}) are restricted to minimum values but may still be significant due to the track width. Also the smoothing capacitors supply a large component of the current to the H-bridge. Therefore, it is necessary to have decoupling capacitor between the smoothing capacitor and H-bridge circuit.

The capacitors required for high frequency may have a small capacitance value but must have an excellent frequency response. They should be designed to handle high transient currents without any failure. The effectiveness of reducing the high frequency current loops lies in distributing multiple high frequency capacitors between the smoothing capacitors and the H-bridge [25]. For this application, WIMA capacitor MKP10 0.068 μF 400 Vdc is selected for C_{dec}.

3.2.4 H-bridge supply design

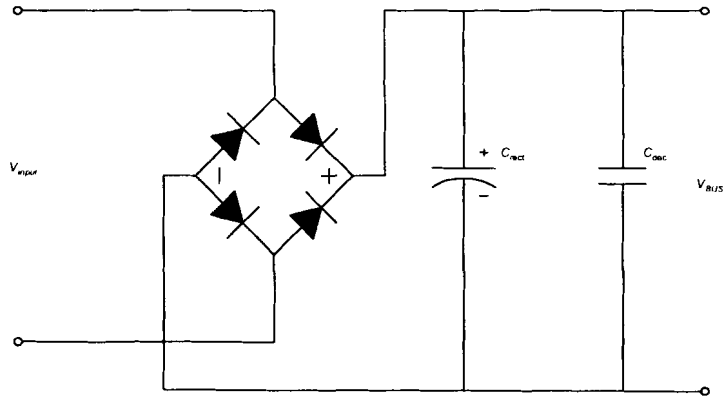

Figure 3-5: Rectifier circuit diagram

Figure 3-5 displays the power supply circuit diagram. The rectifier generates the dc bus voltage by rectifying the ac supply voltage. A low frequency decoupling or a smoothing capacitor (C_{rect}) is an electrolytic capacitor with a high capacitance value and must be able to tolerate large ripple currents.

To specify the smoothing capacitor, one must take into consideration the average power consumption of the H-bridge and the load. For the worst case scenario, the power loss of the double radial AMB system that will be used to test the PA is 52.5 W [19]. This power loss includes the copper and the core losses. The minimum total power required from the rectifier circuit is determined by (3-16).

$$\begin{aligned} P_{rect150V} &= P_{H-bridge} + P_{Load} \\ &= 63.76 + 52.5 \text{ W} \\ &= 116.26 \text{ W} \end{aligned} \tag{3-16}$$

The average power consumption of the H-bridge circuit with the load connected is determined from the total power and minimum supply voltage, (3-17).

$$\begin{aligned} i_{rect} &= \frac{P_{rect}}{V_{BUS(\min)}} \\ &= \frac{116.26}{150} \text{ A} \\ &= 0.755 \text{ A} \end{aligned} \tag{3-17}$$

A single phase bridge rectifier, the BR64 is selected to convert the ac voltage to dc. Since the rectifier is a full-bridge, the output will have a frequency equal to 100 Hz. Thus, a 100 Hz smoothing capacitor is specified to limit the voltage ripple to less than 10 % of the total supply voltage while supplying the average current. The maximum smoothing capacitor value required is determined from the average supply current and the ripple of the minimum dc supply voltage (3-18).

$$\begin{aligned} C_{rect} &= i_{rect} \frac{dt}{dv} \\ &= 0.755 \frac{10 \times 10^{-3}}{0.1 \times 150} \text{ F} \\ &= 503 \text{ } \mu\text{F} \end{aligned} \tag{3-18}$$

For a maximum voltage, the power consumption of the rectifier is 145.96 W and the average current is 0.471 A. The smoothing capacitor is determined in (3-19).

$$\begin{aligned} C_{rect} &= 0.471 \frac{10 \times 10^{-3}}{0.1 \times 310} \text{ F} \\ &= 151.9 \text{ } \mu\text{F} \end{aligned} \tag{3-19}$$

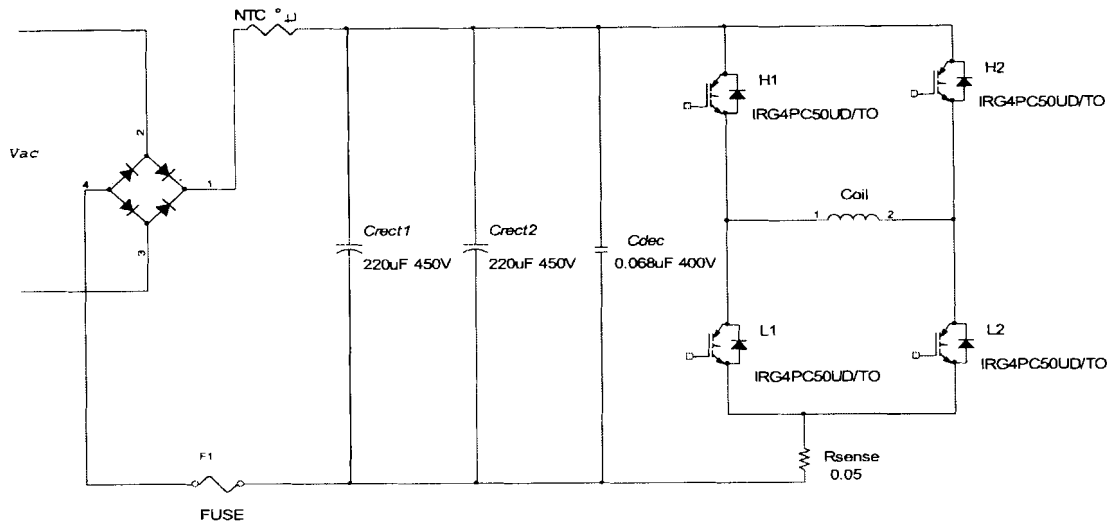

Figure 3-6: Final power circuit

Two Rubycon 220 μF, 450 V large can type electrolytic capacitors are chosen for this application. Figure 3-6 displays the final power circuit diagram.

3.2.5 Thermal design

In all power semiconductor applications like SMPSs, the device temperatures need to be carefully managed. The switching devices used in constructing an H-bridge circuit are the main sources of heat [26]. The heat energy dissipated by these devices must be carefully controlled if safe operating temperatures are to be maintained. To ensure safe operating temperatures, the devices are positioned on a heat sink which reduces the devices' thermal resistances with respect to the ambient. The heat sink provides a thermally conductive pathway from the switching devices to its surroundings. ISOSTRATE 2000 K3, electrically isolating thermal interface pads are used to maintain good thermal contact between the heat sink and the switching devices or the sense resistor.

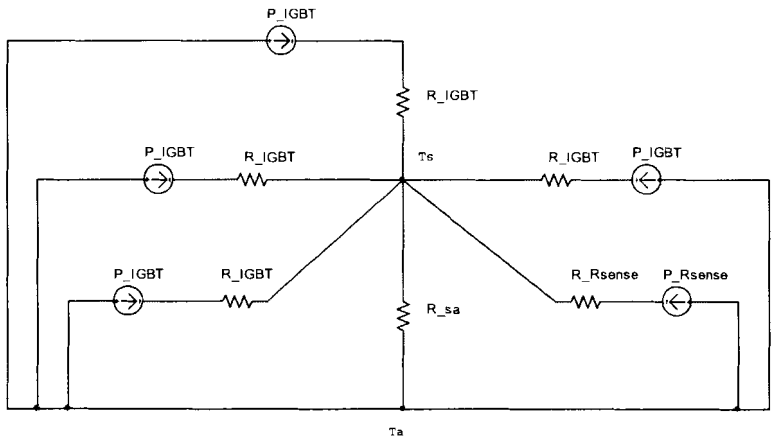

Figure 3-7: Equivalent circuit of thermal system

Figure 3-7 displays the equivalent circuit for the thermal system. $R_{\_IGBT}$ and $R_{\_Rsense}$ are the respective thermal resistances between the component junctions and the heat sink. $R_{\_SA}$ is the heat sink to ambient thermal resistance. Furthermore, $P_{\_IGBT}$ and $P_{\_Rsense}$ are the power dissipated in the devices.

The case to heat sink thermal resistances of the IGBTs packaged in a TO-247 package is given by (3-20).

$$R_{\theta CS} = \frac{0.23}{0.8 \times 0.626} = 0.46\ ^{\circ}\text{C/W} \tag{3-20}$$

The case to heat sink thermal resistances of the sense resistor packaged in a TO-126 package is given by (3-21).

$$R_{\theta CS} = \frac{0.23}{0.32 \times 0.44} = 1.63\ ^{\circ}\text{C/W} \tag{3-21}$$

The thermal characteristics of each component are determined from their respective data-sheets. The allowable heat sink temperature of the mounted devices depends on the power dissipated by the devices. The allowable heat sink temperature of the IGBT device under normal load conditions is determined in (3-22). Since the diodes are internal, its temperature is the same as that of the IGBTs.

$$\begin{aligned} T_S &= T_j - P_{IGBT}\left(R_{\theta JC} + R_{\theta CS}\right) \\ &= 150 - 44.23 \times (0.64 + 0.46) \\ &= 101.35\ ^{\circ}\text{C} \end{aligned} \tag{3-22}$$

The sense resistor has a power rating of 15 W at a case temperature of 25 °C, which decreases to 0 W at 150 °C. This results in a derating factor of 0.12 W/°C. The allowable heat sink temperature for a sense resistor is calculated in (3-23).

$$\begin{aligned} T_S &= \frac{125 \times \left(18 - P_{Rsense}\right)}{15} - P_{Rsense} \times R_{\theta CS} \\ &= \frac{125 \times (18 - 5)}{15} - 5 \times 1.63 \\ &= 100.2\ ^{\circ}\text{C} \end{aligned} \tag{3-23}$$

The device's maximum allowable heat sink temperatures were determined for the case where the maximum current of 10 A flows through the load and a maximum voltage of 310 V is applied..

Comparing the allowable heat sink temperatures of the IGBTs and the sense resistor, the sense resistor is more sensitive to temperature than the IGBTs. For safe and reliable operation of the PA, a derating factor of 15 % is included to guarantee safe operation of the IGBTs [19]. This limits the heat sink temperature to 85.17 °C (3-24) for safe operation of the devices.

$$\begin{aligned} T_{Heat\_s} &= 100.2 - 100.2 \times 15\ \% \\ &= 85.17\ ^{\circ}\mathrm{C} \end{aligned} \tag{3-24}$$

Thermal protection will be incorporated to limit the heat sink temperature increase to minimum allowable temperatures. As discussed in section 3.7, a 75 °C thermal switch will be used to protect the circuit against over temperature. For the PA to operate at a constant load current of 10 A, a maximum thermal resistance of the heat sink at 75 °C is determined form (3-25). A finned aluminium heat sink 200 mm wide and 40 mm high with thermal resistance of 0.65 °C/W is selected for this application. Because of the heat sink's thermal resistance of 0.65 °C/W as compared to the required thermal resistance (3-25), a fan will be used as an extra cooling method to maintain the devices temperature to minimum values.

$$\begin{aligned} R_{\theta SA} &= \frac{T_S - T_A}{P_{H-bridge}} \\ &= \frac{75 - 25}{93.46} \\ &= 0.535\ ^{\circ}\mathrm{C/W} \end{aligned} \tag{3-25}$$

3.3 Gate drive circuit design

To turn on a MOS-gated device utilised as a high side switch, the gate terminal must be set to a voltage at least 10 V greater than the source terminal. An important feature of switching devices like IGBTs is that they have a large stray capacitance between the gate and the other terminals. When pure PWM signals are fed directly to the gate terminal, the charge time of the capacitor will have a negative influence on the time it takes before the gate voltage can reach the 10 - 15 V required to turn-on the device. To ensure fast switching times and low losses the PWM signals are passed through half bridge gate drivers.

3.3.1 Component selection

An International Rectifier IR2113 half bridge gate driver was selected to provide the IGBTs with gate signals. A single driver provides both the high and low side gate signals. The driver has the advantage of

providing very fast switching speeds and low power dissipation. Due to the proposed 4-quadrant controlled H-bridge, two drivers are used. Figure 3-8 displays the gate drive circuitry.

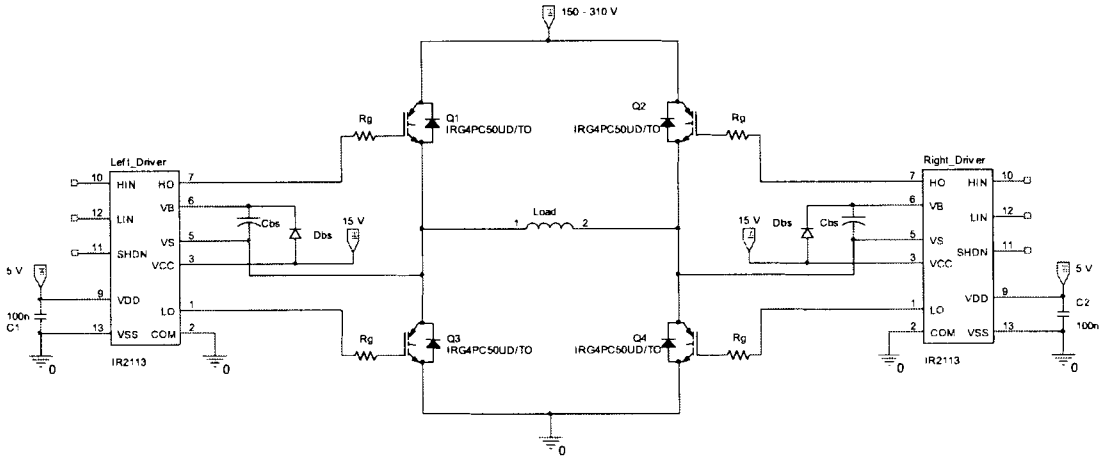

Figure 3-8: Gate drive circuit diagram

The gate resistance (R_g) is chosen based on the driver's maximum output current capability (2 A). The gate resistance is given by (3-26).

$$R_g = \frac{V_{CC}}{I_{g\_max}} = \frac{15}{2} = 7.5\ \Omega \tag{3-26}$$

V_{cc} is the supply voltage, and I_{gmax} is the maximum peak gate current specified by the gate driver. An 8 Ω, ¼ W resistor is chosen.

The low side IGBTs (Q3 and Q4) are driven from the 15V (V_{cc}) supply because their emitter is grounded. However, the high-side switching devices emitter terminals are connected to the collector terminals of the low side IGBTs. To drive the high side devices, a floating supply is required. The bootstrap capacitors (C_{bs}) are used to obtain the floating supplies. The capacitors are charged by the V_{cc} supply through the bootstrap diodes (D_{bs}) when the high side devices are not conducting.

3.3.2 Bootstrap components design

As mentioned in section 3.3.1, the gate charge for the high side IGBTs is provided by the bootstrap capacitor (C_{bs}). The bootstrap capacitors minimum charge requirement is given by (3-27) [27].

$$\begin{aligned} Q_{bs} &= 2Q_g + \frac{I_{qbs}}{f_{sw}} + Q_{ls} \\ &= 2\times 180\times 10^{-9} + \frac{125\times 10^{-6}}{30\times 10^{3}} + 5\times 10^{-9} \\ &= 369.17 \text{ nC} \end{aligned} \tag{3-27}$$

where Q_g is the total gate charge of the IRG4PC50UD, I_{qbs} is the quiescent supply current, f_{sw} is the switching frequency and Q_{ls} is the level shift charge required per cycle. It is important for the bootstrap capacitor to supply the minimum required charge while retaining its voltage. The absolute minimum capacitance value of the bootstrap capacitor is calculated by (3-28) [27].

$$\begin{aligned} C_{bs} &= \frac{2Q_{bs}}{V_{CC} - V_f - V_{ls} - V_{\min}} \\ &= \frac{2\times 369.16\times 10^{-9}}{15 - 1.25 - 1.65 - 8.2} \\ &= 174 \text{ nF} \end{aligned} \tag{3-28}$$

V_{cc} is the supply voltage, V_f is the forward voltage drop across the bootstrap diode, V_{ls} is the voltage drop across the low side IGBT and V_{min} is the minimum voltage between V_B and V_S.

The bootstrap capacitor (C_{bs}) charges when the high side switching device is turned off. The capacitor may be fully charged because of the circuit operation. Increasing the capacitor value by a factor of 15 will minimise the danger of damaging the IC and reduce the ripple component on the V_{bs} voltage [27]. The new C_{bs} is found to be 2.6 μF. A tantalum capacitor is recommended for this application.

The requirements of the bootstrap diode (D_{bs}) are to be able to withstand the full dc bus voltage, which is seen when the high side device is switched on. It should also be an ultra-fast recovery device to minimise the amount of charge fed back from the C_{bs} into the V_{cc} supply and have a high temperature reverse leakage current characteristics [20]. The current rating of D_{bs} is defined from the C_{bs} minimum charge requirement and the switching frequency is given by (3-29).

$$\begin{aligned} I_F &= Q_{ls} f_{sw} \\ &= 369.17\times 10^{-9} \times 30\times 10^{3} \\ &= 11.1 \text{ A} \end{aligned} \tag{3-29}$$

The choice of diode should be able to withstand a voltage of 310 V and conduct a current of 11.1 mA. It is important for the selected device to have a reverse recovery time in the order of 100 ns. The MUR150 ultra-fast diode is identified for this application.

3.4 Current feedback

An average current control scheme is implemented to control the load current. A LEM sensor (LTS 15-NP) is chosen to sense the load current. The sensor has a bandwidth of 200 kHz and is configured to have two primary turns in order to measure a maximum nominal current of 7.5 A. The LEM sensor configured, in this way, can measure a primary current up to 24 A. For the application at hand, the sensor is required to sense a primary current varying from -12.6 to 12.6 A.

The controller will receive a voltage representation of the current flowing through the load. Equations (3-30) and (3-31) show the output voltages related to the minimum and maximum primary currents. At a maximum current of 12.6 A, 3.55 V is obtained and at -12.6 A, 1.45 V is obtained. An output of 2.5 V translates to 0 A flowing through the load.

$$\begin{aligned} V_{out(\max\_current)} &= 2.5 + 0.625\frac{I_P}{I_{PN}} \\ &= 2.5 + 0.625\frac{12.6}{7.5} \\ &= 3.55 \text{ V} \end{aligned} \tag{3-30}$$

and

$$\begin{aligned} V_{out(\min\_current)} &= 2.5 + 0.625\frac{-12.6}{7.5} \\ &= 1.45 \text{ V} \end{aligned} \tag{3-31}$$

Figure 3-9 displays the complete circuit diagram used for sensing the load current and providing feedback to the DSP board. The sensor is supplied from an isolated 5 V supply in order to isolate the DSP from the PEs. The low pass filter with a cut-off frequency of 3 kHz is designed to band limit the output signal, to reduce noise levels and to remove the transient voltages resulting from the switching of IGBTs.

The PWM signal generation will be implemented in the DSP environment. The LEM sensor output will be fed to the TMS320's ADC with additional circuitry as the input to the TMS320 is limited to a

maximum voltage of 3 V. The LEM sensor can provide a maximum voltage of 4.5 V. A voltage divider network of resistance R_d = 390 Ω and R_{14} = 2.2 kΩ are used to scale the LEM output voltage to 3 V.

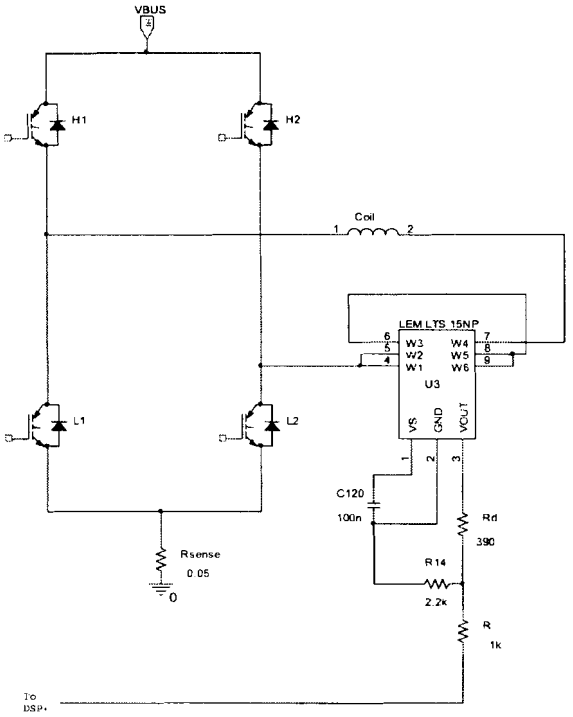

Figure 3-9: Final average current sensing schematic

3.5 Controller design

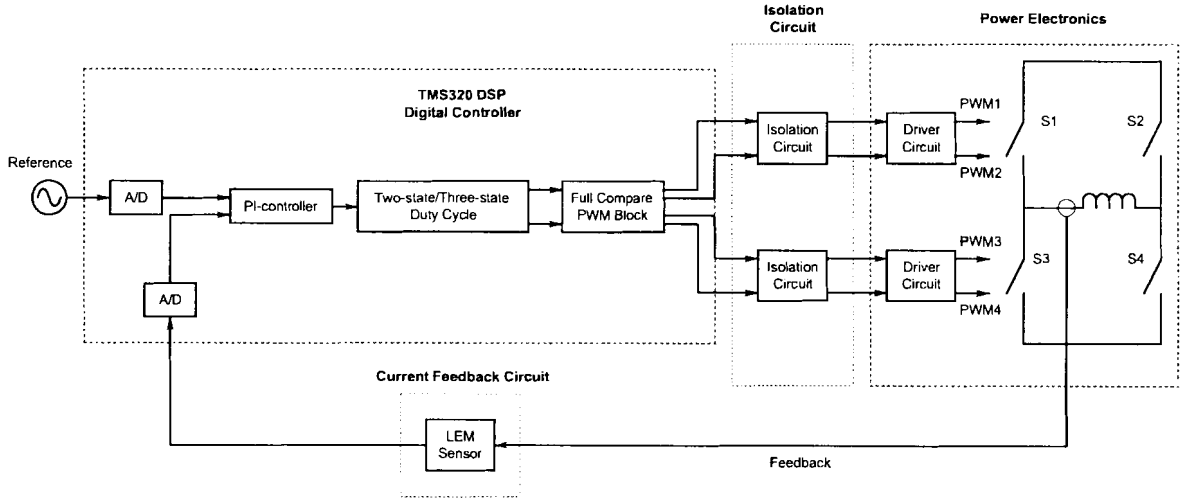

Figure 3-10: Functional block diagram of PEs and digital controller

Figure 3-10 shows the functional block diagram of the digital controller and the PEs. The digital controller is isolated from the PE circuit with high speed opto-couplers. It comprises analogue-to-digital

converters, a PI-controller, a duty cycle converter (for two-state or three-state) and a two-phase PWM generator implemented with a three-phase PWM block.

3.5.1 PI controller design

The PI controller used consists of a proportional gain (K_p) and an integral gain (K_i). The output of the controller is a control signal that is compared to the carrier signal to obtain appropriate PWM signals. In order to obtain the specified PA small signal bandwidth (2 kHz), the K_p value is predicted and the K_i is tuned by trial and error. As mentioned in section 2.5.4, the small signal bandwidth of the PA depends only on the K_p value. The equation for the K_p value is determined from (2-8). The proportional gain of the amplifier for minimum bus voltage is estimated using (3-32).

$$\begin{aligned} \omega_{bw} L A_t &= R A_t + K_p V_{BUS} \\ K_p &= \frac{2\pi f_{bw} L A_t - R A_t}{V_{BUS}} \\ &= \frac{2\pi \times 2\times 10^3 \times 6.6\times 10^{-3} - 0.261}{150} \\ &= 0.55 \end{aligned} \tag{3-32}$$

V_{BUS} is the bridge supply which is variable from 150 V to 310 V, R (0.261 Ω) is the resistance of the AMB coil, L (6.6 mH) is the inductance of the AMB coil, A_t is the amplitude of the carrier or triangular signal and I_{ref} is the reference current signal.

For maximum voltage across the load, the proportional constant is predicted to be 0.276. The integral gain will be predicted to stabilise the actual load current at the expected set point. The gain eliminates the steady-state error between the reference and actual signals when the actual signal reaches the desired level. When the PI-controller constants are properly predicted, the controller will have exceptional control stability.

3.5.2 H-bridge PWM controller

As mentioned earlier, a TMS320 is used to generate the PWM signals. The TMS320 is equipped with a high performance TI DSP chip as well as A/D conversion capability. To realise the development of digital control strategies, VisSim®/Embedded Control Developer software is used to program the TMS320 DSP chip.

VisSim® digital PWM implementation

To obtain PWM outputs required to control an H-Bridge circuit, a Full Compare PWM block is used. The block is a three-phase PWM block used to control PWM channel 1 to 6 of the DSP board. The PWM channels are internally synchronised. The duty cycle of the paired PWM signals can be controlled independent from other pairs thus making it possible to implement two-state and three-state switching techniques. Figure 3-11 displays the Full Compare PWM block. The output of a given PWM pair can be set to active high or active low in the Full Compare PWM dialog settings block illustrated in Figure 3-12.

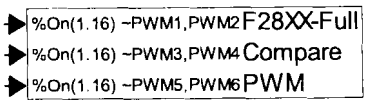

Figure 3-11: VisSim® Full Compare PWM block

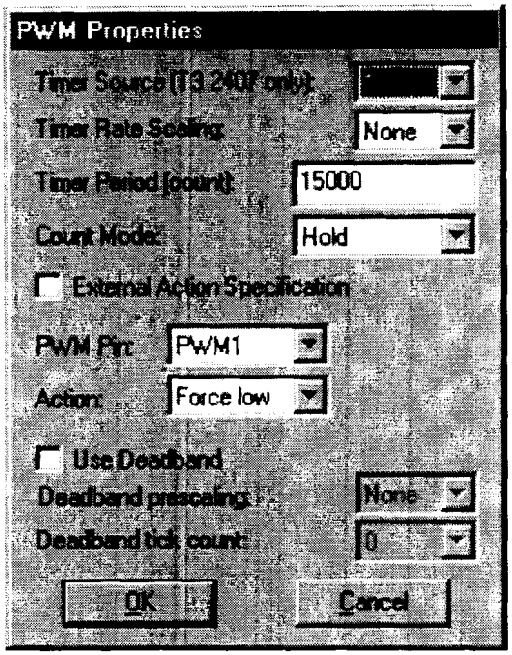

Figure 3-12: Full Compare PWM dialog

The dialog block is used to configure the PWM block properties. Properties like switching frequency, PWM action and the deadband between two PWM signals are configured from this block. The timer source provides a time base for operation of the Full compare block to generate PWM outputs. Timer source T_1 running at a clock frequency of 150 MHz is selected for this application because the Full compare block is exclusively based on T_1 [28]. Timer period is used to set the switching frequency of the PWM signals. For 30 kHz switching frequency, the timer count mode is set to continuous Up/down mode for symmetric PWM signals. The timer period is scaled as shown in (3-33).

$$\begin{aligned} T_{Period} &= \frac{T_1}{2f_{sw}} \\ &= \frac{150\times10^6}{2\times30\times10^3} \\ &= 2500 \end{aligned} \tag{3-33}$$

The deadband of 1 μs is desired between the PWM signals controlling the same leg of the H-bridge. The PWM block's deadband pre-scaling is set to $T_{dprescaling} = \frac{1}{32}$ and the tick count ($T_{d(TickCount)}$) is determined form (3-34). From (3-34), the tick count is approximated to 5.

$$\begin{aligned} T_d &= \left(\frac{T_{d(TickCount)}}{T_1 T_{d(prescaling)}} \right) \\ T_{d(TickCount)} &= T_d T_1 T_{d(prescaling)} \\ &= 1\times10^{-6}\times150\times10^6 \frac{1}{32} \\ &= 4.7 \end{aligned} \tag{3-34}$$

Figure 3-13 (not drawn to scale) displays the Full compare PWM control signals and the output PWM signals with added deadband. PWM1 is set to active low and PWM2 to active high to ensure that the two signals are complements of each other. When PWM1 receives a command to turn-on, the switching transition is delayed by time T_d and the same applies to PWM2.

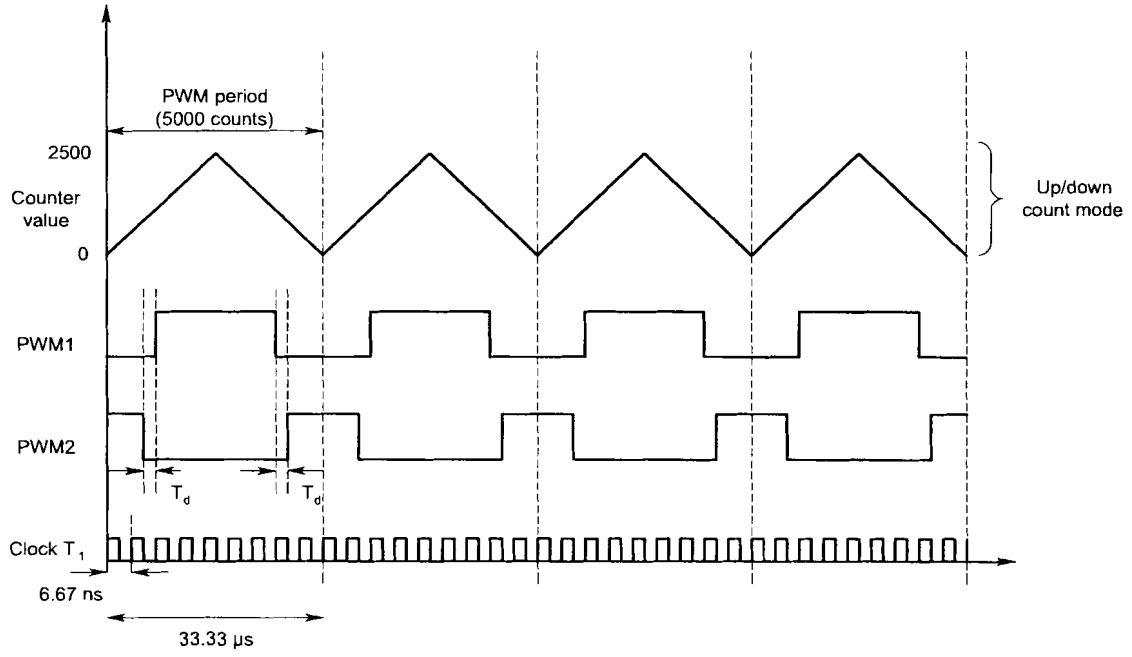

Figure 3-13: Full Compare PWM switching waveforms

Feedback and reference signal

As indicated in Figure 3-10, a single signal measurement is needed to implement CMC. The average current of the load is sensed with a LEM sensor and fed to the DSP via analogue-to-digital converter (ADC) channel 0. The output of the LEM sensor has a dc offset voltage of 2.5 V for a current of 0 A. The output is scaled to 2.12 V. When a sinusoidal reference signal is generated in the DSP, a heavy computational burden is placed on the DSP controller. Thus, a reference signal with an offset of 1.5 V is generated from the signal generator and it is fed into the ADC1. The offset is selected because a full resolution of the ADC channel is used. Besides the offset in the LEM sensor output signal, the actual current is scaled down by a gain of $\frac{1}{14.127}$. This gain is compensated for in the DSP environment. Figure 4-16 shows how signals from the external electronics are provided to the DSP with ADC channels.

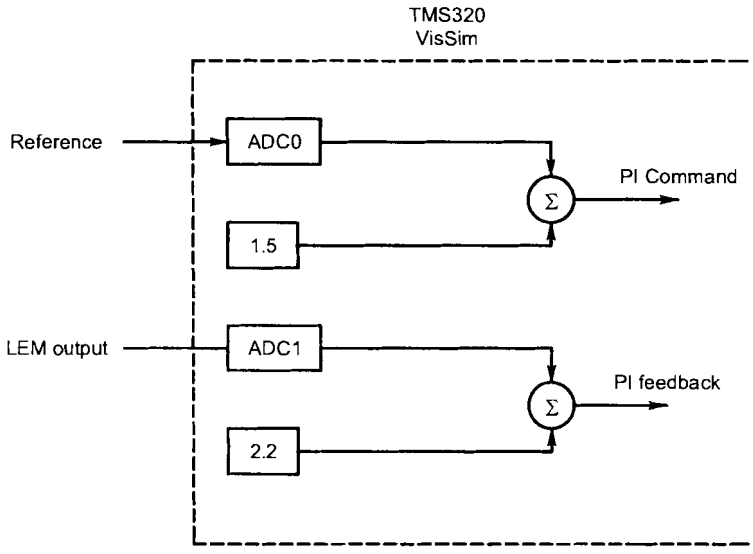

Figure 3-14: Implementation of feedback in DSP

PI controller

The sensed feedback signal is compared to the reference signal inside the VisSim® PI-controller to determine the error signal. The PI-controller utilises the design constants of section 3.5.1 to ensure that the output signal tracks the reference signal and at the same time achieves the desired dynamic performance. The output of the PI-controller provides the duty cycle command to the duty cycle converter. The PI-controller duty cycle is manipulated to produce duty cycles required to produce the two-state and three-state PWM signals. Figure 3-15 shows the PI block used to implement the controller.

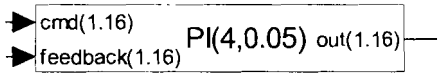

Figure 3-15: VisSim® PI controller block

As discussed in section 3.5.1, the proportional gain for the controller is set to 0.276 because of the amplitude of the carrier signal. Due to the implementation of the two-state and three-state techniques, the amplitude of the output of the controller is limited to 0.5 for the two-state and to 1 for the three-state technique. Thus, controller's gains of the two techniques will differ by a factor of 2.

Two-state and three-state duty cycle

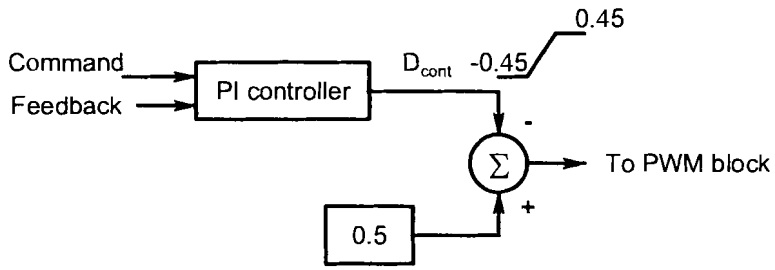

Figure 3-16: Two-state duty cycle converter

To control the PA in two-state, the output of the PI controller is set to a lower limit of -0.45 and an upper limit of 0.45 in order to vary the PWM duty cycle from 5 % to 95 %. Figure 3-16 displays the two-state duty cycle converter. The duty cycle is fed directly to the PWM pairs (PWM1,2 and PWM3,4) and a deadband is added between the pairs of PWM signals. PWM2 and PWM4 of the Full compare PWM block are set to active high and PWM1 and PWM3 are set to active low to compensate for the inverting effect of the opto-couplers. PWM1 and PWM2 respectively drive the high and the low side switches on the left leg of the bridge while PWM3 and PWM4 respectively drive the high and low side switches on the right side of the bridge.

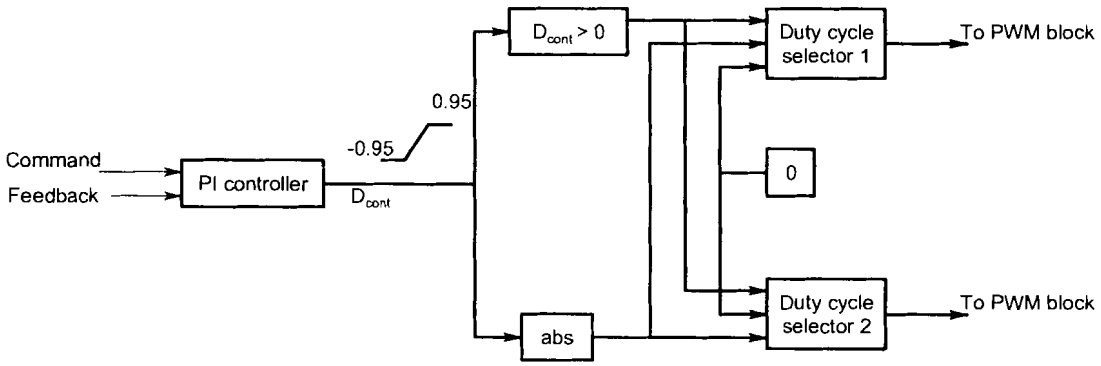

Figure 3-17: Three-state duty cycle converter

In order to realise the three-state switching technique, two separate PWM signals are generated. The output of the PI controller is now limited to a minimum of -0.95 and a maximum of 0.95. Figure 3-17 shows how the PI-controller's output is manipulated to produce the three-state PWM control signals. The duty cycle selector block is used to generate a constant duty cycle of 0 % (or 100 %) to control one leg of the bridge or a varying duty cycle from 5 % to 95 % to toggle the switches in the other leg of the bridge.

The deadband is also added and the PWM pairs are configured in the same manner as in the two-state control. Figure 3-18 displays the proposed H-bridge controller programmed with VisSim®/Embedded Controls Developer software. The Two-state/Three-state generator block refers to either a two-state or three-state duty cycle converter as illustrated by Figure 3-16 and Figure 3-17.

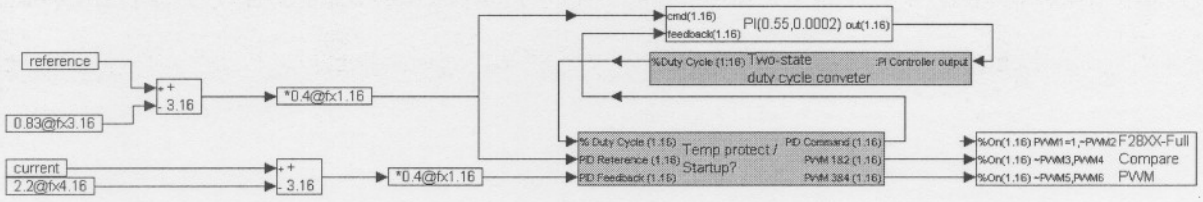

Figure 3-18: DSP PWM based H-bridge controller

Over temperature and soft start

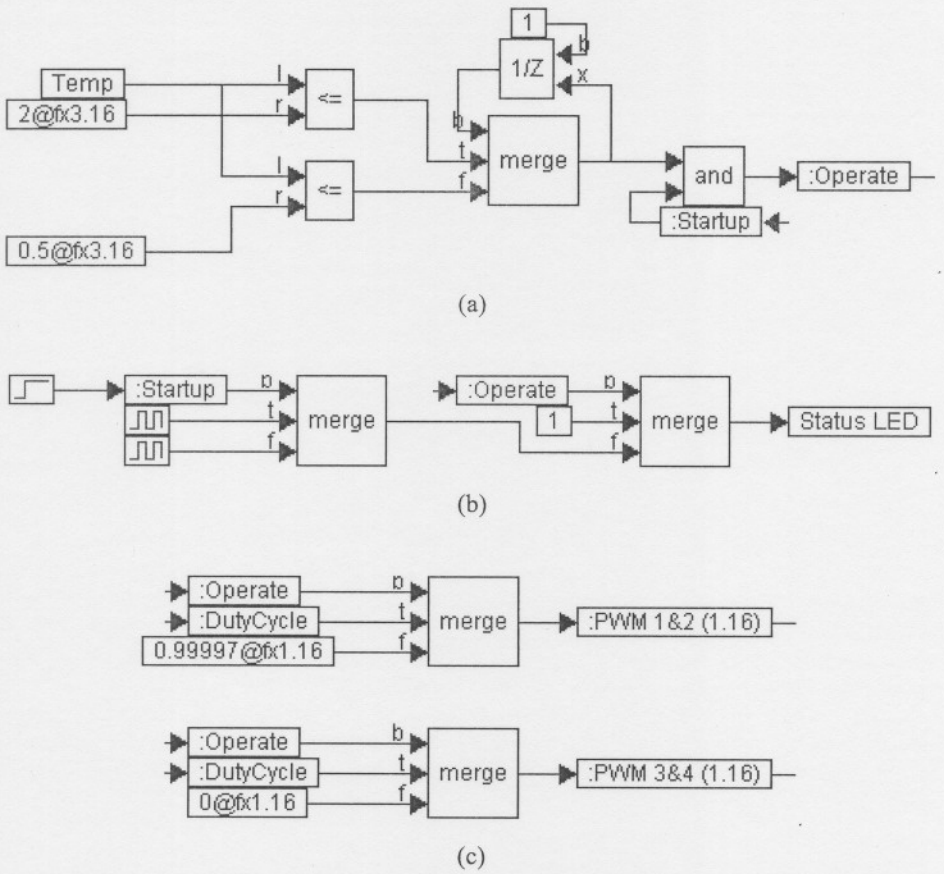

Figure 3-19: DSP based over temperature protection and soft start (a) over-temperature (b) over temperature and soft strat output signals (c) soft start delay

The over-temperature is implemented in VisSim®. The output of the thermal switch is sent to the TMS320 via ADC2. Figure 3-19 displays how the over-temperature protection and soft start was realised in

VisSim®. The sensed temperature of the heat sink is continuously compared to a value representing over-temperature conditions. For normal conditions, the PWM block is controlled by the PI-controller output signal. When over-temperature conditions are reached, the PI-controller output is terminated and PWM block receive a command that output a low duty cycle. Figure 3-19(a) and (b) illustrates the operation of the over temperature protection.

Figure 3-19(a) and (c) display the implementation of soft start in VisSim®. A soft-start is implemented by delaying the normal operation of the PA. During start-up, the soft start terminates the PI controller's duty cycle command for a while thereafter, allowing the generation of PWMs to take place. A 10 s operational delay is provided by the soft start circuit. The soft start is implemented to stabilise the voltage across the power circuit and the electronic devices.

3.6 Isolation circuit design

To interface the analogue electronic circuit and the digital circuit of the PA, a high speed opto-coupler is used. The output signals are isolated because they are not referenced to the same ground as the analogue electronic circuit. Figure 3-20 displays the isolation circuit diagram. The circuit provides the isolation barrier between the TMS320 and the PEs.

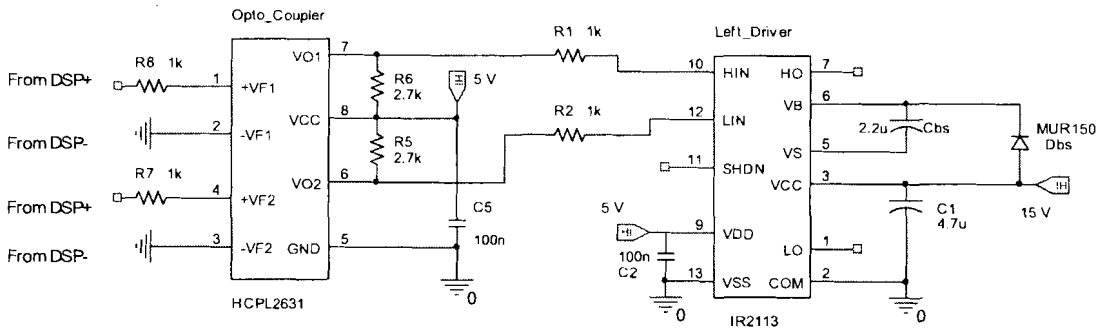

Figure 3-20: Isolation circuit diagram

A high speed opto-coupler HCPL-2631 is selected for this application. The opto-coupler is capable of transferring the generated PWM signals to the PEs with minimum distortion and delay in the signals. The left side of the device is referenced to the DSP ground while the right side is referenced to the power ground.

3.7 Protection

It is a prerequisite for AMB PAs to be reliable. The reliability of PAs relate to immunity against failure such as over-voltage, over-current and over-temperature. The PA is integrated with current limiting

circuitry to protect the load and switching devices against over-currents. Short circuit protection is also realised with this circuit which safeguards the switching devices from short circuit conditions. A thermal protection circuit protects the PEs from over-temperatures.

3.7.1 Short circuit protection

One of the key issues in designing a reliable short circuit or current limiting circuitry is to continuously sense the current through the load in all the possible modes of the H-bridge. The current is sensed with a non-inductive sense resistor as shown in Figure 3-3. When the resistor is located in this position, the total current flowing through the H-bridge and the load flows through the sense resistor, even in the event of switch failure and when both the switches on the leg are switched together, the total current will be picked up.

During the energy addition period in the AMB load, the current flowing through the coil may increase to peak values greater than the required current value due to the positive slope of the coil current. In addition, there may be an instance where the two switches on the same leg of the H-bridge are active. The two conditions are monitored continuously. In general, the current limiting circuitry monitors the current flowing through the load and works by terminating the gate pulses in the event of an over-current and short circuit condition.

The circuit responsible for terminating the gate pulse during possible short-circuit or over-current condition is shown in Figure 3-21. Due to switching transients present in the sensing circuitry, a low pass filter is placed across the sense resistor. The voltage across the sense resistor is compared to a reference voltage generated by the shunt regulator circuitry. As soon as the sense resistor voltage exceeds this reference voltage, the output of the high speed comparator becomes active high. This output is directly connected to the shutdown pin of IR2113. The shutdown pin of the half-bridge driver is given a high value to terminate the gate pulses.

During normal operation of the PA, the maximum current required to flow through the load is 10 A. With a sense resistor of 0.05 Ω, the voltage produced by the R_{sense} equals 0.5 V. The minimum output voltage produced by shunt regulator (LM4041) is 1.24 V. The current through the coil may increase to an acceptable current of 12.65 A. Thus, the reference voltage of the shunt regulator is scaled to 0.65 V. The resistance value of 1.2 kΩ scales the shunt regulator reference to appropriate value. If the amplifier fails to regulate the coil current to values lower than 12.65 A, the shutdown pins of the driver will be pulled high and the gate signals will be terminated.

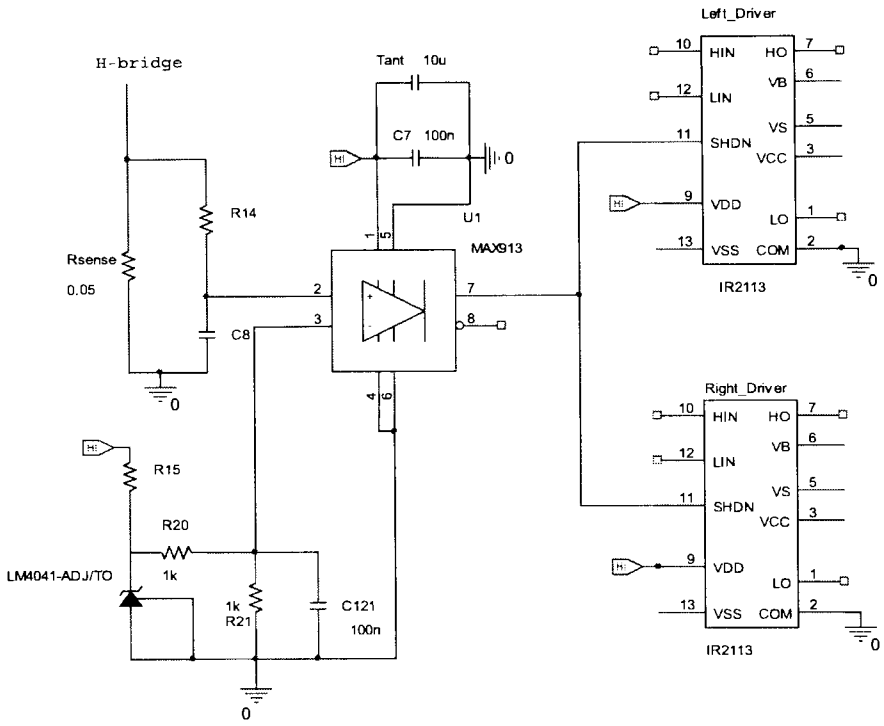

Figure 3-21: Short circuit protection

3.7.2 Thermal protection

To protect the PA against over-temperature conditions, a 75 °C thermal sensor (T_S) is used to sense the temperature of the heat sink where the temperature sensitive devices are mounted. The circuit diagram is shown in Figure 3-22.

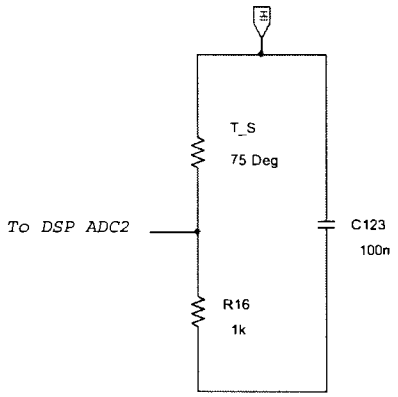

Figure 3-22: Thermal protection schematic diagram

The thermal protection circuitry will send a low voltage signal to the DSP controller when the components temperature is within the safe operating limits and a high voltage signal in the event of temperatures higher than 75 °C. Initially, the resistance of the temperature sensor is at a high value (100 kΩ). The high resistance value of T_S instantly decrease to a minimum value (100 Ω) when the heat

sink's temperature increases above 75 °C. In the DSP environment, the high voltage value will terminate the PWM signals. The PA will then self recover as soon as the temperature returns to safe operating limits.

3.8 Electronic supply design

The electronics power supply of the PA is divided into two sections, the analogue and the digital (isolated) supply. The analogue voltage section provides +17 V and a regulated +5 V and the digital supply provides a regulated +5 V for the LEM sensor. Table 3-3 displays the circuit's components and their respective power supply voltage.

Table 3-3 Electronic circuit power supply

Power supply (V)	Components
17	2x IR 2113
5	2x IR2113, 2x HCPL 2631, MAX 913
5	LTS 15NP

3.8.1 Transformer specifications

Table 3-4 Current consumption of electronic devices

	Description	IR2113	HCPL	MAX913	LM4041	LEM
I_C	Current	340 µA	13 mA	6 mA	1 mA	23 mA
I_{CDD}	Logic I input current	15 µA				
I_{CQ}	Gate current	32.4 mA				

The suitable transformers are selected based on the current requirements of the integrated electronic components of the PA. The current consumption of each component is obtained from the components data sheet and the power rating of the transformer is determined. Table 3-4 shows the current consumption of the components.

From the analogue 17 V power supply, two half bridge gate drivers each drawing a current of approximately 330 µA and gate current of 32.4 mA at a switching frequency of 30 kHz (3-35) are supplied.

$$\begin{aligned} I_{cq} &= Q_g \times f_{sw} \times n \\ &= 270\times10^{-9}\times30\times10^{3}\times4 \\ &= 32.4\ \text{mA} \end{aligned} \tag{3-35}$$

Q_g is the total gate charge of the IGBT, f_{sw} is the switching frequency and n is the number of IGBTs. The total current consumption from a 17 V supply is given (3-36) and the required rating of the transformer is obtained using (3-37).

$$\begin{aligned} I_{C17V} &= I_{cq} + 2I_c \\ &= 32.4 + 2\times0.34\ \text{mA} \\ &= 33.1\ \text{mA} \end{aligned} \tag{3-36}$$

$$\begin{aligned} P_{rating\_17V} &= VI \\ &= 12\sqrt{2}\times33.1\times10^{-3}\ \text{VA} \\ &= 0.56\ \text{VA} \end{aligned} \tag{3-37}$$

The requirement of the +17 V power supply result in a transformer power rating of 0.56 VA. Therefore, a 1.5 VA, 220-12 V transformer is selected.

The regulated analogue +5 V power supply supplies two opto-couplers each drawing a current of 13 mA per channel, a high speed comparator drawing 6 mA, two half-bridge drivers each drawing 8 μA for the logic supply and a shunt regulator drawing 1 mA. The total current consumption from this +5 V is given by (3-38).

$$\begin{aligned} I_{analoque\_5V} &= 13\times4+6+0.015\times2+1 \\ &= 59.03\ \text{mA} \end{aligned} \tag{3-38}$$

The requirements for the 5 V power supply results in a transformer of power rating given by (3-39).

$$\begin{aligned} P_{rating\_5V} &= 6\sqrt{2}\times59.02\times10^{-3} \\ &= 0.5\ \text{VA} \end{aligned} \tag{3-39}$$

Thus, the power rating of the transformer is 0.5 VA. A 0.5 VA, 220-6 V transformer is selected.

The digital regulated supply is used to supply a LEM sensor drawing a current of approximately 28 mA. Thus, the power rating of the transformer for the LEM is given by (3-40).

$$P_{rating\_digital} = 6\sqrt{2} \times 28 \times 10^{-3} = 0.24 \text{ VA} \quad \textbf{(3-40)}$$

The selected transformer for the LEM sensor is a 0.5 VA, 220-6 V transformer.

3.8.2 Rectifier design

The secondary sides of the three transformers are rectified using DB105 full wave rectifiers. The three output voltages are required to have a voltage ripple of less than 5 %. The capacitor values are determined from (3-41).

$$C = i_{rect} \frac{dt}{dv} \quad \textbf{(3-41)}$$

For the 12 V transformer, the capacitor value is obtained as (3-42).

$$C_{17V} = 0.0331 \frac{10 \times 10^{-3}}{0.05 \times 17} = 388 \text{ } \mu\text{F} \quad \textbf{(3-42)}$$

For the analogue supply 6 V transformer, the capacitor value is obtained as (3-43).

$$C_{5V} = 0.059 \frac{10 \times 10^{-3}}{0.05 \times 8.4} = 1405 \text{ } \mu\text{F} \quad \textbf{(3-43)}$$

(3-44) gives the capacitor value for the 6 V transformer required for the digital supply.

$$C_{5V\_LEM} = 0.028 \frac{10 \times 10^{-3}}{0.05 \times 8.4} = 667 \text{ } \mu\text{F} \quad \textbf{(3-44)}$$

Figure 3-23 displays the electronic supply circuit diagram of the PA. The outputs of the 6 V transformers are regulated to 5 V with 5 V voltage regulators.

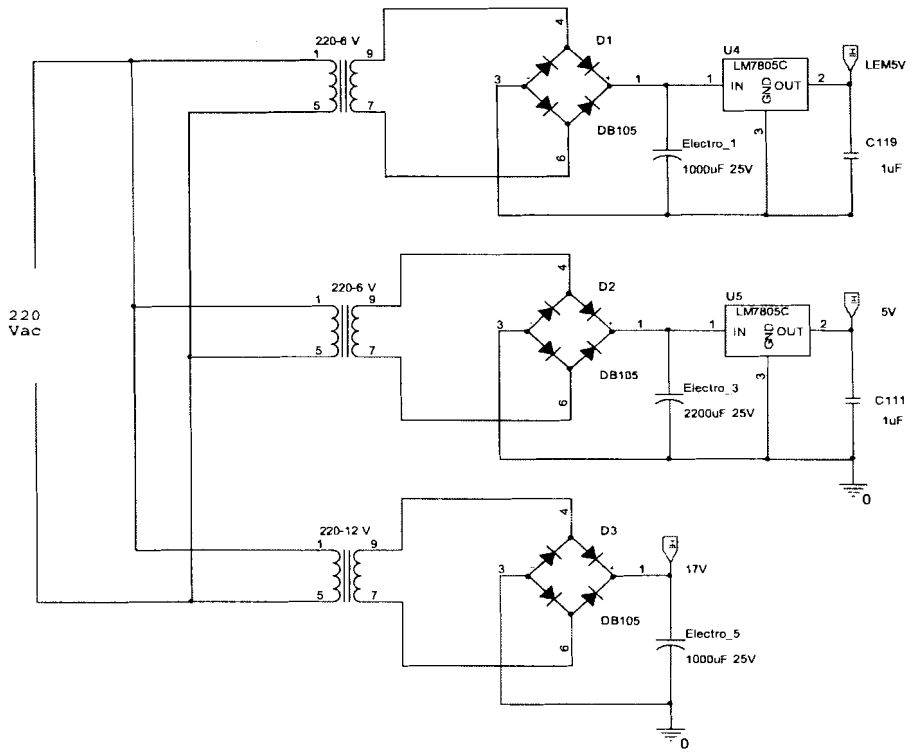

Figure 3-23: Schematic diagram of the electronics power supply

3.9 Circuit layout

In order to minimise the area of the high *di/dt* current loops and the high *dv/dt* surfaces mentioned in section 3.2.3, the components forming an H-bridge are placed as close as possible to each other. The critical factors that are looked at are:

- H-bridge layout i.e. the arrangement of switching devices
- H-bridge decoupling capacitor position with respect to H-bridge and
- IR2113 placement with respect to the IGBTs

Figure 3-24 shows the suggested circuit layout. The IR2113 drivers are placed as close as possible to the high side IGBTs' sources to minimise stray inductance between the V_s pin and the high-side IGBTs' sources. The high frequency decoupling capacitor (WIMA) is positioned next to the IGBTs and the thermal sensor is also located as close as possible to the temperature sensitive devices.

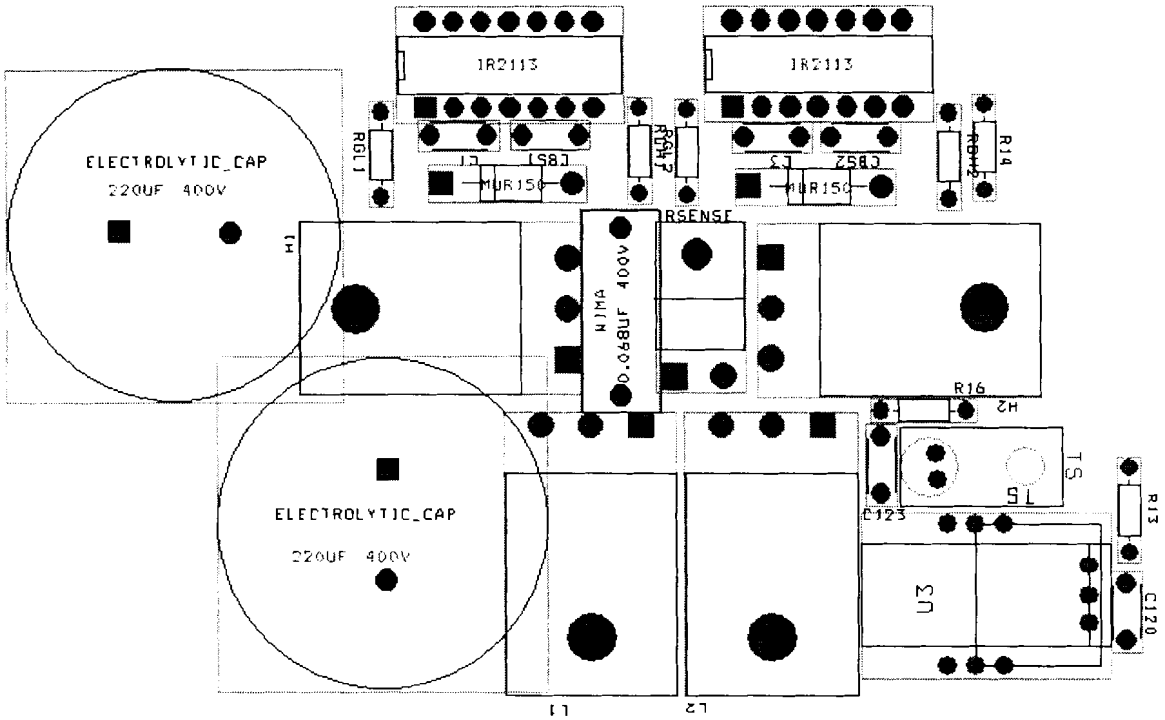

Figure 3-24: Suggested H-bridge circuit layout

In chapter 3, the design of the PEs, protection circuit and VisSim® PWM control for the two-state and three-state average current controlled switching PA was conducted. The design of the PEs section involved the H-bridge and the driver circuit. Short-circuit and over-temperature protections were designed to ensure that the PA will be able to respond to conditions that may lead to the failure of the amplifier. A digital PWM generator was implemented for the TMS320 by using VisSim® development software. The next chapter will discuss the characterisation of the PEs and the actual operation of the two-state and three-state PA.

4
Chapter
Power amplifier simulation

Chapter 4 discusses power amplifier (PA) simulations. The main aim of conducting the simulations is to evaluate the performance of the amplifier and to predict the experimental setup's behaviour. The simulations are conducted with the help MATLAB®/Simulink toolbox. The simulink model of the PAs is based on Zhang Liang PA switching models. For comparison purposes, two-state and three-state PAs are simulated simultaneously. The two PAs are compared in terms of the switching waveforms, coil current and the coil voltage. The bandwidth prediction of the amplifier is also verified in this chapter.

4.1 Power amplifier simulation model

Table 4-1 Simulation parameters

Parameter	Value
DC supply	310 V
Reference current	±10 A maximum
Switching frequency	30 kHz
Power bandwidth	1.5 kHz
Small signal bandwidth	2 kHz
Coil resistance	0.2631 Ω
Coil inductance	6.6 mH

The simulation setup parameters are shown in Table 4-1. A dc voltage of 310 V is applied across the H-bridge and a 10 A sinusoidal reference current (4-1) is allowed to flow through the coil. The switching frequency of the PA is set to 30 kHz. The desired power bandwidth of the PA is 1.5 kHz and the small signal bandwidth is designed at 2 kHz. An AMB coil is modelled as an *RL* circuit.

$$i_{ref} = 10\sin(2\pi f_{ref} t) \tag{4-1}$$

Figure 4-1 contains a Simulink® model of the average current controlled PA. This figure corresponds to Figure 3.11 in chapter 3. The PAs simulation model is from the work presented in [29]. The model is

constructed with the power circuit block which is the H-bridge circuit, the current feedback for average current sensing, a PID controller and the PWM generator block. The generation of PWM signals is implemented with two different techniques i.e. the two-state and three-state PWM techniques.

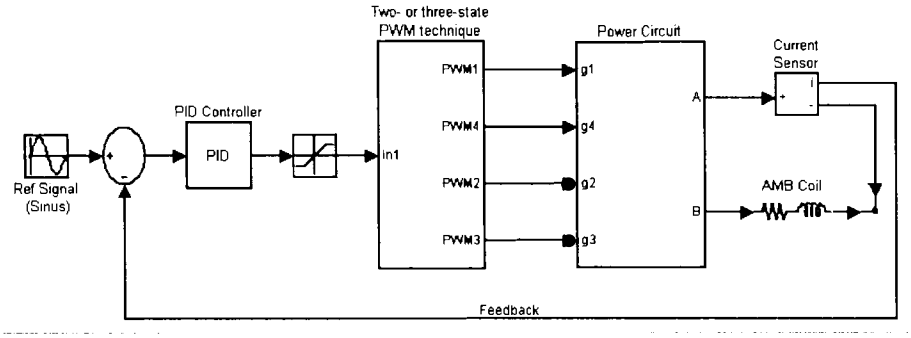

Figure 4-1: Simulink® block diagram representing average current controlled PA

Power circuit

Figure 4-2 displays an H-bridge circuit with a dc voltage supply. A power circuit is implemented with four MOSFETs in order to allow bi-directional current to flow through the coil. The selected MOSFETs are integrated with diodes. The diodes will provide a path for the current during the deadband periods and freewheeling states. An AMB coil is connected between terminal A and B.

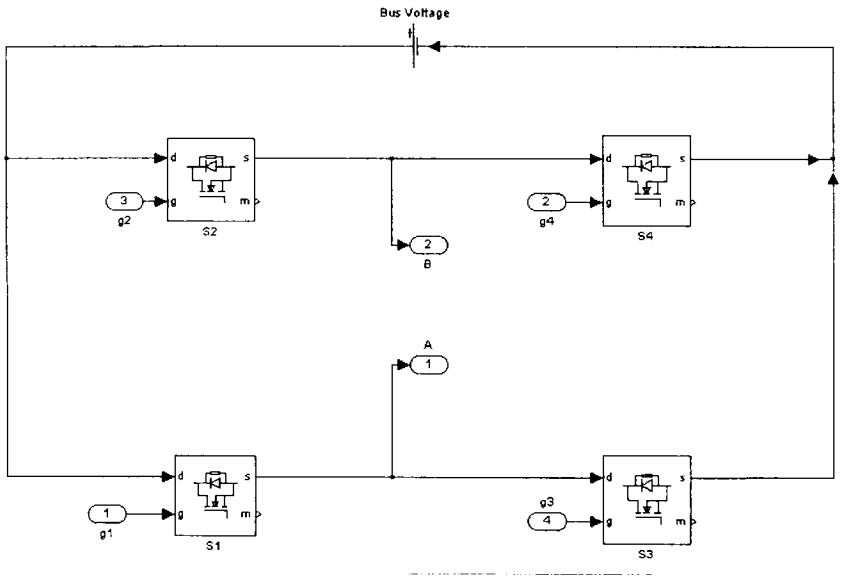

Figure 4-2: An H-bridge power circuit

PWM generator

Figure 4-3 and Figure 4-4 respectively illustrates the two-state and three-state PWM block diagrams. In a two-state PA, a single PWM signal with its complement is used to drive the H-bridge circuit. The PWM signals are generated by comparing a control command with a carrier signal of amplitude of ±1V and a

frequency of 30 kHz. A single PWM signal will control the two diagonal switches S1 and S4 while the other two diagonal switches S2 and S3 are controlled by the complement of the signal.

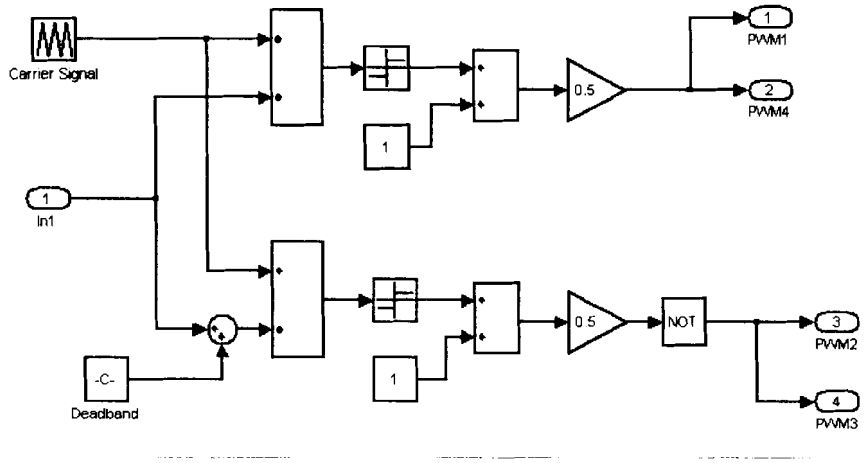

Figure 4-3: Two-state PWM generator

As shown in Figure 4-4, the three-state technique uses two different PWM signals with their complements to drive the H-bridge circuit. One PWM with its complement will drive the switches on the one leg (S1 and S3 or S2 and S4) while the other PWM with its complement drives the other leg (S2 and S4 or S1 and S3) of the H-bridge circuit. The simulation model of the three-state achieves the freewheeling state by turning S3 and S4 on.

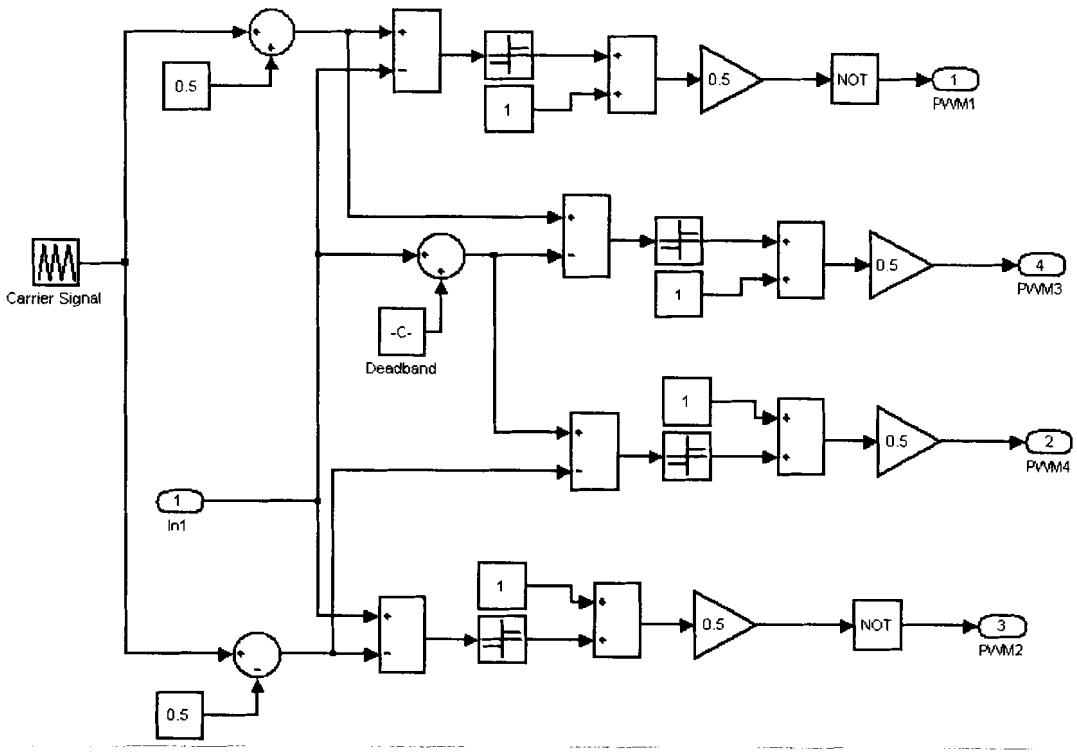

Figure 4-4: Three-state PWM generator

For both the two-state and three-state PWM techniques, the PWM duty cycles are generated according to the difference in the desired current and the actual coil current. To avoid transconductance of switches on the same leg, a deadband is added between the PWM signals controlling the switches on the same leg of the H-bridge circuit.

4.2 Simulation results

4.2.1 PWM simulation

A 1 μs dead band (T_d) is introduced between the PWM signals. Figure 4-5 displays a deadband time between the two-state PWM signals controlling a single leg of the H-bridge.

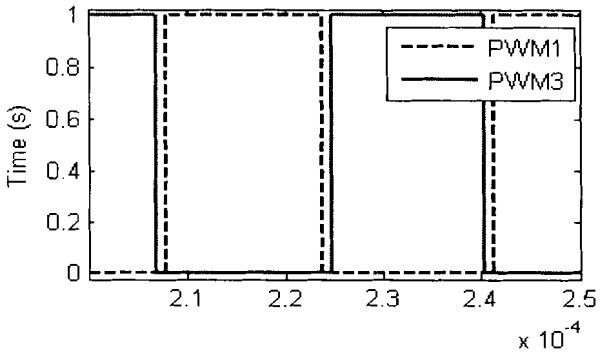

Figure 4-5: A 1 *μs* deadband period between two switching waveforms

Figure 4-6 and Figure 4-7 displays the PWM switching waveforms of the two-state and three-state switching PAs when zero current is desired. It is noticeable in Figure 4-6 that for a two-state operating PA; the two diagonal switches are turned on at the same time. For a three-state PA, it can be seen in Figure 4-7 that the two bottom switches of the H-bridge circuit are switched on for longer period of time.

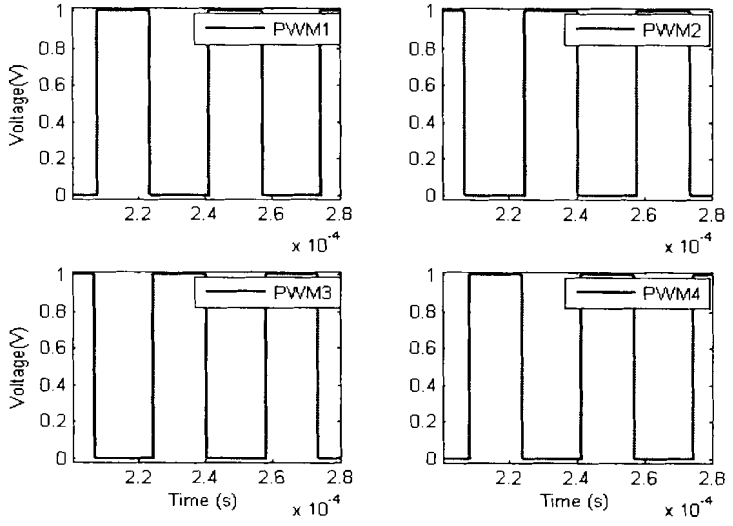

Figure 4-6: The two-state PA switching waveforms

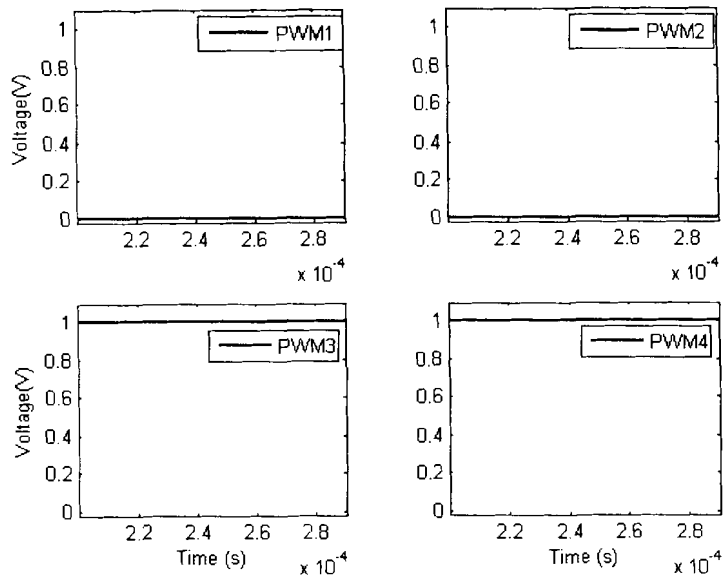

Figure 4-7: The three-state PA switching waveforms

The generated PWM signals are then fed directly to the gate terminal of the corresponding MOSFET. The driver circuit is not modelled in the simulations. The PWM signals relates to gate-to-emitter signals of the switching devices.

The simulated H-bridge collector-emitter voltage waveforms for the two-state and the three-state PA are respectively displayed in Figure 4-8 and Figure 4-9. The overshoot in the signals is due to the switching transient of the devices.

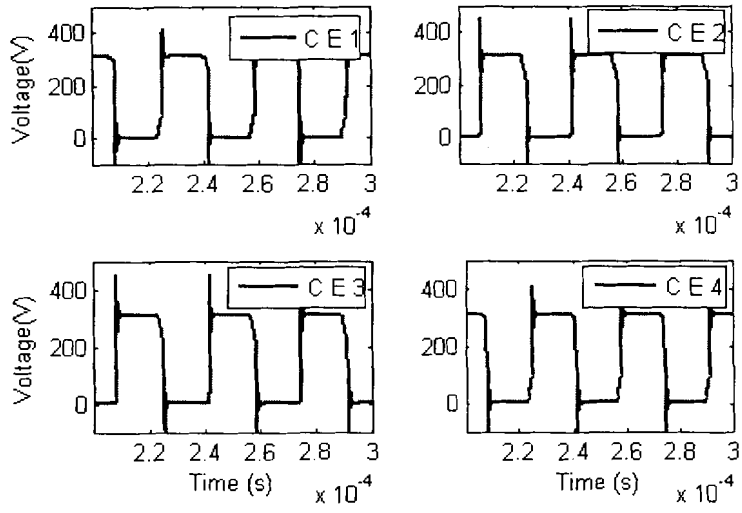

Figure 4-8: The two-state PA collector-emitter voltage waveforms

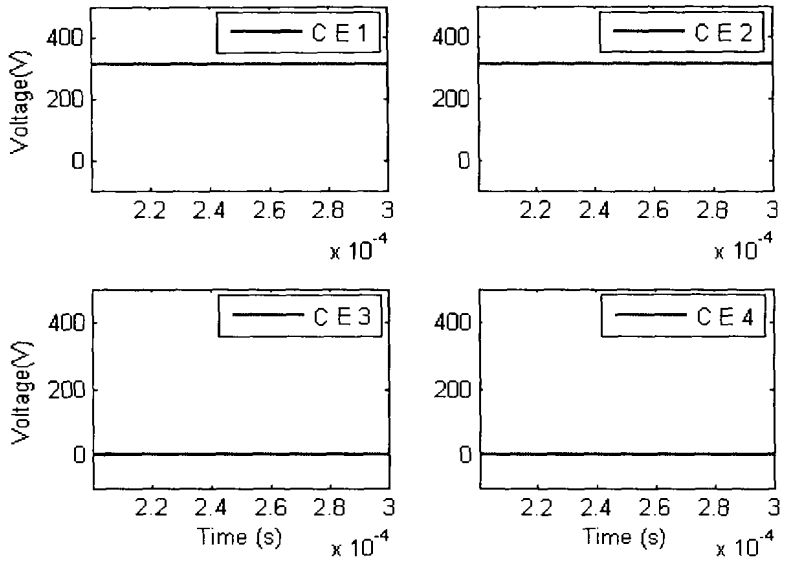

Figure 4-9: The three-state PA collector-emitter voltage waveforms

For a positive current through the coil, the collector-emitter voltages across the three-state H-bridge switches are shown in Figure 4-10. S1 is switched on with an approximately 1 % duty cycle and S2 with approximately 99 % duty cycle.

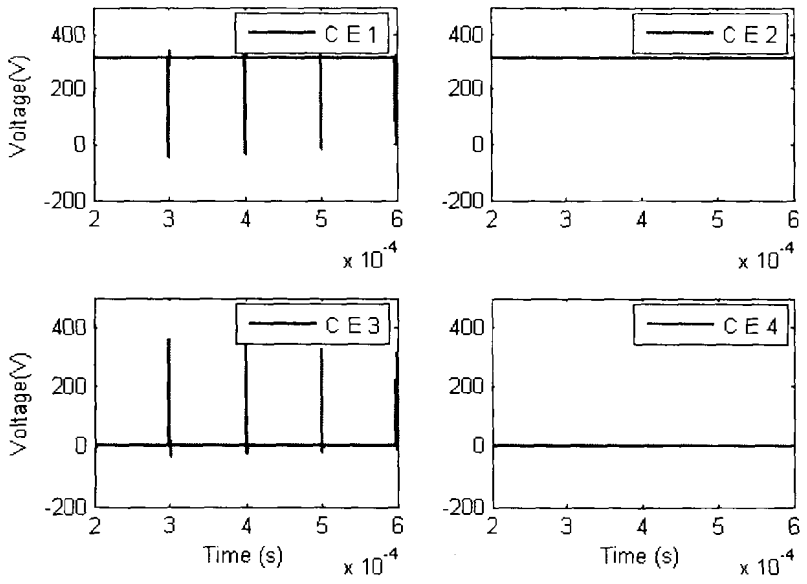

Figure 4-10: Three-state PA collector-emitter voltage waveforms for positive current

4.2.2 *Load simulation*

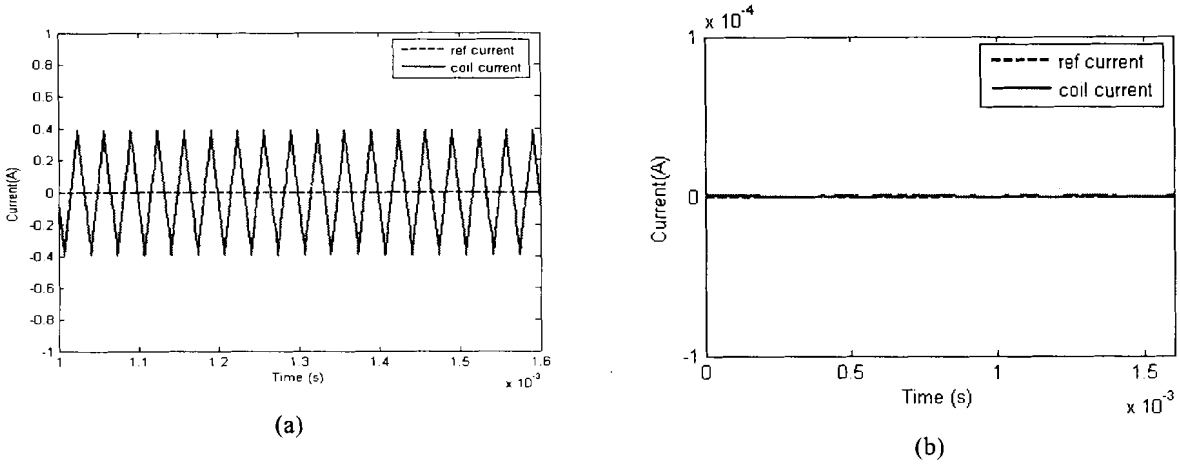

Figure 4-11: A zero current flowing through the coil (a) two-state PA and (b) three-state PA

Figure 4-11(a) and (b) respectively shows a ripple component in the coil current for the two-state and the three-state PA, when 0 A is desired. The current ripple in a two-state PA is approximately 740 mA and very close to 0 A in a three-state PA. Figure 4-12 displays a 10 A current flowing through the load for both two-state and three-state switching techniques. The ripple component did not change much. A current ripple of approximately 10 mA is measured in a three-state PA. In a two-state PA, the current ripple component is still the same for zero and maximum current levels. As the ripple current component induces eddy currents in the magnetic circuit and the eddy current losses are a function of the amplitude of the ripple component. The reduced ripple component due to the three-state technique will greatly minimise the eddy current losses in the AMB coil.

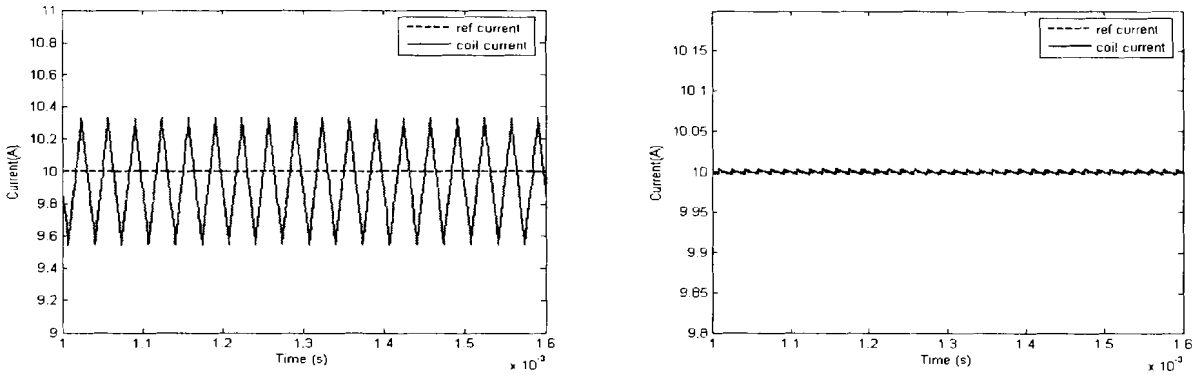

Figure 4-12: 10 A current flowing through the coil (a) two-state PA and (b) three-state PA

Figure 4-13(a) and (b) displays the coil current and voltage for the two-state PA and three-state PA, respectively. A two-state PA maintains the current to the desired level by switching the coil voltage between a positive and negative voltage. A three-state PA switches the coil voltage between a positive and zero voltage for positive current and between negative and zero voltage for negative current.

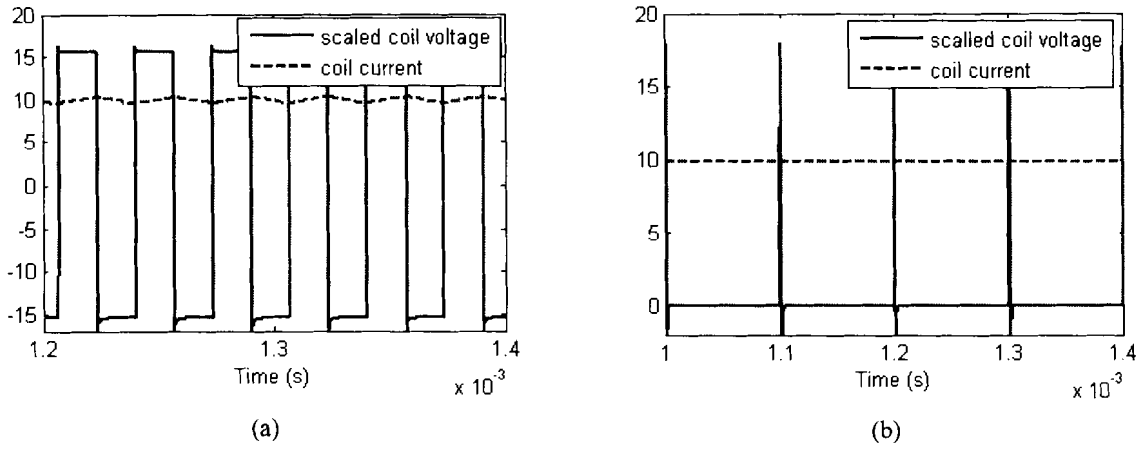

Figure 4-13: Simulated coil waveforms (a) two-state PA and (b) three-state PA

Figure 4-14(a) and (b) displays a sinusoidal reference and actual current flowing through the coil for a two-state and a three-state PA, respectively. The reference signal is changing at a frequency of 250 Hz. For both the two-state and three-state techniques, the coil current is able to track the reference signal with minimum error in amplitude and phase-lag.

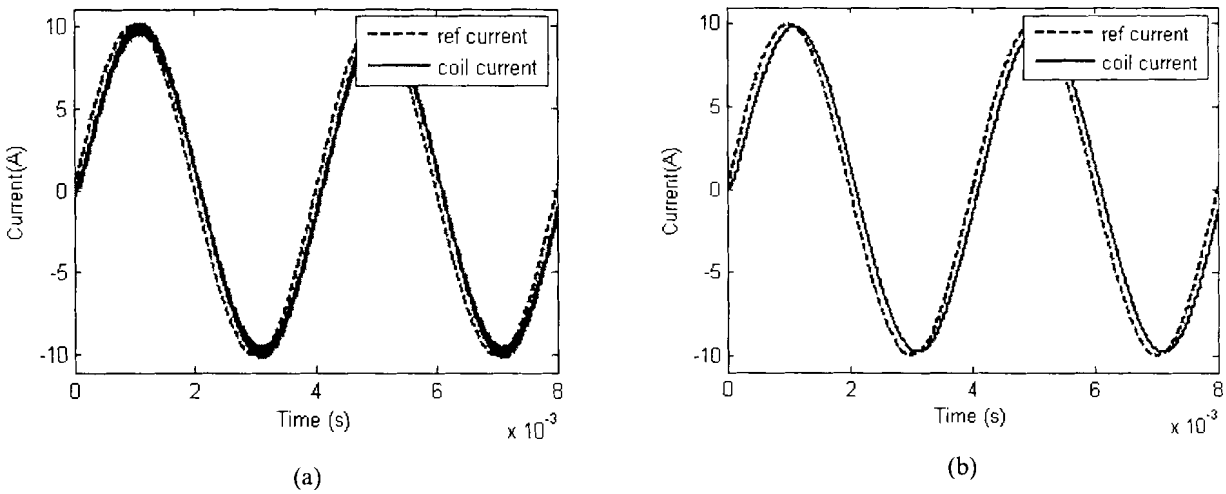

Figure 4-14: Simulated coil current for sinusoidal reference of 250 Hz (a) two-state PA and (b) three-state PA

These results show that both the techniques can reproduce the reference signal with minimum distortion. The only difference in the response of the two techniques is the ripple current component.

The controller produces a control signal that varies the coil voltage in order to make the actual simulation coil current follow the reference signal. Figure 4-15 and Figure 4-16 displays the resulting coil waveforms for a sinusoidal reference input. The two-state PA's coil voltage varies between +310 V and -310 V whereas the three-state PA's coil voltage varies between +310 V, 0 V and -310 V. Note that a three-state PA changes the coil voltage between +310 V and 0 V for an increasing current and between 0

and -310 V for a decreasing current. When zero voltage is applied across the coil, the coil current freewheels and slowly decreases due to the losses in the resistive component of the load.

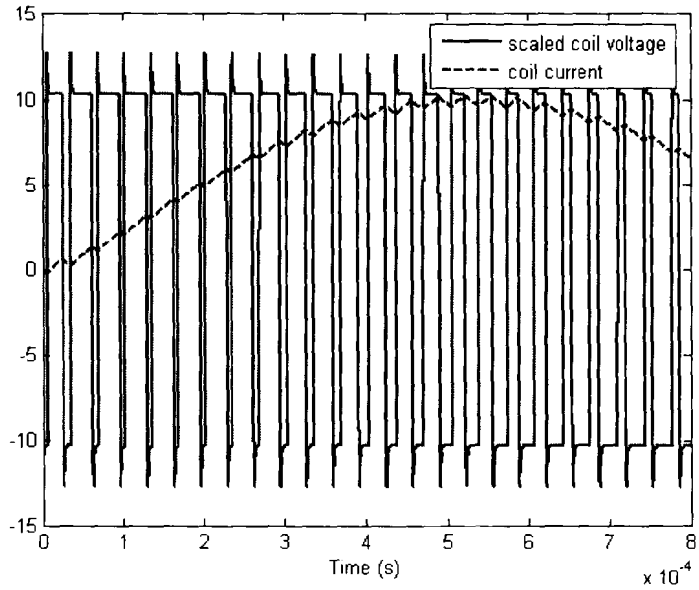

Figure 4-15: Simulated coil current and voltage for sinusoidal reference of 250 Hz for a two-state PA

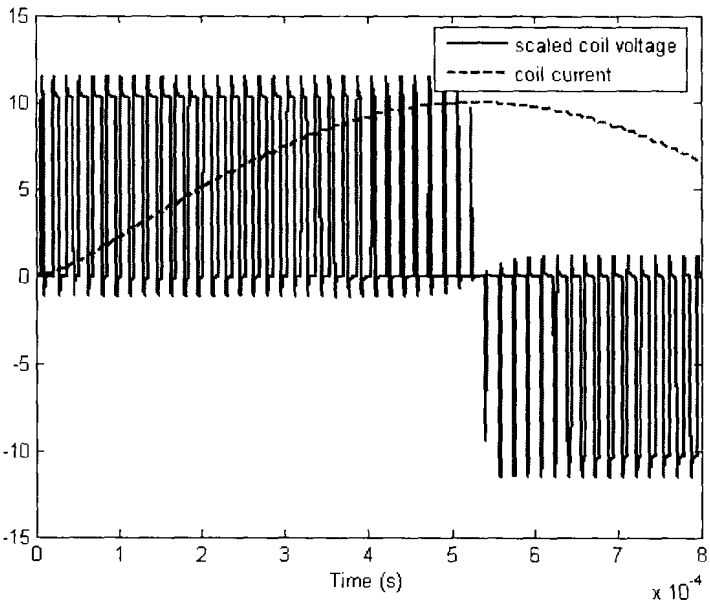

Figure 4-16: Simulated coil current and voltage for sinusoidal reference of 250 Hz for a three-state PA

4.3 Frequency response and power bandwidth

The power bandwidth of the PAs is designed to be 1.5 kHz and the small signal of 2 kHz. The controller constants were predicted in section as K_p = 0.267 and K_i = 0.5. The K_p values was determined from the small signal specifications with (4-2) and K_i was selected based on trial and error method.

$$K_p = \frac{A_t\left(2\pi f_{bw}L - R\right)}{V_{BUS}} \tag{4-2}$$

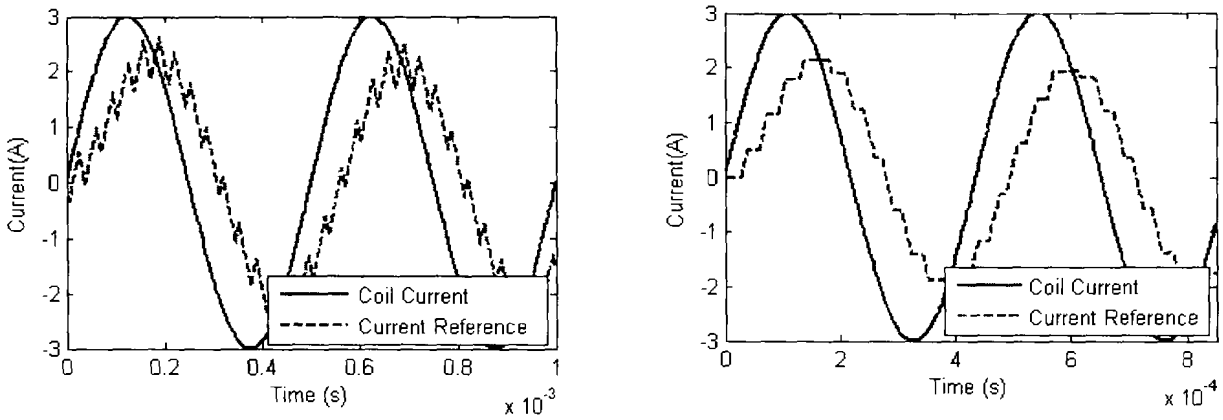

Figure 4-17: PA small signal bandwidth at 2.1 kHz (a) two-state PA and (b) three-state PA

Figure 4-17 displays the coil current signals at the frequency of 2.1 kHz. The reference signal's amplitude was set to 3 A in order to test the small signal bandwidth. The resulting simulation coil current has amplitude which is 70.7 % of the reference satisfying the small signal bandwidth specifications. Both the PAs provides the same frequency response. As expected, the simulated current signals have phase shift when compared to the reference signal at the small signal bandwidth frequency.

Table 4-2 shows the simulated coil current amplitude at different frequencies of the reference signal of amplitude 3 A. The frequency response graph is displayed in Figure 4-18.

Table 4-2 Small signal frequency response of the PA for a reference of 3 A

Frequency (Hz)	**Simulated coil current amplitude (A)**	$Gain = 20\log\left(\frac{I_{act}}{I_{ref}}\right)$ **(dB)**
400	2.8133	-0.55
500	2.825	-0.522
600	2.768	-0.699
800	2.699	-0.918
900	2.704	-0.902
1000	2.648	-1.08
1100	2.577	-1.320
1200	2.564	-1.364
1300	2.5225	-1.538

Frequency (Hz)	Simulated coil current amplitude (A)	$Gain = 20\log\left(\frac{I_{act}}{I_{ref}}\right)$ (dB)
1400	2.463	-1.713
1500	2.441	-1.795
1600	2.392	-1.945
1700	2.324	-2.218
1800	2.311	-2.226
1900	2.28	-2.383
2000	2.234	-2.576
2100	2.1366	-2.947
2200	2.098	-3.106
2300	2.0659	-3.240

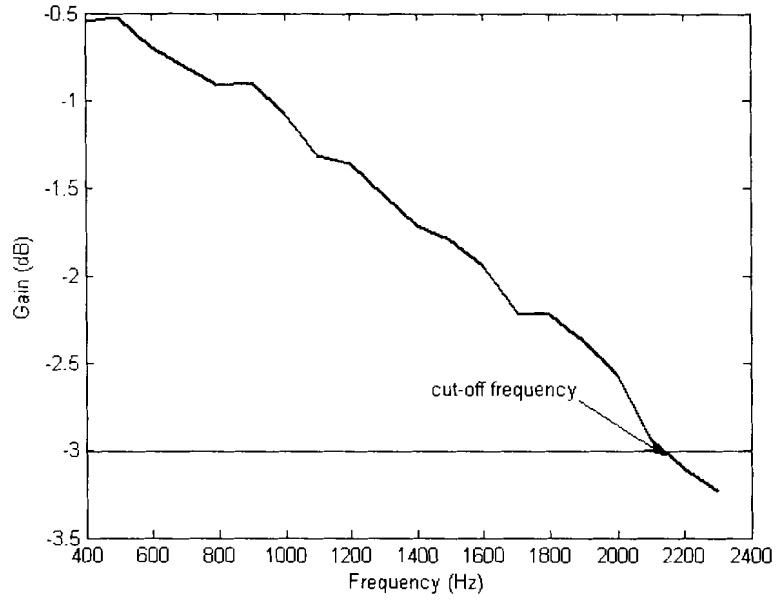

Figure 4-18: Frequency response of the PAs

To simulate the power bandwidth of the PAs, the reference signal of half the amplitude of maximum current is desired to flow through the coil. Figure 4-19 displays the simulated coil current waveforms at the specified power bandwidth frequency of 1.5 kHz; it is seen that both the two-state and three-state PAs response have a linear region when the reference signal is increasing and/or decreasing. This shows that the PAs reaches the specified power bandwidth. Figure 4-20 displays the simulated coil current waveforms at a frequency above the specified power bandwidth. Neither the two-state nor the three-state PA is able to track the reference current signal. The resulting coil current still maintains the amplitude of

the desired current but ramps to minimum or maximum current level with a constant slope. Both the PAs reach the power bandwidth at the specified value.

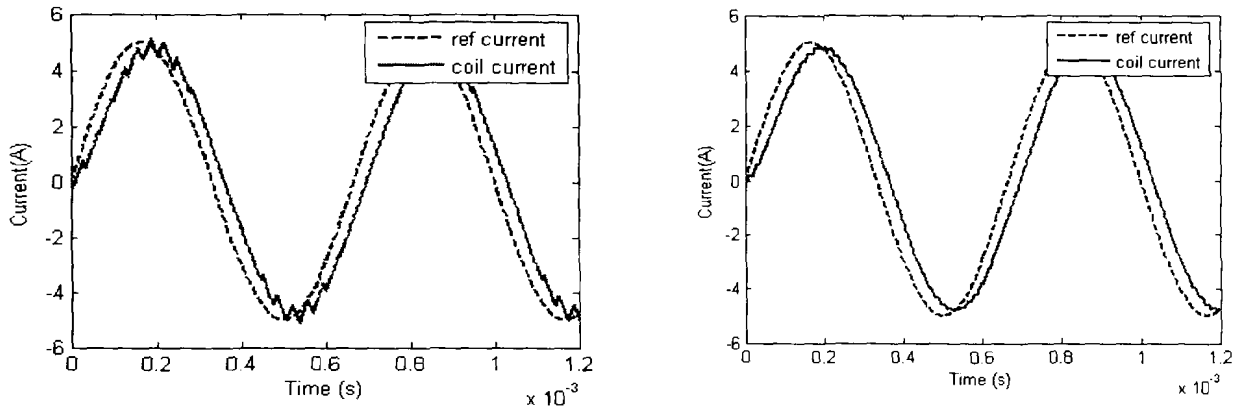

Figure 4-19: PA simulated coil current at a frequency of 1.5 kHz (a) two-state PA and (b) three-state PA

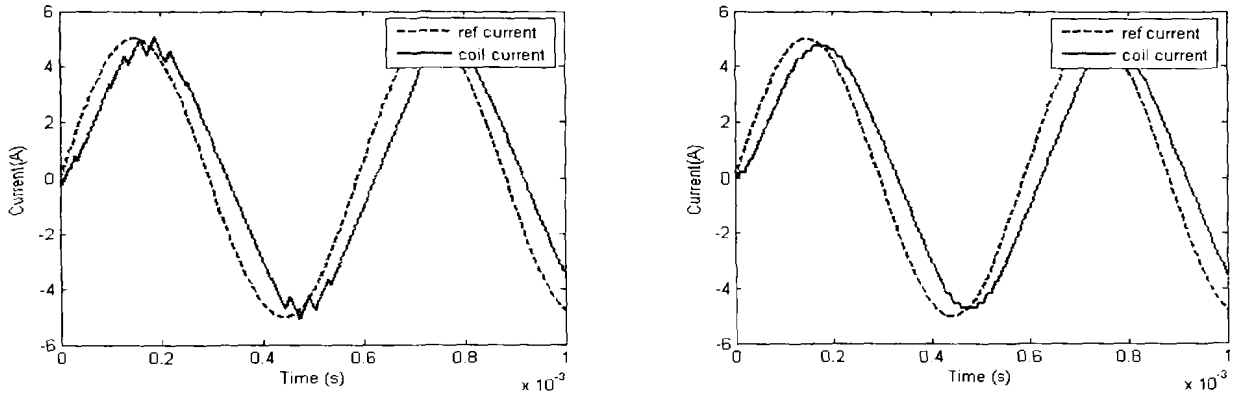

Figure 4-20: PA simulated coil current at a frequency of 1.7 kHz (a) two-state PA and (b) three-state PA

The chapter presented the simulation results of the two-state and the three-state PA. The two PAs were compared based on the control of the H-bridge circuit for different current levels and the power bandwidth of the amplifiers. Simulation results show that the PA with three-state switching technique regulates the coil current with minimum current ripple. The implementation of the three-state technique produces a current ripple of about 1% of the maximum current reference. The reduced ripple in the coil current reduces the coil losses. The analytical prediction of the small signal bandwidth and the power bandwidth using the controller constant also proved reliable. The next chapter will discuss the experimental results of the two PAs.

5
Chapter

Power amplifier implementation and verification

Chapter 5 discusses the procedure followed to verify and to characterise the power amplifier (PA) circuit. Measurements are taken on different sections of the PA. The protection circuits are evaluated and tested for worst case scenarios. The small signal bandwidth and the power bandwidth of the PA are measured and discussed. The losses resulting on the load due to the PA and the losses on the PA itself are monitored while the efficiency measurements are conducted. All the measurements and tests are conducted on both the two-state and three-state switching techniques in order to compare the two techniques.

5.1 Testing procedure

Figure 5-1 shows the experimental test set-up of the entire system. An AMB coil is connected to the PA circuit and the power supply across the H-bridge. A signal generator is used to generate the desired input reference signals.

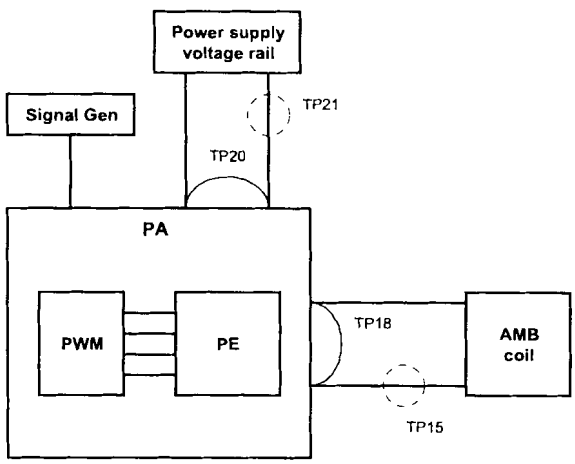

Figure 5-1: Experimental test set-up

Figure 5-2 and Figure 5-3 displays the PA's PE prototype board and the schematic circuit, respectively. Figure 5-3 display the test points (TPs) on the electronics. The TPs are the points where different

waveforms can be observed. The inputs to the opto-couplers are the PWM signals generated by the TMS320P2812 as seen in Figure 5-3. The PWM signals are measured at TP1 - TP4 before they pass through the gate drivers. Test points TP5 - TP8 measure the PWM signals driving the gates of the IGBTs.

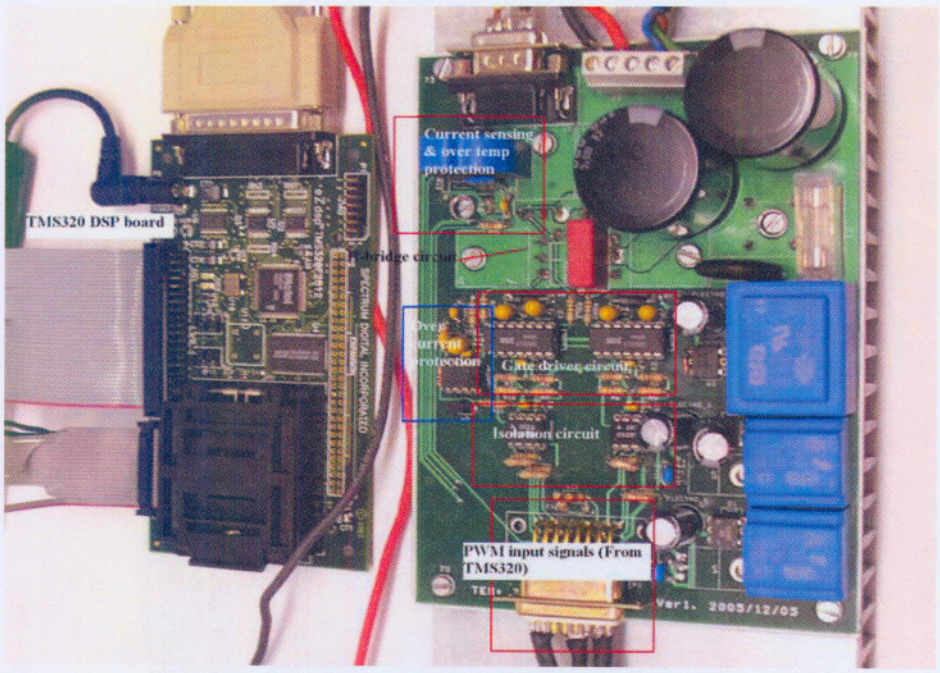

Figure 5-2: The PA prototype board

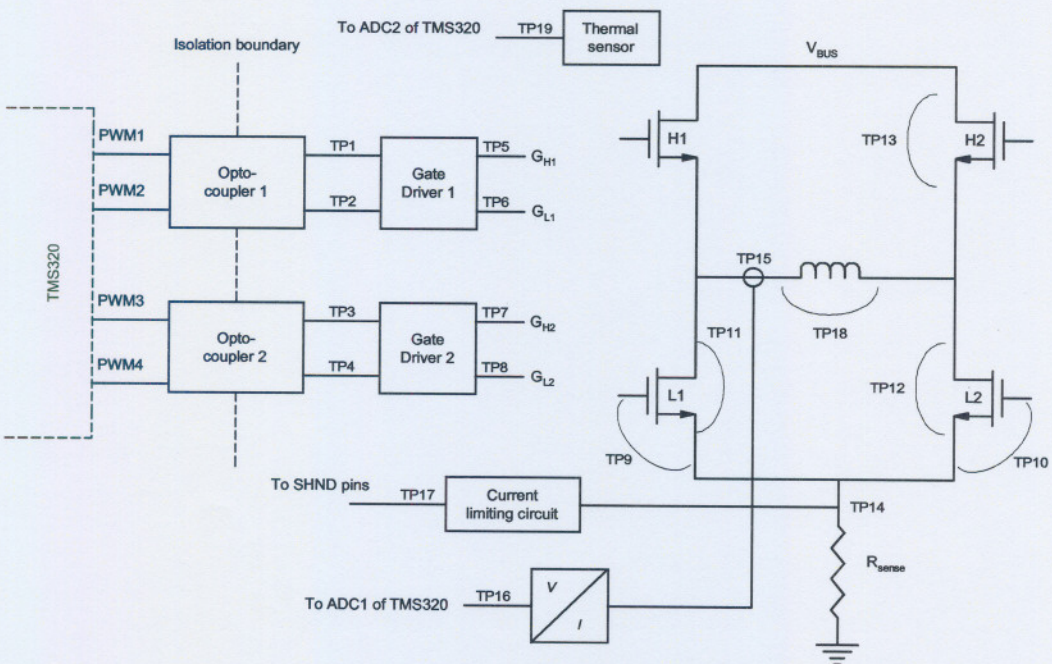

Figure 5-3: PE circuit test points

To study the differences in the two implemented switching techniques, the PWM generation and PE circuit are tested first. At this stage, an AMB coil is connected to the H-bridge circuit and the voltage across the bridge is set to 0 V. The PWM signals are measured at the appropriate output's of the TMS320P2812, the opto-couplers outputs and the gate driver outputs. While observing the PWM waveforms, attention will be on the:

- PWM signals' overshoots,
- PWM signals' phasing and deadband and
- gate signal with incorrect output levels

The next phase of measurements will be to supply the H-bridge with maximum dc voltage. This phase monitors the gate-emitter and collector-emitter signals of the IGBTs when there is no current flowing through the load. The signals are observed at test points TP9 - TP12 for the two low-side IGBTs. The focus on the signals will be at:

- the peak voltages during turn-on and turn-off transients and
- transients in the gate driver signals as this may cause the IGBTs to change states when it is not yet time.

To complete the tests on the PE circuit; a minimum, a zero and a maximum current is allowed to flow through the coil. At this stage, the ripple component of the current will be monitored. Special attention is given to the current sensor output and the current regulation of the two-state and the three-state techniques. The measurements are observed at test points TP15 and TP16.

While the PA is regulating the coil current, an intentional short circuit will be applied by short circuiting the output ports of the H-bridge. The short circuit test is conducted at minimum dc voltage. The maximum peak current that results due to the shorting of the H-bridge output ports and the time it takes the current limiting circuit to respond to this condition will be observed. The test measurements are taken at test point TP15 and TP17 of Figure 5-3. Test point TP17 is the output of the current limiting circuit. The circuit will apply a voltage of 5 V at the shutdown pin of the H-bridge drivers when a current exceeding the set maximum current value, is observed.

The final phase of measurements is to evaluate the performance of the two-state and the three-state PAs in terms of the frequency response and the losses in the load. The frequency response refers to the measurement of the PA's small signal bandwidth and the power bandwidth. The small signal bandwidth will be observed by requesting a signal of lesser amplitude than the specified 10 A amplitude while the power bandwidth will be observed by setting the reference signal to half the specified 10 A and by gradually increasing the frequency of the reference signal to the frequency where half the maximum current can still be achieved without any deformation in the current the coil current signal.

The load losses and the amplifier losses will be measured and evaluated. The efficiency of the PA circuit will be determined by monitoring the input and the output power of the circuit at different current levels.

5.2 Power electronic measurements

The experimental set-up was operated at 20 kHz instead of 30 kHz since more stable operation could be realised. The operation at 30 kHz was limited by the synchronisation of the PWM signals and the cycle time of the DSP. This resulted in significant noise problems.

The PE measurements are conducted to test the PWM generators and the power circuit. The measurements taken are the PWM signals, the gate driver waveforms, collector-emitter waveforms and the resulting coil waveforms for a specific PWM pulse train. The evaluation of the PEs will highlight the difference in the two-state and three-state technique with respect to the PWM switching pattern.

5.2.1 PWM and gate driver waveforms

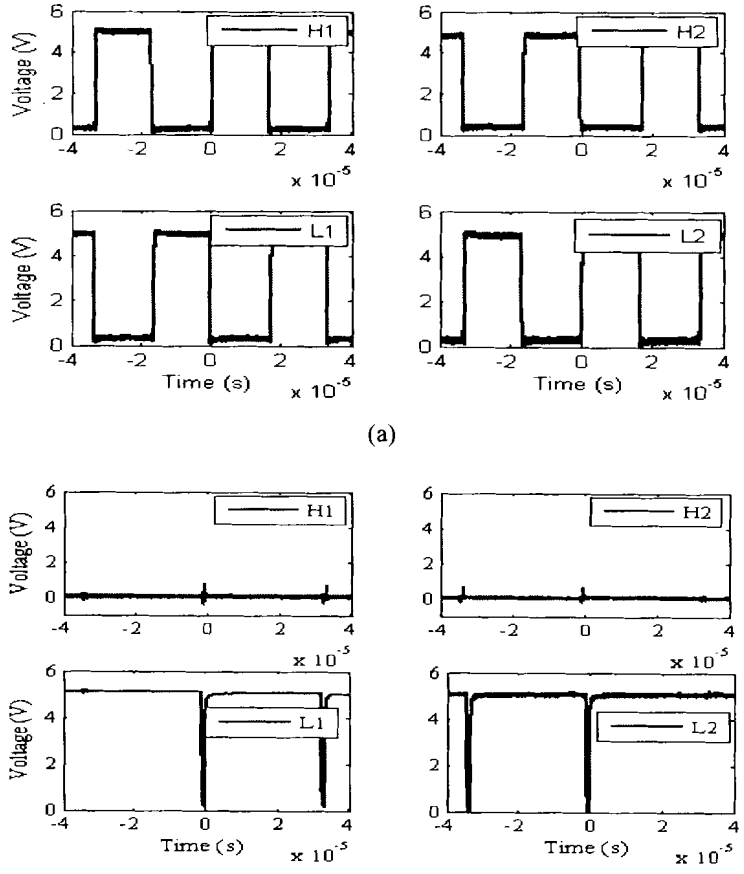

Figure 5-4: PA switching waveforms (a) two-state PA and (b) three-state PA

Figure 5-4(a) and (b) display the PWM waveforms generated by a TMS320P2812 for the two-state and the three-state switching techniques, respectively. The signals are observed at TP1 - TP4 as shown in Figure 5-3. Note that PMW1, PWM2, PWM3 and PWM4 respectively controls high-side 1 (H1), low-side 1 (L1), high-side 2 (H2) and low-side 2 (L2). The two-state PWM signals have a 50 % duty cycle resulting in an average voltage of 0 V across the AMB coil. The three-state technique controls the H-bridge in a different manner as compared to the two-state technique. In a sense that the bottom switches of the H-bridge are controlled with a 100 % duty cycle while the top switches are controlled with a 0 % duty cycle. The signals have a maximum voltage of 5 V.

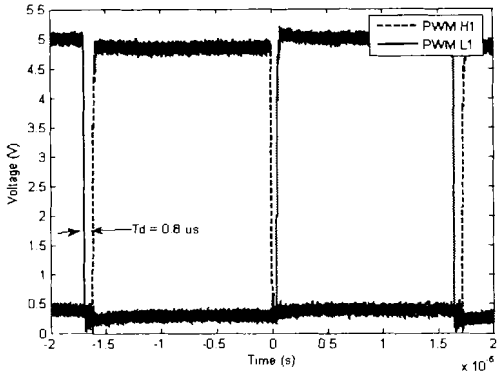

Figure 5-5: Two-state PWM waveforms displaying a deadband period

A transient on the three-state PWM signals controlling the bottom switches is due to the VisSim®'s fixed point maximum value i.e. a duty cycle of 100 % is represented as 0.99997. Ideally, the bottom switches should be on and the top switches should be off for a 0 % duty cycle. Figure 5-4 implies that the two-state technique maintains the coil current by continuously switching the IGBTs with 50 % duty cycle whereas the three-state technique only switches the low side IGBTs fully on in order to maintain the current to a zero level.

Figure 5-5 displays the two-state PWM signals driving one leg of the H-bridge. The PWM waveforms display a deadband time of 0.8 μs which is introduced to eliminate short circuits in the H-bridge legs.

Figure 5-6 displays the two-state PWM signals after being passed through the gate driver circuit. The PWM waveforms reach a maximum voltage of above 15 V which is required to turn-on the IGBTs. The generated PWM waveforms have no overshoot and the signals driving a single leg of an H-bridge circuit are complements of each other. In order to utilise the IGBTs in hard switching mode, the IGBTs require a gate voltage between 10 V and 20 V to turn-on. Therefore, the output levels of the PWM signals are at the acceptable level to switching the IGBTs.

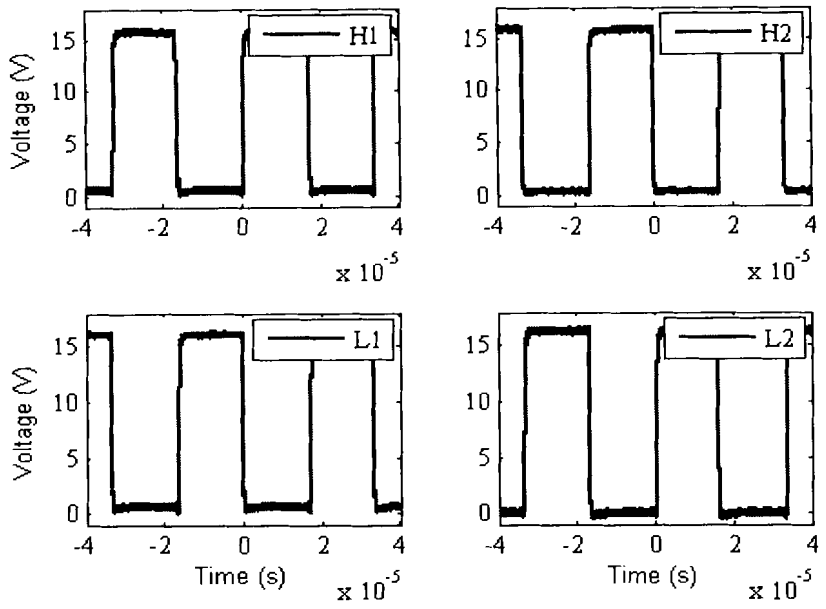

Figure 5-6: Two-state PWM waveforms at the outputs of the gate drivers with 0 V across the H-bridge

As the voltage is applied across the coil, the gate-emitter voltage waveforms of the low side IGBTs are measured at TP9 and TP10. Figure 5-7 displays the IGBTs gate-emitter waveforms at a bus voltage of 310 V. It is observed that the gate-emitter waveforms experience the switching transients when the switches on the same leg of the H-bridge change states. The switching transients will be discussed in detail when the collector-emitter voltages of the IGBTs are analysed.

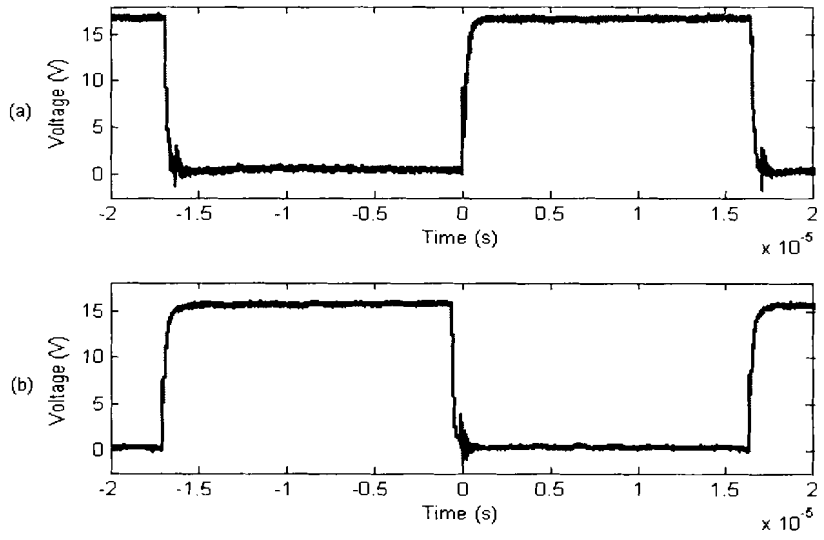

Figure 5-7: Two-state gate-emitter voltage waveforms, V_{BUS} = 310 V (a) high side 1 and (b) low side 1

5.2.2 *Coil waveforms and collector-emitter waveforms*

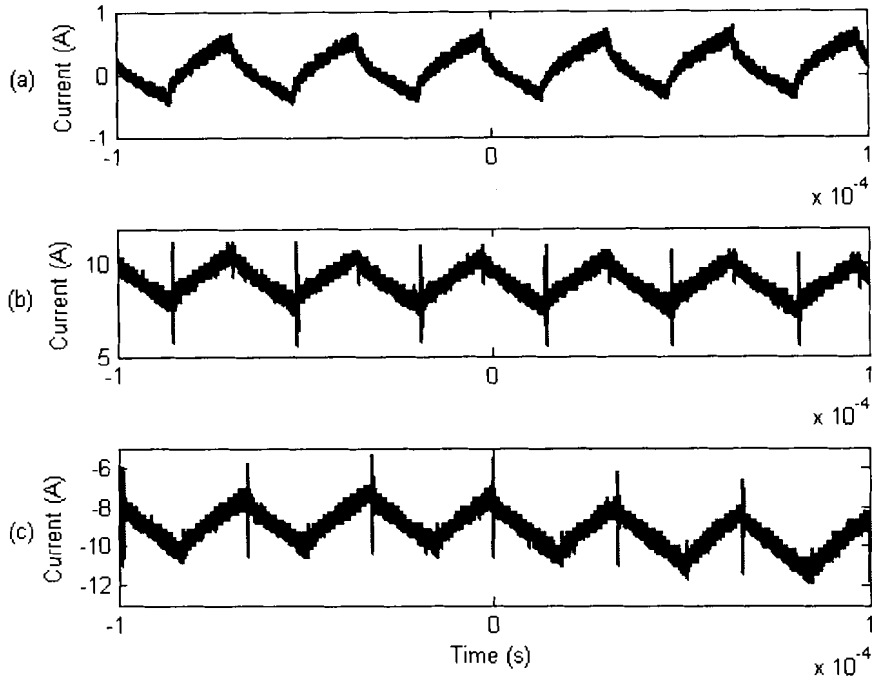

Figure 5-8: Two-state PA coil current (a) at zero current and (b) positive current and (c) negative current

Figure 5-8(a), (b) and (c) display the two-state coil current waveforms for zero, +9A and -9A respectively. The recorded current ripple in the load is 0.8 A for a reference current of 0 A and 2 A for a reference current of +9 A and -9 A.

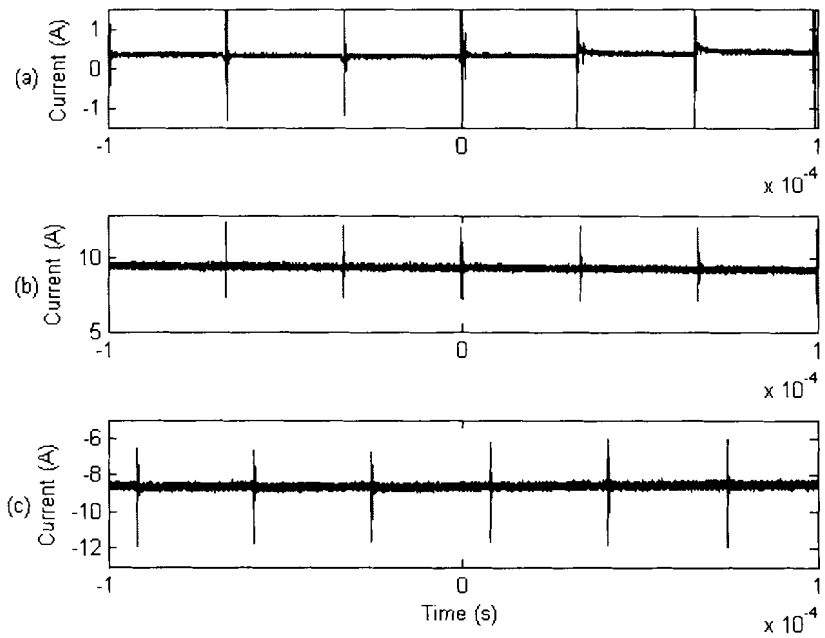

Figure 5-9: Three-state PA coil current (a) at zero current and (b) positive current and (c) negative current

For the three-state PA, the coil currents are shown in Figure 5-9. The recorded ripple component in the currents is approximately 0 A. The three-state technique achieves low ripple current due to the freewheeling state it incorporates.

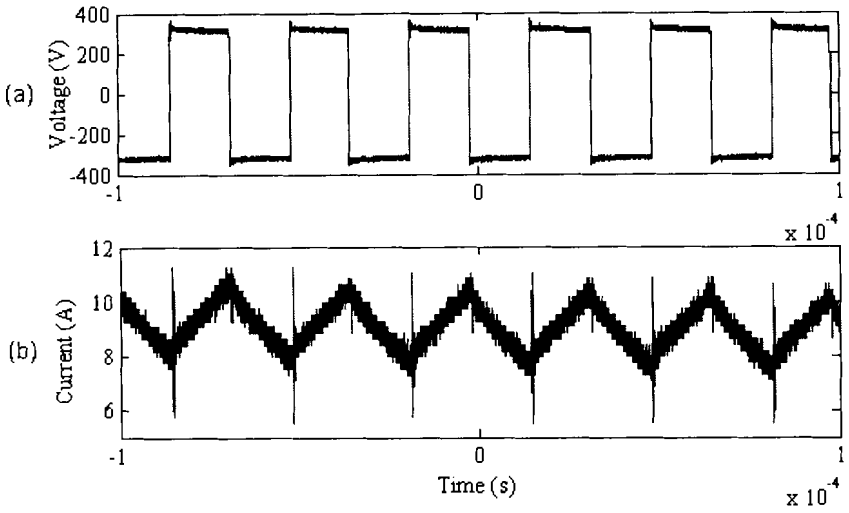

Figure 5-10: Two-state PA coil waveforms (a) applied voltage and (b) coil current

Figure 5-10(a) and (b) displays the coil voltage and current for the two-state operating PA. Note that for a positive voltage across the coil; the high-side 1 and low-side 2 IGBTs are switched-on and the current increases with a positive slope. A negative voltage across the coil result when high-side 2 and low-side 1 are switched on and the current decreases with a negative slope.

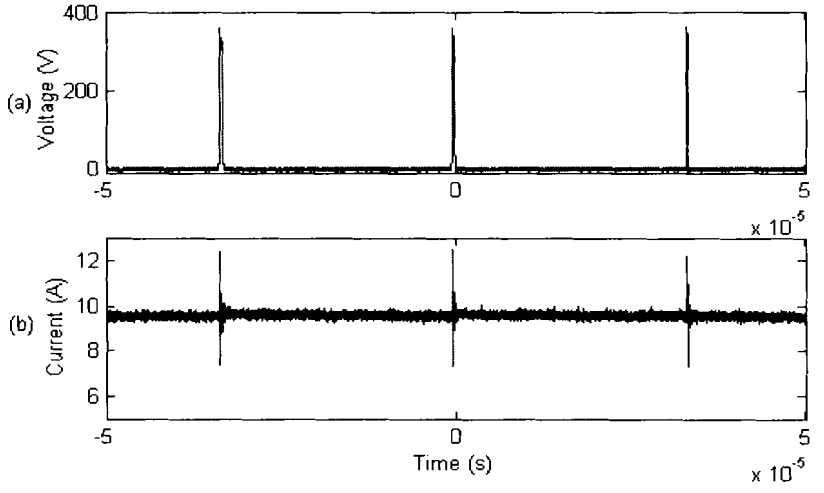

Figure 5-11: Three-state PA coil waveforms for a current of 9.5 A (a) applied voltage and (b) coil current

The three-state PA coil waveforms are shown in Figure 5-11. Most of the time, a zero voltage is applied across the load in order to maintain the coil current at a constant level-freewheeling state. During the freewheeling state, the current slowly decreases with a negative slope. A positive voltage is only applied across the coil to change the coil current level.

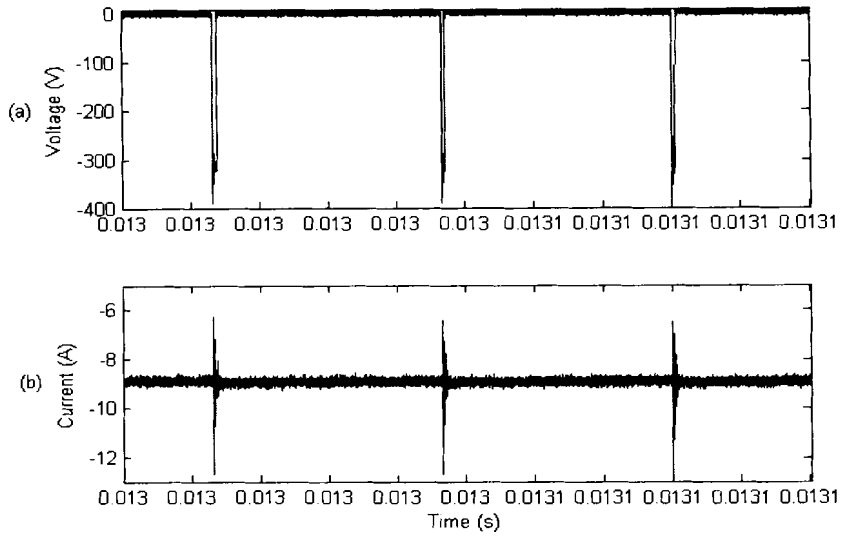

Figure 5-12: Three-state PA coil waveforms for a current of –9 A (a) applied voltage and (b) coil current

Figure 5-12(a) displays the coil voltage for a constant negative current and Figure 5-12(b) displays the resulting coil current. For a constant negative current, a negative and a zero voltage are applied across the load. It is important to note that for an increasing coil current, only a positive and zero voltage will be applied across the load. Also, a decreasing coil current will result in a negative and zero voltage being applied across the load.

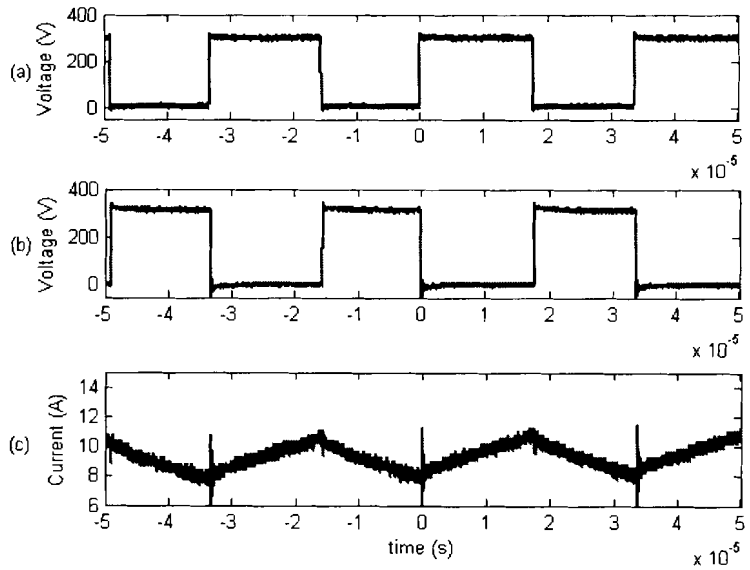

Figure 5-13: The two-state collector-emitter waveforms for the low side IGBTs (a) low side 1 (b) low side 2 and (c) coil current

Figure 5-13 displays the collector-emitter voltages of the low side IGBTs together with a maximum coil current of 10 A for the two-state switching technique. The low-side 1 conducts only the negative slope of the coil current and the low-side 2 conducts only the positive slope of the coil current.

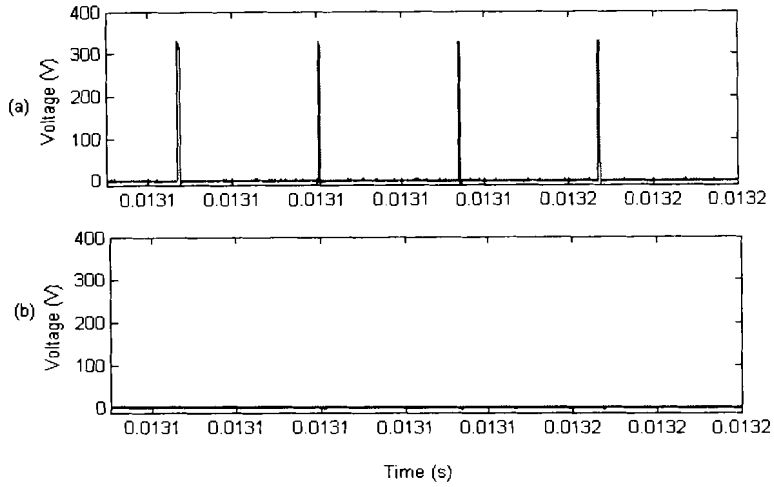

Figure 5-14: The three-state collector-emitter waveforms for the low side IGBTs (a) low side 1 (b) low side 2

For the three-state PA regulating a positive current, the collector-emitter waveforms of the low side IGBTs are displayed in Figure 5-14. The low side 1 IGBT will conduct the negative slope of the current. Note that the low side 2 IGBT conduct both the negative and positive slope of the coil current. This is due to the fact that for positive coil currents, the low side 2 IGBT is always on. For negative coil currents, the low side 1 IGBT is always on. Therefore, the IGBT conducts both the negative and positive slope currents and the low side 2 will conduct only the positive slope current.

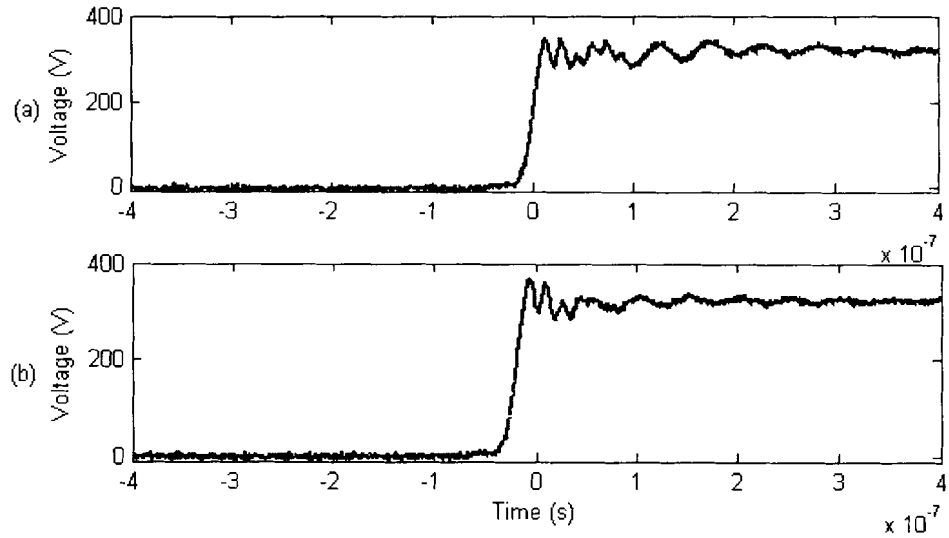

Figure 5-15: Low side 1 IGBT switch off voltage (a) two-state switching technique (b) three-state switching technique

Figure 5-15(a) and (b) display the low-side switch on transient for the two-state and the three-state switching techniques respectively. For both the switching techniques, the IGBT takes approximately 50 ns to switch to the on-state.

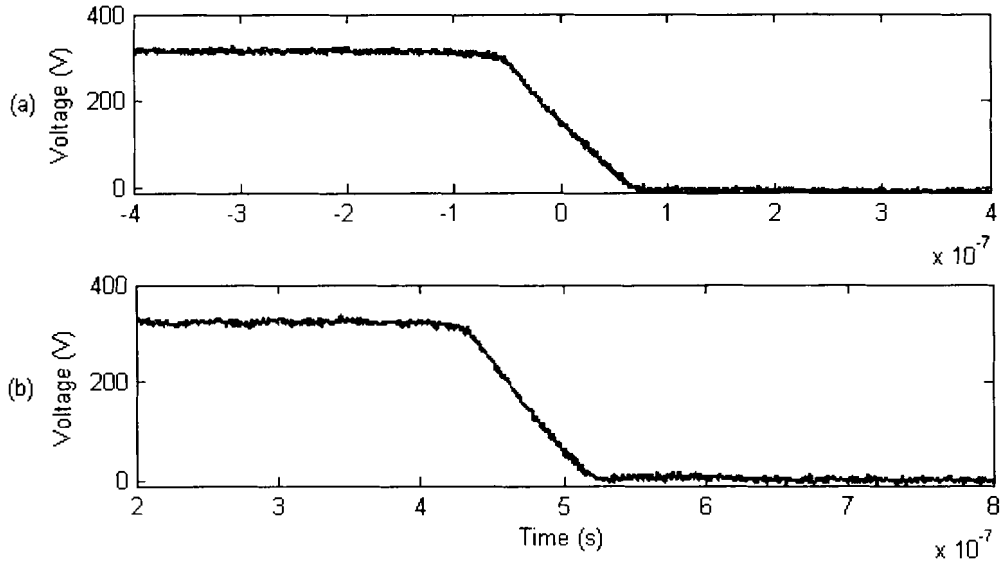

Figure 5-16: Low side 1 IGBT switch on voltage (a) two-state switching technique (b) three-state switching technique

Figure 5-16(a) and (b) display the low-side IGBT switch-off transients for the two-state and three-state switching PAs, respectively. For both the PAs, the IGBT takes approximately 110 ns to switch to the off-state position.

5.3 Control

This section evaluates the control loop of the PAs. It characterises the two-state and the three-state switching topologies in terms of the dynamic and the frequency response.

5.3.1 Feedback

Figure 5-17(a) and (c) display the output voltage waveforms of the LEM sensor for a current of +11 A and -11 A as shown in (b) and (d) respectively. It is clear that a mean current of 11 A flowing through the coil translates to approximately 3.3 V at the output of the LEM sensor. Also, for a mean current of -11 A, the LEM sensor will output a mean voltage of approximately 1.6 V. The output voltage of the LEM for a three-state PA is shown in Figure 5-18. The figure only shows the output for 11 A flowing. Note that the output of the LEM is the replica of the coil current. It is in the form of a small signal due to the LEM sensor gain. The gain is compensated in the DSP.

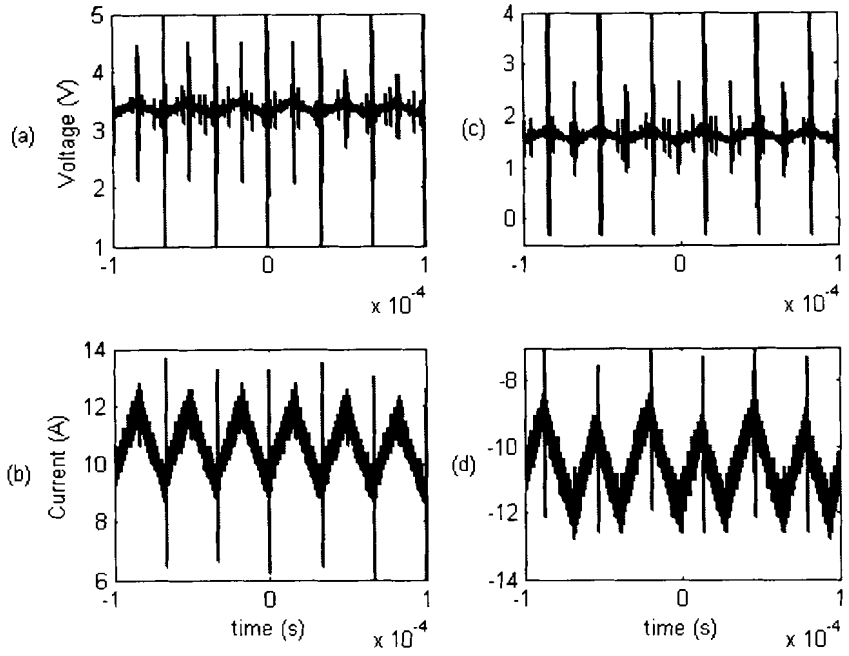

Figure 5-17: The LEM sensor output voltage and the coil current (a) LEM output for 11 A current (b) 11 A coil current (c) LEM output for -10 A current and (d) -11 A coil current

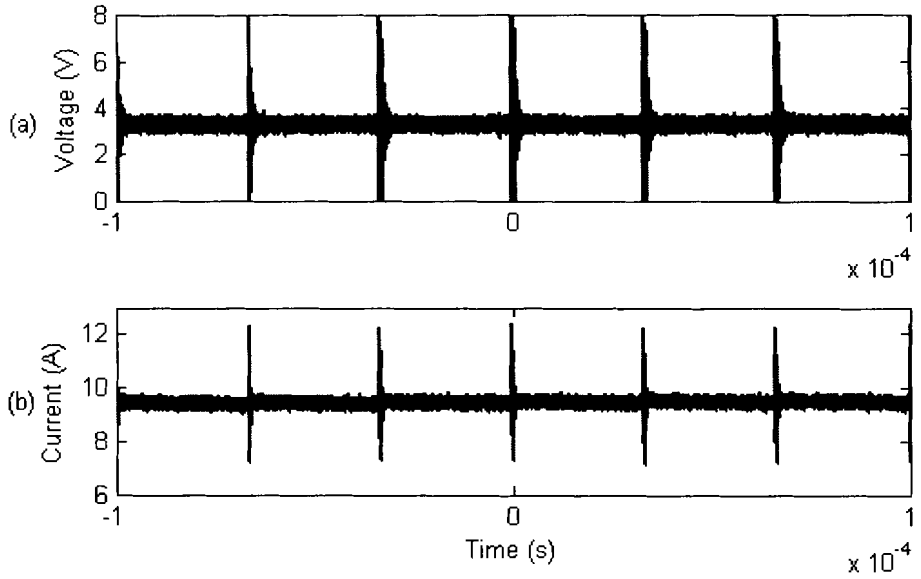

Figure 5-18: The LEM sensor output voltage and the coil current for three-state PA (a) LEM output for 9 A current (b) 9 A coil current

5.3.2 Dynamic response

The PA's response to a ±10 A sinusoidal reference current for the two-state and the three-state techniques is displayed in Figure 5-19(a) and (b) respectively. The voltage across the H-bridge is set to 310 V. The

resulting coil current of both the techniques follows the reference signal. The response of a PA controlled by the three-state switching technique has a minimum ripple component. As mentioned in section 5.2.2 under the coil current discussion, the reduced ripple component in the actual waveform is due to the freewheeling state employed by the three-state technique.

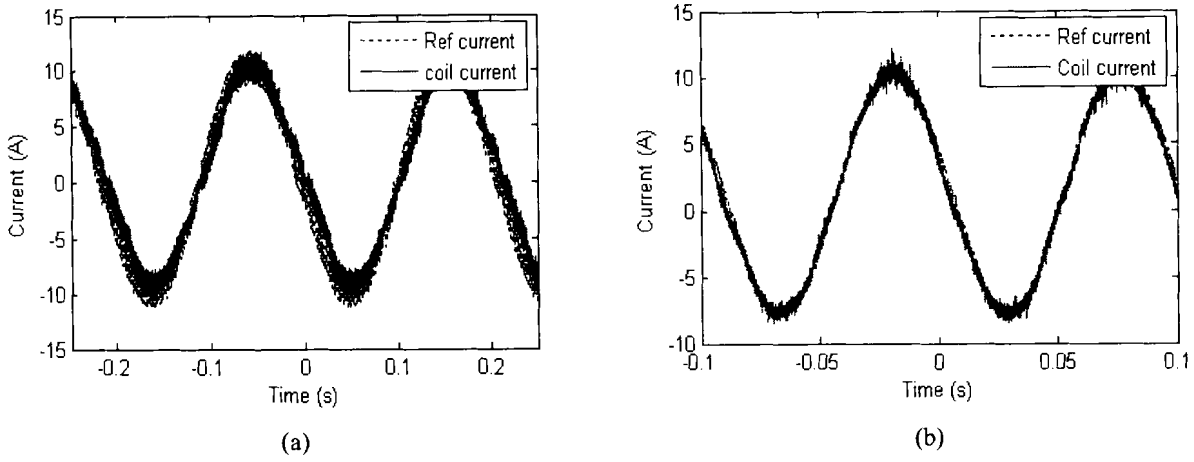

Figure 5-19: Sinusoidal response (a) two-state PA (b) Three-state PA

5.3.3 Frequency response

Power bandwidth

The power bandwidth of the amplifier is determined by applying a sinusoidal reference signal with amplitude equal to half of the PA's maximum current level. The frequency is increased to a point where the resulting coil current can no longer track the reference signal without distortion. Figure 5-20 and Figure 5-21 respectively display the response of the PAs operating at a bus voltage of 310 V across the H-bridge for a 200 Hz and 500 Hz sinusoidal reference. The responses of the PAs appear noisy at this frequency levels. As the reference signal's frequency is increased, the response becomes more susceptible to noise.

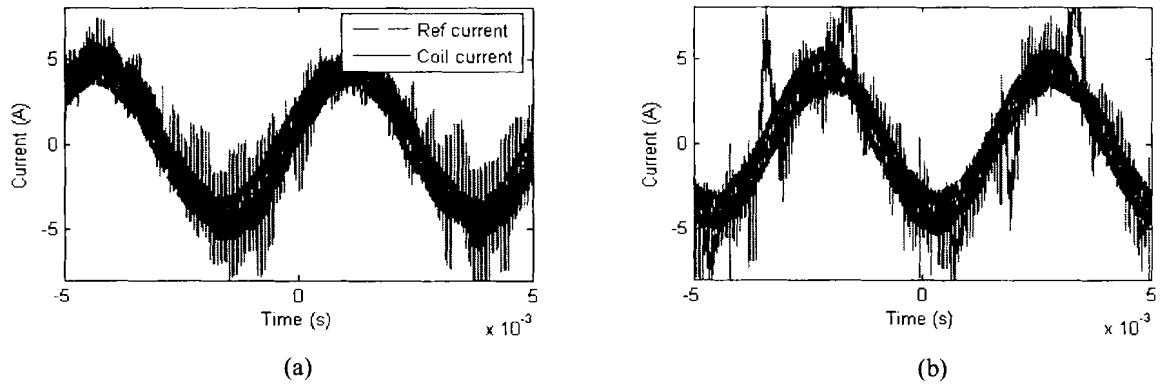

Figure 5-20: PAs response at 200 Hz, 310 V across the H-bridge (a) two-state and (b) three-state

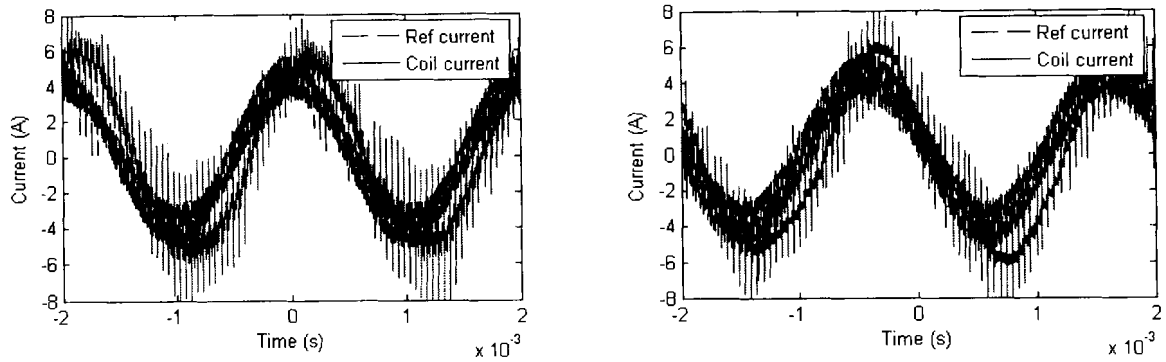

Figure 5-21: PAs response at 500 Hz, 310 V across the H-bridge (a) two-state and (b) three-state

Due to the excessive noise levels produced for high frequency reference signals, the power bandwidth of the PAs could not be measured at 310 V across the H-bridge. To verify the power bandwidth prediction, the voltage across the H-bridge is reduced to 50 V and 130 V. The new power bandwidth is then estimated for the two voltage levels across the H-bridge. The estimated power bandwidth at the bus voltages is predicted by (5-1).

$$f_{pbw} = \frac{V_{BUS}}{\pi L I_{\max}} \tag{5-1}$$

V_{BUS} is the voltage applied across the AMB coil, L is the inductance of the coil and I_{max} is the maximum current level. For a bus voltage of 50 V and 130 V, the expected power bandwidth is 217 Hz and 550 Hz respectively. Figure 5-22(a) and (b) respectively displays the PA power bandwidth of the two-state and three-state PAs when a voltage of 50 V is applied across the H-bridge. The two-state reaches a power bandwidth of 200 Hz and the three-state reaches a wide power bandwidth of 220 Hz. Notice that the resulting power bandwidth are within ranges of the predicted power bandwidth.

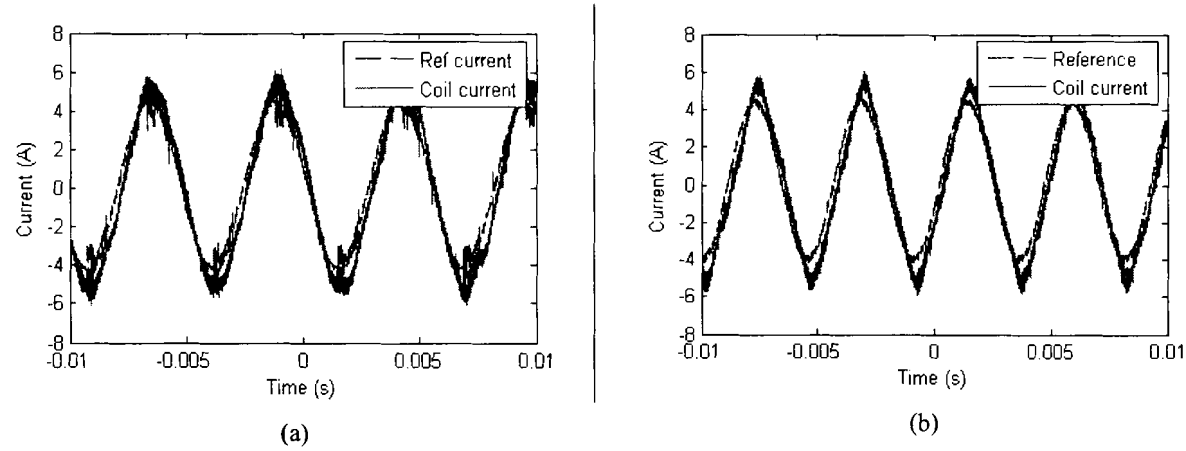

Figure 5-22: PAs power bandwidth, 50 V across the H-bridge (a) two-state power bandwidth at 200 Hz and (b) three-state power bandwidth at 220 Hz

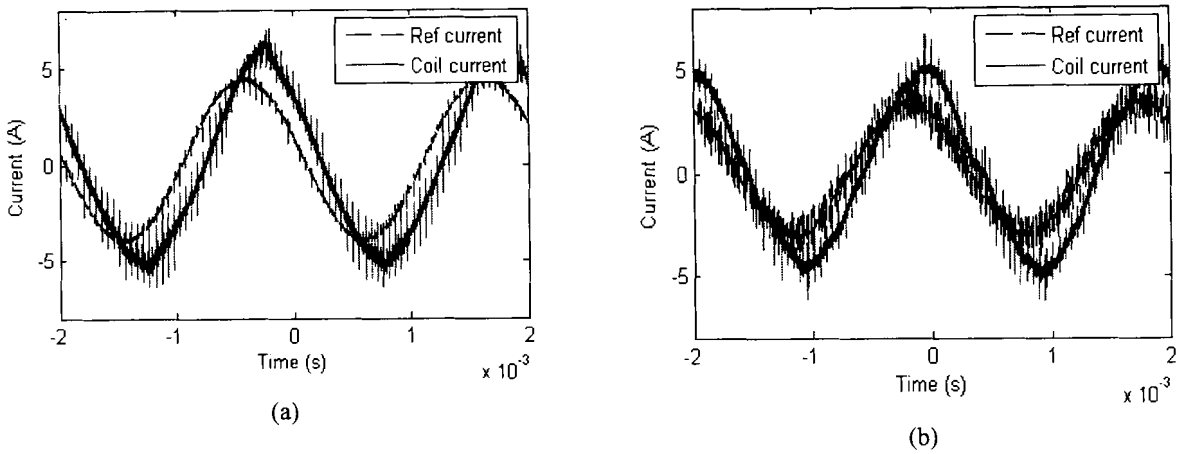

Figure 5-23: PAs power bandwidth, 130 V across the H-bridge (a) two-state power bandwidth at 470 Hz and (b) three-state power bandwidth at 520 Hz

Figure 5-23 shows the power bandwidth at 130 V. The PAs exhibit the power bandwidth of 470 Hz and 520 Hz for the two-state technique and three-state technique respectively. The measured power bandwidth has a percentage error of less than 20 % as compared to the predicted power bandwidth of 560 Hz.

Small signal bandwidth

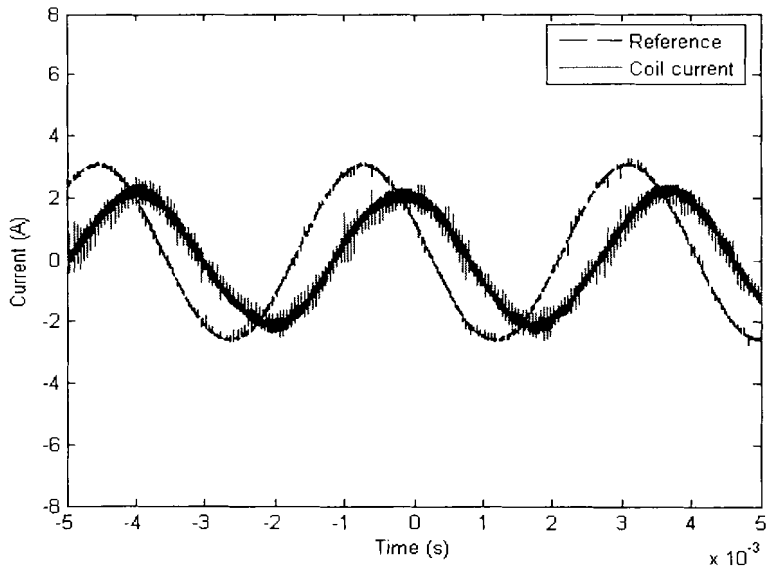

Figure 5-24: Small signal bandwidth of the two-state PA, for 50 V across the H-bridge

The small signal bandwidth is measured at lower current levels and bus voltage levels. At a 50 V bus voltage, the two-state PA displayed a small signal bandwidth of 260 Hz. The two-state's small signal bandwidth response is shown in Figure 5-24. A small signal bandwidth higher than 500 Hz could not be measured, as the response of the PA became noisy at high frequencies.

5.4 Protection

5.4.1 Over current protection

Figure 5-25 displays the short circuit condition at 80 V across the H-bridge. Figure 5-25(a) and (b) respectively shows the voltage on the shutdown pin of the half-bridge driver and the resulting current waveform. When a short circuit condition occurs, it takes the current limiting circuit approximately 350 ns to terminate the gate drive pulses. The gate drive pulses are terminated when the IGBTs conduct a current of 55 A.

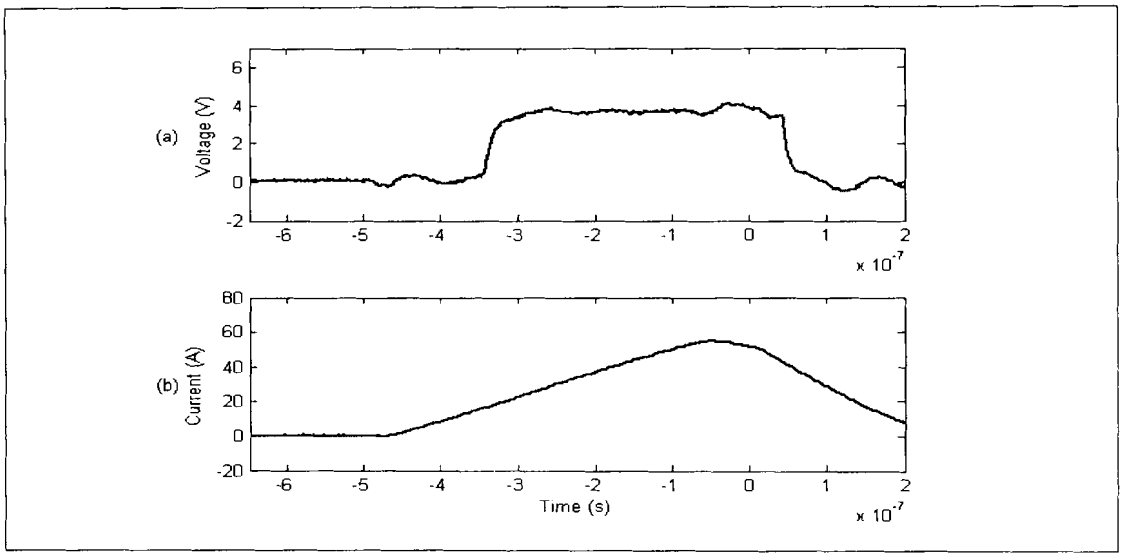

Figure 5-25: Short circuit condition, 80 V across the bridge (a) shutdown pulse and (b) current waveform

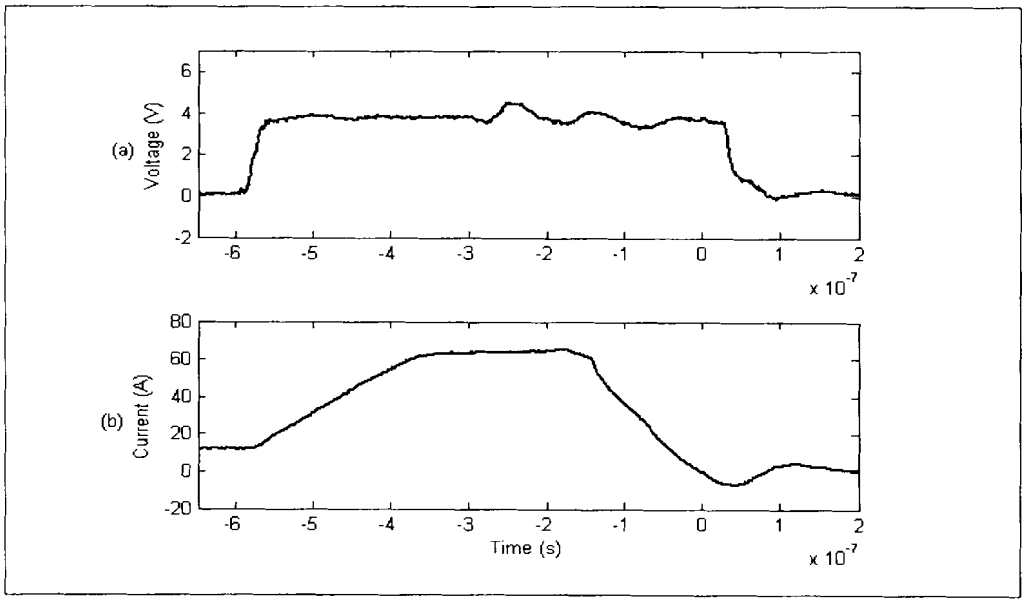

Figure 5-26: Short circuit condition, 80 V across the bridge (a) shutdown pulse and (b) current waveform

Figure 5-26 displays the resulting short circuit condition at 150 V across the H-bridge. The current waveform flattens when it reaches a current of 60 A. This is due to the current probe that was used for the measurements. The probe can measure a maximum current of 60 A.

The short circuit current levels at 80 V and 150 V, are used to predict the short circuit current peak at a voltage level of 310 V to be 227 A. The peak current of 227 A does not guarantee the safe operation of the H-bridge circuit. This current level is above the IGBT's repetitive peak current rating of 220 A. The PA will therefore not be short-circuit protected at 310 V.

5.5 Power measurements

The power measurements on the PAs were conducted by varying the current level from a minimum to a maximum value. A (6.6 mH + 0.261 Ω) AMB coil was used to conduct the power measurements. Table 5-1 and Table 5-2 respectively show the power measurements of the two-state and the three-state PAs at different current levels.

Table 5-1: Two-state PA power measurements

I_{Coil} (A)	P_{in} (W)	P_{out} (W)	$P_{H\text{-}bridge}$ (W)
0	67.8	55	12.8
0.66	70.2	56.3	13.9
1.873	76.7	57.9	18.8
2.770	82.4	60.32	22.08
3.854	91.1	64.6	26.5
4.761	99.9	69.2	30.7
5.732	110.0	71.8	38.2
6.785	122.1	77.2	44.9
7.845	135.7	84.3	51.4
8.970	150.9	94.6	56.3
10.090	168.9	103.8	65.1

Table 5-2: Three-state PA power measurements

I_{Coil} (A)	P_{in} (W)	P_{out} (W)	$P_{H\text{-}bridge}$ (W)
0.946	13.6	2.23	11.37
2.058	17.4	5.07	12.34
3.284	23.32	4.87	18.45

3.933	26.76	6.06	20.70
5.03	32.76	8.83	23.93
6.40	41.4	13.3	28.10
7.06	46.0	15.2	30.8
7.88	52.8	23	29.8
8.71	60.0	25.1	34.9
9.33	65.6	27.4	38.2
10.16	73.4	32.6	40.8

Figure 5-27 displays the relationship between the output power and the current levels in the two-state and the three-state PAs. The figure indicates that the two-state PA produces high losses compared to the three-state PA. As the current level is increased, the output power of the two switching topologies increases at the same rate. At maximum current, the two-state and the three-state PAs produce output powers of 104 W and 33 W, respectivcly. The output power is dominated by the eddy current losses as it will be seen later.

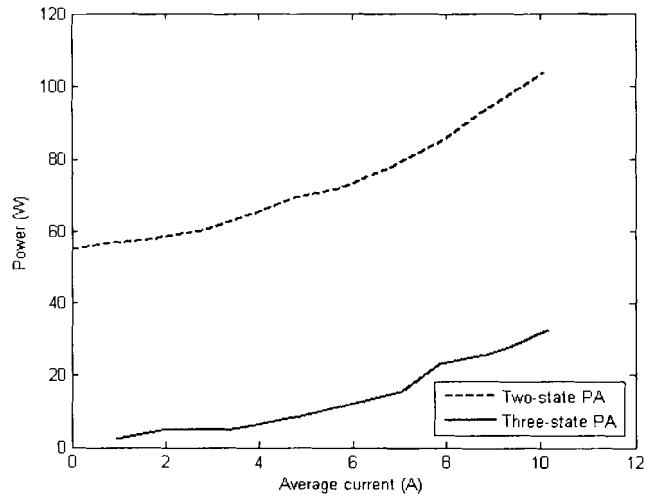

Figure 5-27: Output power vs. coil current

The losses experienced by the PA are obtained by (5-2).

$$P_{H-bridge} = P_{in} - P_{out} \tag{5-2}$$

P_{in} is the input power and P_{out} is the output power. Figure 5-28 graphically reprcsents the H-bridge losses against the coil current. The three-state PA experiences low losses in the H-bridge as compared to a two-state PA. The losses are due to the switching technique employed by the two-state and the three-state PAs.

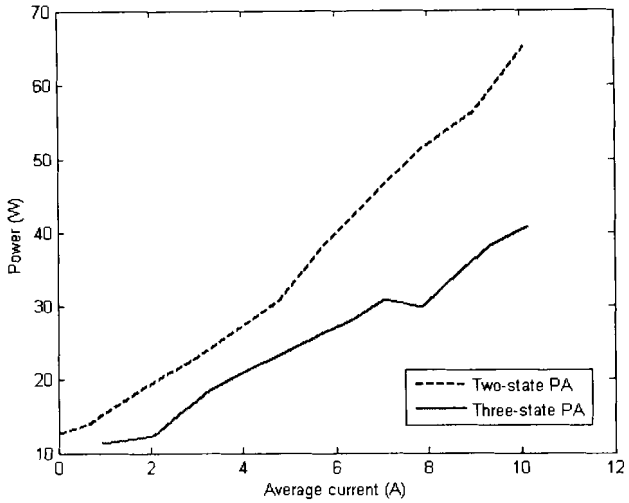

Figure 5-28: PA losses vs. coil current

The copper losses (5-3) experienced by the coil for changing current levels are graphically displayed in Figure 5-29.

$$P_{cu} = I_{rms}^2 R \tag{5-3}$$

I_{rms} is the root-mean-square (rms) value of the actual current and it depends on the ripple component of the actual current. Figure 5-29 illustrates that an AMB coil experiences higher copper losses when the output current is regulated with a two-state PA. The copper losses resulting due to the employment of the two-state technique also dominate at a zero current level. It is due to the high current ripple component in the load current.

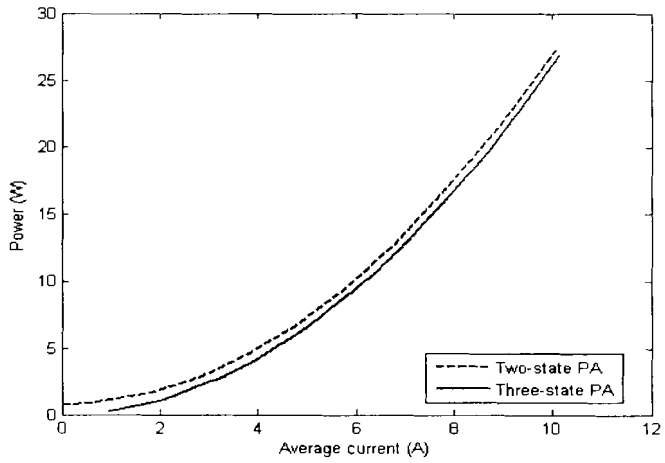

Figure 5-29: Copper losses vs. coil current

The resulting eddy current losses due to the employment of the two-state and three-state PA topologies are displayed in Figure 5-30. The eddy current losses are obtained from (5-4).

$$P_{eddy} = P_{out} - P_{cu} \tag{5-4}$$

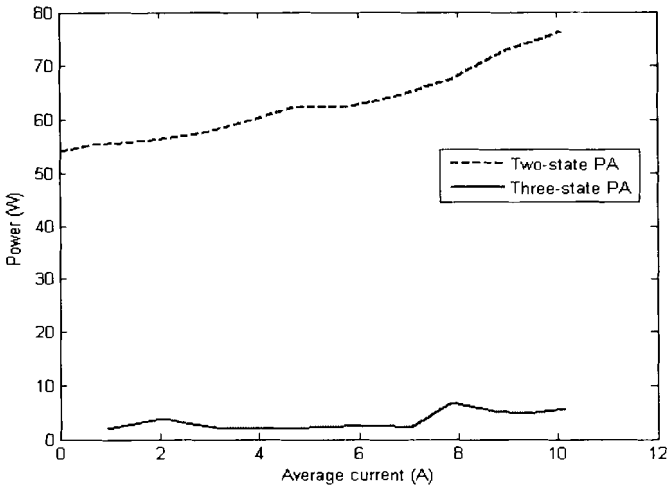

Figure 5-30: Eddy current losses vs. coil current

Here, P_{out} is the output power and P_{cu} is the copper losses of the coil wire. Note that the eddy current losses due to the use of the two-state PA is approximately 55 W at 0 A whereas the three-state PA achieves minimum eddy current losses of about 0 W. As the desired current is increased to maximum level, the eddy current losses drastically increase to almost 80 W in an AMB controlled with a two-state PA. The use of the three-state PA topology results in eddy current losses below 10 W when the desired current is increased to maximum level. The extreme increase in eddy current losses from the use of the two-state PA is due to the high ripple component present in the AMB coil current.

Chapter 5 presented the implementation and verification of the PAs. The reliability of the PE board was tested with short circuit. The two-state and three-state switching techniques were evaluated by regulating the flow of current in the AMB coil. The dynamic response, frequency response and power measurements were used to characterise the switching techniques. Chapter 6 discusses the simulation and practical results, the difference in switching techniques and give the recommendation in improving the PAs.

6
Chapter
Conclusions and Recommendations

Chapter 6 includes the discussion of the results obtained from the two-state and three-state power amplifiers (PAs) in terms of the simulation and practical results and differences in the switching techniques. Recommendations are made for improving the PA performance. A further investigation in the application of power electronics (PE) in the active magnetic bearing (AMB) using other available DSP boards is proposed.

6.1 Conclusion

6.1.1 Simulation and experimental results

The two-state and the three-state PWM switching techniques were implemented in simulations and practically realised. The simulation models of the PAs did not include all the components of the actual PAs. The models were constructed with ideal components and the AMB coil was only modelled as an *RL* circuit which restricted the analysis to the power measurements. Because of difficulty in simulating digital PWM signals and current sensing devices, the generation of the two-state and the three-state PWM signals as well as the current sensing device were constructed with ideal components. The switching frequency of the experimental set-up was at 20 kHz as compared to 30 kHz used for the simulation models. A 20 kHz frequency was used since 30 kHz produced high noise levels due to the limitations on the cycle time of the DSP.

The switching topologies were only implemented in the simulations in order to compare them and to predict the behaviour of the actual system. Useful results were obtained as the simulation and experimental results displayed a close correlation in terms of the coil current regulation at constant levels and sinusoidal reference current of low frequencies. Figure 6-1 and Figure 6-2 display the simulation and the experimental set-up coil current regulation results obtained from a two-state PA and the three-state PA, respectively. The ripple component resulting from the experimental results of the two-state PA at a maximum current level is about 3 A as compared to 0.8 A from the simulation results. The mismatch in

the current ripple value is due to the switching frequency of 20 kHz used in the experimental setup. Nonetheless, the practical results are in agreement with the simulation results. The results of the actual three-state PA gave a close correlation with the simulations. The overshoots in the practical results are due to the stray inductance found in the practical PE circuits.

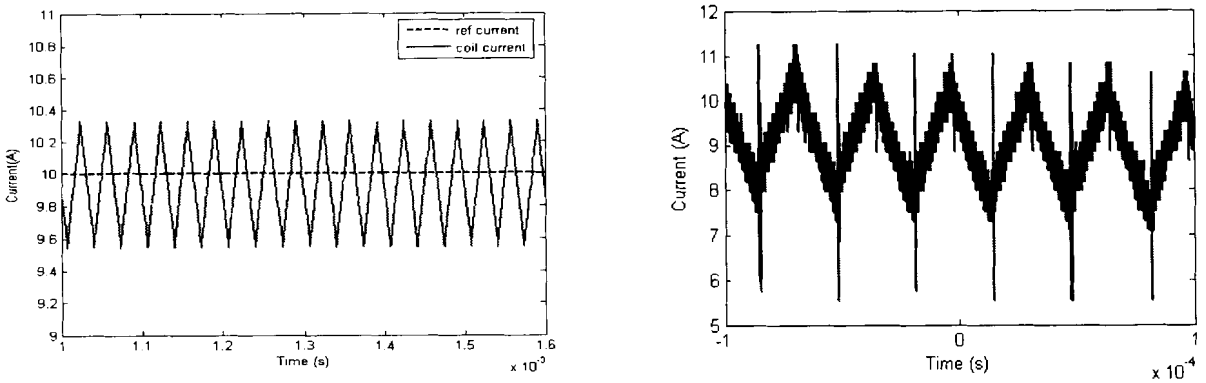

(a) (b)

Figure 6-1: Two-state PA current waveforms (a) simulation results (b) experimental results

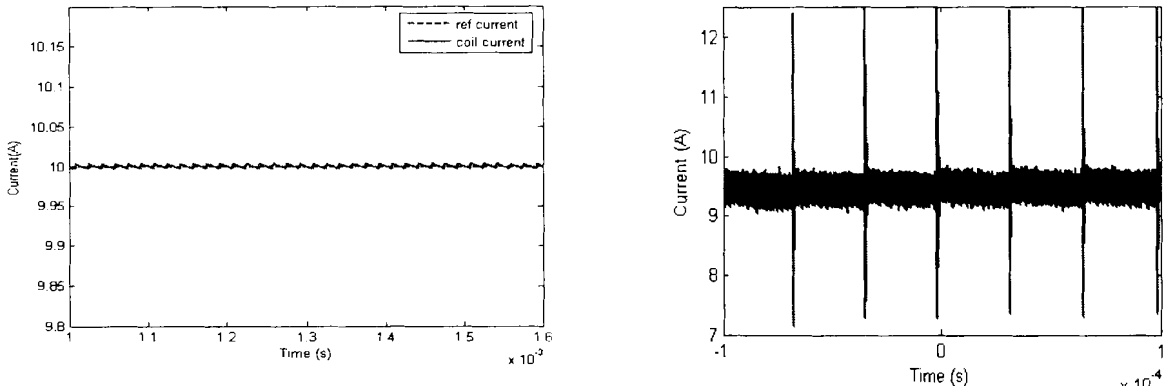

(a) (b)

Figure 6-2: Three-state PA current waveforms (a) simulation results (b) experimental results

For the small signal bandwidth and the power bandwidth, the practical results did not correlate with the simulation results as it is shown in Figure 6-3. Figure 6-3(a) shows the power bandwidth of 1.5 kHz obtained from the simulations while Figure 6-3(b) displays the practical setup's response reaching the power bandwidth at a frequency of 500 Hz. The frequency of the practical PA could not be further increased beyond this frequency. The experimental results are inferior as compared to the simulation results. The poor results are attributed to the high noise levels resulting from the practical set-up. The extreme noise levels results due to the layout of the PE board. The placement of the DSP board significantly affected the overall performance of the hardware as the TSM320 is connected to the PE prototype board with long cables.

The current sensor signal may also have contributed to the poor results. Its output could not be filtered as the filter made the controller more unstable. Low pass filters with different cut-off frequencies were implemented but did not make any difference in the controller's performance. An attempt to filter the signal in the DSP environment caused the controller to malfunction. Unfortunately, the limitation of filtering the sensor output in the DSP environment could not be further investigated.

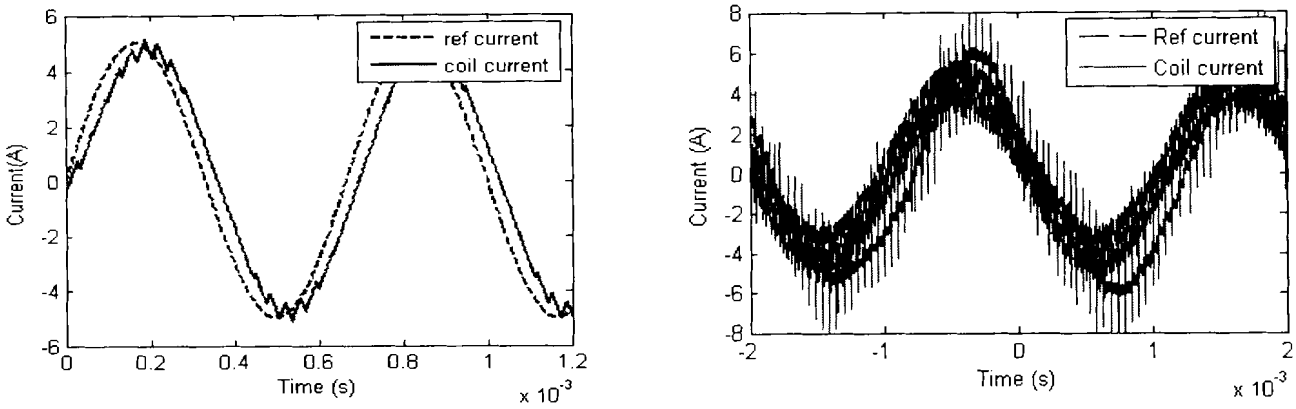

Figure 6-3: Two-state PA power bandwidth (a) simulation results (b) experimental results

Since the switching devices were ideal and the AMB coil was not modelled in terms of the type of the core used, the power losses could not be predicted from the simulations. The conclusion on the comparison of the simulation results power losses can be drawn from the resulting current ripple when the two-state PA is used. The copper losses will be more significant than the losses that will result due to the employment of the three-state PA.

The predicted switching losses of the H-bridge circuit operating at a switching frequency of 20 kHz are given by (6-1) and (6-2) for the IGBT and the freewheeling diode, respectively.

$$\begin{aligned} P_{sw} &= E\big|_{ts\_new} f_{sw} \\ &= 880\times10^{-6}\times20\times10^{3}\ \text{W} \\ &= 17.6\ \text{W} \end{aligned} \tag{6-1}$$

$$\begin{aligned} P_{Dsw} &= \frac{V_{rr} I_{rr} t_{rr} f_{sw}}{2} \\ &= \frac{310\times10\times74\times10^{-9}\times20\times10^{3}}{2}\ \text{W} \\ &= 2.29\ \text{W} \end{aligned} \tag{6-2}$$

Therefore, the total H-bridge losses for the two-state and the three-state PA operating at a switching frequency of 20 kHz are respectively estimated by (6-3) and (6-4).

$$\begin{aligned} P_{H-bridge\_2state} &= 2P_{sw} + 2P_{Dsw} + 2P_{on} + 2P_{D\_on} + P_{Rsense} \\ &= 2\times 17.6 + 2\times 2.29 + 2\times 8.25 + 2\times 6.25 + 5 \text{ W} \\ &= 73.78 \text{ W} \end{aligned} \quad \text{(6-3)}$$

$$\begin{aligned} P_{H-bridge\_3state} &= P_{sw} + P_{Dsw} + P_{on(S1)} + P_{on(S4)} + P_{D\_on} + P_{Rsense} \\ &= 17.6 + 2.29 + 0.3 + 16.5 + 12.29 \\ &= 48.83 \text{ W} \end{aligned} \quad \text{(6-4)}$$

For the two-state and the three-state PA, the measured losses in the experimental set-up are respectively measured as 65.1 W and 40.8 W. The measured losses are lower than the predicted losses by approximately 8 W for both the two-state and the three-state switching techniques. The difference in the predicted and the measured losses are attributed to the various assumptions in the theoretical prediction.

6.1.2 Two-state and three-state

The two amplifiers were compared based on the resulting current ripple, the power losses and the power bandwidth. Both PAs are in agreement with the theoretical levels of the current ripple components. The two-state PA has significant ripple component whereas the three-state PA showed considerably low current ripple components. It was observed in the practical set-up that the ripple component of a three-state is independent of the supply voltage and that of the two-state increases with the supply voltage. This is evidence that the use of the three-state PA results in improved AMB performance as the dynamic responses and stiffness of an AMB system can be increased by the supply voltage without inducing eddy current losses in the system.

Power losses

The power losses occurring in the H-bridge and the load due to the use of the two-state PA are significant as compared to the three-state PA. Figure 5-30 showed that the eddy current losses in the AMB coil results due to the high ripple current components resulting from the use of the two-state PA. The considerably lower losses in the AMB coil due to the three-state PA are the reason why the three-state PA is preferred in the AMB systems.

Power bandwidth

The power bandwidth of the two PAs could not be measured at the supply voltage of 310 V due to high noise levels. The use of long cables to connect the DSP board to the PE made the PA very susceptible to

noise. The PA's power bandwidth was measured at low supply voltages. The results of the two amplifiers correlated with the power bandwidth predictions at low supply voltages.

6.2 Recommendations

Characterising the AMB PAs in terms of the operation of the specific topology of the PA does not quantify the use of the PA in AMB systems. The prototype PAs presented in this work clearly show the expected differences in the two techniques but needs more work in order to make them applicable to the double radial AMB system in the MBMC lab. The dynamic performance of the PAs is important to AMB systems. Improvements need to be made as this PAs failed to exhibit a wide power bandwidth and small signal bandwidth for the desired specifications. The limitation on the dynamic performances is attributed to the high noise levels produced when the PAs operate at high supply voltages. The high noise levels result from the PCB layout of the prototype board. The layout of the prototyped board should be reviewed and the grounding policy of the PA should be revisited. Factors such as heating of transformers, placement of current sensing devices and placement of the DSP board affected the overall performance of the PA circuit. Also, the electronic supply should be replaced with the flyback converter. In addition, the use of common mode filters should be considered in future designs.

Since, the use of VisSim® program caused inconsistencies in the implementation of the switching techniques. The implemented PI controller and the use of a fixed point number system are likely the main reasons for undesired responses. It is recommended in future that the control algorithm be done in C-compiler. The use of a Field Programmable Gate Array (FPGA) may also be the possible solution to the digital implementation of the switching topologies. Therefore it is advantageous to investigate the use of FPGAs in the realisation of both the two-state and the three-state switching PAs.

6.3 Closure

The objective of the study was to develop the platform to facilitate the analysis of the two switching techniques possible for the AMB switch-mode PAs. The two-state and the three-state switching techniques were successfully designed, implemented and tested on the flexible rotor double radial AMB model.

The results obtained showed good correlation with the conducted simulations. Also, the use of the three-state PA resulted in low power losses.

APPENDIX

Appendix A: Power Amplifier Circuit Diagram

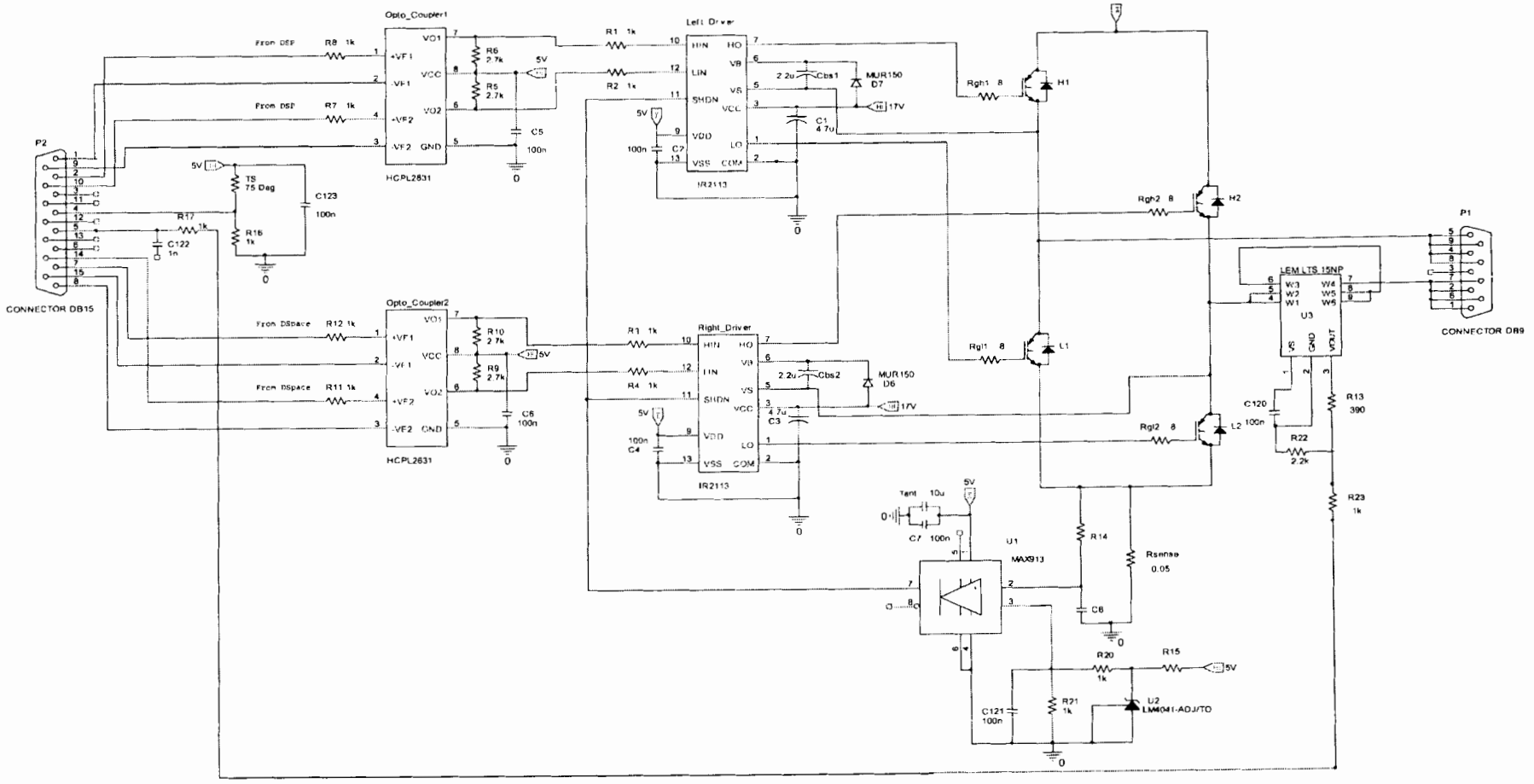

Figure A- 1: Power electronic schematic circuit

Appendix B: Data CD

1. **Dissertation in MS Word format**
2. **Simulink® simulation models**
3. **VisSim® program**
4. **Orcad® schematic file and PCB Layout files**

REFERENCES

[1] J. Zhang, J.O. Schulze, N. Barletta, "Synchronous three-phase PWM power amplifier for active magnetic bearings," Proc. 8th International Symposium on Magnetic Bearings, August 1996, Japan, pp. 277-282

[2] G. Schweitzer, H. Bleuler, A. Traxler, "Active Magnetic Bearings: Basics, Properties and Applications of Active Magnetic Bearings", Authors Reprint, Zürich, 2003.

[3] E. Maslen, "Magnetic bearings." Revised, University of Virginia, June 2000

[4] R.C. Lebron-Velilla, R.H. Jansen, *et al*, "Magnetic bearing amplifier output power filters for flywheel systems," *NASA/TM-2003-212510*, 2003

[5] P. Alleire, C.R. Knospe, *et al*, "Short course on magnetic bearings," Alexandria Virginia United states of America: University of Virginia 1997

[6] J. Zhang, N. Karrer, "IGBT power amplifier for active magnetic bearings of high speed milling spindle" Proc. IECO'95, Orlando Florida, pp. 596-601

[7] S. Pradhananga, "Experimental validation of smart-bias active magnetic bearing controller," The Graduate Fuculty of the Louisiana State University and Agricultural and Mechenical college 2004

[8] Burwen, "Kilowatts on order," *IEEE Spectrum,* 1993, pp. 32-37

[9] T.P Denver, A.B. Pallazzolo, *et al*, "Evaluation and improvement of eddy current position sensors in magnetically suspended flywheel systems," *NASA/CR-2001-211137*, 2001

[10] A. Schammass, H. Bleuler, "Experimental results on self-sensing AMB using a three-state PWM amplifier" 8th International Symposium on Magnetic Bearing," 2002, pp 289-292

[11] T. Mizuno, T. Ishii, K. Araki. (1998) Self sensing magnetic suspension using hysteresis amplifiers. *Control Engineering Practice 6.* pp. 1133-1140. Available: http://www.sciencedirect.com [Date of access: August 2005]

[12] H. Lloyd, J. Doxon. Closing the feedback loop. Texas Instrument Application Note. [Onlinc] Available: http://www.ti.com

[13] R. Mammano. Switching power supply topology-voltage mode vs. current mode. Unitrode Design Note. [Online] DN-62, pp. 1-4. Available: http://www.ti.com

[14] L. Dixon (May, 2003). Average current mode control of switching power supplies. Unitrode Application Note. [Online]. U140, pp. 3-356 – 3-369. Available: http://www.ti.com

[15] J. Holtz, "Pulsewidth modulation – A survey" IEEE Transactions on Industrial Electronics, Vol 32, 1992, pp. 410-419

[16] G Schweitzer, "Active magnetic bearings – chances and limitations", International Centre for Magnetic Bearings, ETH Zurich, CH-8092 Zurich

[17] B. Mammano, "Current sensing solutions for power supply designers"

[18] R. Dickinson, S. Milano. Isolated open loop current sensing using Hall Effect technology in an optimized magnetic circuit. Allegro Application Note [Online]. pp. 1-12. Available: http://www.allegro.com

[19] E.O. Ranft, "The Development of a Flexible Rotor Active Magnetic Bearing System", North West University, School of Electrical and Electronic Engineering, 2005

[20] J.P. Agrawal, "Power electronic systems: theory and design" Prentice Hall, New Jersey, 2001

[21] M. Edmunds. (May 2003). Hard Switching vs Soft Switching: A Case Study. [Online]. Available

[22] M. Borage, S. Tiwari, S. Kotaiah (May 2003). MOSFET-Assisted Soft-Switching of IGBTs: A Re-Examination. [Online] Available: http://www.techonline.com/community/tech_topic

[23] N. Mohan, T.M. Undeland, W.P. Robbins, "Power electronics: converters, applications, and design" John Wiley & Sons, United States of America, 2003

[24] A.R. Turner, "Design and implementation of a single phase transconductance inverter", University of Sydney, School of Electrical and Information Engineering, 2003

[25] C.R. Paul, "Effectiveness of Multiple Decoupling Capacitors" IEEE Transactions on EMC, May 1992.

[26] V.R Moorthi, "Power electronics : devices, circuits and industrial applications" New Delhi ; Oxford : Oxford University Press, 2005

[27] J. Adams. (2003, May). Bootstrap component selection for control IC's. International Rectifier Design Tip. [Online]. DT 98-2a. pp1-4. Available: http://www.irf.com

[28] Texas Instruments. (1997). TMS320C24x general purpose timer 1 symmetric mode. Texas Instruments Technical report. [Online]. Spra368. Available: http://www.ti.com

[29] L. Zhang, J. Fang, G. Liu, " Modeling and simulation of the switching power amplifier for magnetic suspending flywheel" Proc. 8th International Symposium on Magnetic Bearings, September 2005, Dresden, pp. 240-244